**UNIVERSIDADE FEDERAL DE SÃO CARLOS**
**CENTRO DE CIÊNCIAS EXATAS E DE TECNOLOGIA**
**DEPARTAMENTO DE QUÍMICA**
**PROGRAMA DE PÓS-GRADUAÇÃO EM QUÍMICA**

# SURFACE MODIFICATION WITH POLYMERS AS A TOOL TO FUNCTIONALIZE FABRICS, FABRICATE GRADED MATERIALS AND DESIGN INTERFACE OF COMPOSITES

REBECCA FAGGION ALBERS*

Tese apresentada como parte dos requisitos para obtenção do título de DOUTORA EM CIÊNCIAS, área de concentração: FÍSICO-QUÍMICA.

Orientador: EDSON ROBERTO LEITE
*Bolsista FAPESP

São Carlos – SP
2021

To my father, who has never had the chance to see this adventure,
but I know is proud somewhere.

"You can't connect the dots looking forward; you can only connect them looking backward. So you have to trust that the dots will somehow connect in your future. […]

Almost everything — all external expectations, all pride, all fear of embarrassment or failure — these things just fall away in the face of death, leaving only what is truly important. Remembering that you are going to die is the best way I know to avoid the trap of thinking you have something to lose. You are already naked. There is no reason not to follow your heart."

Steve Jobs

"Cheguei onde cheguei porque tudo o que planejei deu errado."

Rubem Alves

# ACKNOWLEDGEMENTS

I am thankful to Prof. Dr. Edson R. Leite for the opportunity of being guided through the Ph. D. by him. I am enormously grateful for him propelling me towards pursuing my dreams since our first conversation back in 2016.

I would like to thank Prof. Dr. André Studart for accepting me in the Complex Materials Group as an exchange Ph. D. student for 2.5 years and for the precious contributions during this period.

I am indebted with Dr. Rafael Libanori, who has been patiently guiding me through the composites' world, teaching me about mechanical properties of materials, motivating me and opening up new perspectives every time I believed there was no way out.

Special thanks to Dr. Edmondo M. Benetti for leading me through the fascinating ATRP chemistry, teaching me about organic synthesis and believing I was capable of doing the job.

I would like to thank Prof. Dr. Nicholas Spencer for his support and precious contributions.

I am grateful for my father Beto (in memoriam), my mother Sônia, my sister Sarah and my brother Pedro for all the love and for believing in me, even when I doubted myself.

Special thanks to Stefano Menasce for being present even when I was not the best company, for all the food we have shared, nice memories we have made and for encouraging me in the times when I felt lost.

Many thanks to Tommaso Magrini for the scientific contributions and for being a good friend, making me laugh with the daily pranks at the lab.

I would like to acknowledge Isabelle Lendvai for being supportive and not letting me give up when I tried to.

I would like to address my gratitude to Marco Binelli, Alessandro Dutto and Yannick Nagel for the friendship and for all the dinners and lunches shared at ETH.

I am thankful to Gilberto Siqueira for his friendship and support during these years.

I am grateful to Julia Carpenter for her valuable support in hard moments during the PhD period and for her friendship.

I would like to thank the Complex Materials Group members, who replied to my uncountable ciaos, making me feel home, specially to Wilhelm Woigk, Erik Poloni, Ahmet Demirörs, Alessandro Ofner, Etienne Jeoffroy, Fabio Bargardi, Fergal Coulter,

Iacopo Mattich, Lorenzo Barbera, Matthias Haug, Nicole Kleger, Manuel Schaffner, Petar Stefanov, Akin Gursoy, Madeleine Grossman, Martina Pepicelli, Rafael Heeb, Rani Boons, Sara Velásquez, Silvan Gantenbein, Ahmad Rafsanjani, Florian Bouville, Kunal Masania, Michael Hausmann, Patrick Rühs, Lucas Castro, Anton Kan, Enrico Scoccimarro, Chirstian Furrer, Julie Laurent, Lena Tervoort, Noemi Kaufmann, Lun Han and Veronika.

I am thankful to the Laboratory for Surface Science and Technology members, for the support and contributions, specially to Wenqing Yan, Matteo Romio, Moh Divandari, Lucca Trachsel, Amine Layadi and Benjamin Kessel.

I would like to thank the friends I have made in Zurich Francesca Victorelli, Liliane Manny, Maribal Gonzalez and Timothée Schaeffer for all the good moments we have spent together.

I am truly grateful for my therapist Thais Chaves, who has carefully guided me through the tortuous paths of my mind.

I am thankful for the friends from UFSCar Fabrício Destro, Cipriano Gozzo and Josiane Carneiro, for the good moments in São Carlos.

Many thanks to the friends from LNNano Murillo Rodrigues, Carolina Torres, Joao Batista Souza Jr., Cibele Pessan and Danilo for the laughs we shared during the pandemic time in Brazil.

I would like to express my gratitude to my Brazilian friends Ana Laura Biancolli, Leticia Ortiz, Munique Mendes, Patrícia Trajano, Isadora Sabater, Larissa Zibordi and Luma Garcia for being present and supportive in the hardest moments of this journey.

I am thankful to my aunts Lu and Bel (in memoriam), who have become even closer after my father's death.

Many thanks to the employees who have made the office work at UFSCar, LNNano, ETH Zürich and EMPA during the five years of my PhD.

I would like to acknowledge the Brazilians and Swiss institutions Federal University of São Carlos (UFSCar), Brazilian Nanotechnology National Laboratory (LNNano), Swiss Federal Institute of Technology (ETH Zürich) and Swiss Federal Laboratories for Materials Science and Technology (EMPA St. Gallen) for the infrastructure.

I am thankful to FAPESP (2016/14493-7 and 2017/22304-2), EMPA and the Complex Materials Group for the financial support.

# LIST OF FIGURES

# LIST OF SCHEMES

# SUMMARY

SURFACE MODIFICATION WITH POLYMERS AS A TOOL TO FUNCTIONALIZE FABRICS, FABRICATE GRADED MATERIALS AND DESIGN INTERFACE OF COMPOSITES

Tailoring the properties of a material for a target application often depends on combining features of different components. To effectively arrange these components in a material, several methods have been developed to chemically modify surfaces, tuning its chemical composition, morphology and properties. Chemically modifying both organic and inorganic substrates enables the fabrication of coatings, the modification of scaffolds and the modulation of mechanical properties of composites. In this work, chemical functionalization through Atom Transfer Radical Polymerization (ATRP) was explored to fabricate coatings on $SiO_x$ substrates and cotton-based wound dressings; modifying scaffolds for the fabrication of 3D polymer-based graded materials; and designing the interface of polymer matrix composites. Conventional ATRP in solution is sensitive to oxygen and often requires lengthy deoxygenation processes of the polymerization mixture. When a zero-valent metal ($Mt^0$) is introduced to the system in surface-initiated ATRP, it acts as a reducing agent, consuming oxygen from the polymerization mixture and enables the grafting of polymer brushes under ambient conditions. $Zn^0$ was used as a reducing agent in $Zn^0$ SI-ATRP to favor a cheap, fast and oxygen-tolerant fabrication of polymer brushes. Chemically different polymers were grafted from $SiO_x$ substrates using microliter volumes of polymerization mixture and the applicability of the process was demonstrated by grafting polymer brushes from cotton-based wound dressings. SI-ATRP is also a polymerization method in which the grafting density depends on the distance between the initiator and the reducing agent. Such feature enables the fabrication of materials with a gradient of chemical composition and morphology. A scaffold containing ATRP initiator in its structure was fabricated through free radical polymerization (FRP) of a high internal phase emulsion (HIPE) and functionalized through $Cu^0$ SI-ATRP, yielding single and multiple polymer gradients. Poly(oligoethylene glycol methacrylate) (POEGMA) and poly(N-isopropylacrylamide) (PNIPAM) single gradients and poly(2-Hydroxyethyl methacrylate) PHEMA and POEGMA double gradients were fabricated and investigated through attenuated total refection Fourier-transform infrared spectroscopy (ATR-FTIR) and image analysis of scanning electron microscopy (SEM) images. Moreover, polymers with different functionalities were synthesized through ATRP for the interfacial design of polymer matrix composites. Chemical compatibility

between matrix and reinforcing elements enhances mechanical properties of composites, however interfacial architecture also influences the mechanical response of the final material. Interfacial vulcanization between the exposed S of 2D-$MoS_2$ and the polybutadiene block of polystyrene-block-polybutadiene-block-polystyrene (PSBS) leads to the formation of loop-chain entanglements at the interface of the composite. To investigate the transference of stress from the matrix to the reinforcing elements at the interface of such composites, controlled architecture polymers were synthesized through conventional ATRP in solution, grafted to 2D-$MoS_2$ and used as reinforcing elements in PSBS matrix composites. Such composites with interfacial brushes and loops were cyclic tested in tensile mode and revealed how molecular events taking place at the interface during loading and unloading cycles impacts the mechanical performance of polymer matrix composites.

# RESUMO

MODIFICAÇÃO DE SUPERFÍCIE COM POLÍMEROS COMO UMA FERRAMENTA PARA FUNCIONALIZAR TECIDOS, FABRICAR MATERIAIS COM GRADIENTE E PROJETAR A INTERFACE DE COMPÓSITOS.

Ajustar as propriedades de um material para uma aplicação específica frequentemente depende da combinação de características de diferentes componentes. Para que esses componentes sejam efetivamente arranjados num material, diversos métodos foram desenvolvidos para modificar superfícies quimicamente, adaptando suas composição química, morfologia e propriedades. Modificar quimicamente substratos orgânicos e inorgânicos permite a fabricação de revestimentos, a modificação de suportes e a modulação de propriedades mecânicas de compósitos. Neste trabalho, funcionalização química através da Polimerização Radicalar por Transferência de Átomo (ATRP) foi explorada para fabricar revestimentos sobre substratos de $SiO_x$ e curativos à base de algodão; modificar suportes para a fabricação de materiais poliméricos em três dimensões (3D) com gradientes, e projetar a interface de compósitos de matriz polimérica. ATRP convencional em solução é sensível a oxigênio e frequentemente requer processos demorados de desoxigenação da mistura de polimerização. Quando um metal de valência zero ($Mt^0$) é introduzido ao sistema em ATRP iniciado em superfície (SI), ele atua como um agente redutor, consumindo oxigênio da mistura de polimerização e permite o enxerto de cadeias de polímero sob condições ambiente. $Zn^0$ foi usado como um agente redutor em $Zn^0$ SI-ATRP para favorecer uma fabricação barata, rápida e tolerante a oxigênio de cadeias de polímero. Polímeros quimicamente diferentes foram enxertados em substratos de $SiO_x$ usando volumes de mistura de polimerização da ordem de microlitros e a aplicabilidade do processo foi demonstrada por enxerto de cadeias de polímero em curativos à base de algodão. SI-ATRP também é um método de polimerização em que a densidade de enxertia depende da distância entre o iniciador e o agente redutor. Tal característica possibilita a fabricação de materiais com gradiente de composição química e morfologia. Um suporte contendo o iniciador de ATRP em sua estrutura foi fabricado através da polimerização radicalar livre (FRP) de uma emulsão de alta fase interna (HIPE) e funcionalizado através de $Cu^0$ SI-ATRP, originando gradientes poliméricos únicos e múltiplos. Gradientes simples de poli(oligoetilenoglicol metacrilato) (POEGMA) e poli(N-isopropilacrilamida) (PNIPAM) e gradientes duplos de poli(2-hidroxietil metacrilato) PHEMA e POEGMA foram fabricados e investigados por espectroscopia de infravermelho com transformada de Fourier com reflectância total

atenuada (ATR- FTIR) e análise de imagens de imagens de microscopia eletrônica de varredura (SEM). Além disso, polímeros com diferentes funcionalidades foram sintetizados através de ATRP para projetar a interface de compósitos de matriz polimérica. A compatibilidade química entre a matriz e os elementos de reforço melhora as propriedades mecânicas dos compósitos, no entanto a arquitetura da interface também influencia a resposta mecânica do material final. A vulcanização interfacial entre o S exposto do 2D-$MoS_2$ e o bloco de polibutadieno do copolímero em bloco poliestireno-polibutadieno-poliestireno (PSBS) leva à formação de emaranhamentos do tipo ciclo-cadeia na interface do compósito. Para investigar a transferência de tensão da matriz para os elementos de reforço na interface de tais compósitos, polímeros de arquitetura controlada foram sintetizados através de ATRP convencional em solução, enxertados em 2D-$MoS_2$ e usados como elementos de reforço em compósitos de matriz de PSBS. Esses compósitos com cadeias e ciclos interfaciais foram testados ciclicamente em modo de tração e revelaram eventos moleculares que ocorrem durante os ciclos de carregamento e descarregamento.

## CONTENTS

# CHAPTER 1

# INTRODUCTION

## 1.1 AIM AND ORGANIZATION OF THE THESIS

The main goal of this thesis is to explore the surface modification of organic and inorganic materials through Atom Transfer Radical Polymerization (ATRP) to tailor chemical, morphological and mechanical properties of the final material. In particular, this thesis aims to tune properties of two-dimensional (2D) flat substrates, three-dimensional (3D) supports and modulate the interface of polymer matrix composites. Exploring the mechanism of zero-valent metal ($Mt^0$)-mediated surface-initiated (SI) ATRP ($Mt^0$ SI-ATRP) is the key to modify 2D substrates under ambient conditions and create technologically relevant approaches for the functionalization of fabrics. Understanding the mechanism of $Mt^0$ SI-ATRP to modify 2D substrates paves the way to functionalize 3D supports and fabricate polymer-based materials with a gradient of chemical composition and morphology. Besides, the synthesis of polymers through conventional ATRP allows the fabrication of architectured polymers, enabling the investigation of the stress transfer mechanism at the interface of polymer matrix composites. Comprehending the mechanism of $Zn^0$ SI-ATRP, fabricating polymer-based graded materials through $Cu^0$ SI-ATRP and modulating the interface of polymer matrix composites compose the three pillars that sustain this thesis, Figure 1.1.

The thesis is divided in six chapters and three appendices. Chapter 1 is a general introduction into the surface modification of inorganic and organic materials with polymers through "grafting to", "grafting from" and "grafting through" approaches. Subsequently, we discuss the characters of conventional Free Radical Polymerization (FRP) and the most applied Controlled/Living Radical Polymerization (CLRP) methods, including Nitroxide Mediated Polymerization (NMP), Reversible Addition-Fragmentation chain Transfer (RAFT) and ATRP, as well as their advantages and drawbacks. Finally, ATRP approach is discussed thoroughly, comprising the mechanism of classical ATRP performed in solution, how to vary technical features to fabricate polymers with controlled architecture and the challenges and limitations of such method.

Chapter 2 focuses on understanding the mechanism of $Zn^0$ SI-ATRP through investigation of reaction kinetics of various chemically different polymers grafted from 2D $SiO_x$ controlled substrates, Figure 1.1a. Furthermore, such methodology is applied to modify cotton-based wound dressings with polymer under ambient conditions.

Chapter 3 explores the manufacture of polymer-based graded materials through $Cu^0$ SI-ATRP, Figure 1.1b. An elastomeric 3D support containing ATRP initiator in its structure is fabricated and subsequently functionalized through $Cu^0$ SI-ATRP. Chemically and morphologically tunable 3D supports are obtained, enabling the fabrication of single and multiple gradients without the need of lengthy deoxygenation processes.

Chapter 4 explores the interface modulation of 2D-$MoS_2$ rubbery composites, Figure 1.1c. Polymers with controlled chemical composition, site specific functionalities and topology were fabricated through conventional ATRP method and used to decorate 2D-$MoS_2$ particles with linear brushes and loop-forming polymers. Architectured interface composites were mechanically tested to understand the stress-transfer mechanism from the matrix to the reinforcing elements of interfacial vulcanized composites. Appendices A, B and C provide supplementary information to the chapters 2, 3 and 4, respectively.

Finally, chapter 5 describes the conclusions of the thesis and chapter 6 gives an outlook with open questions for further investigations.

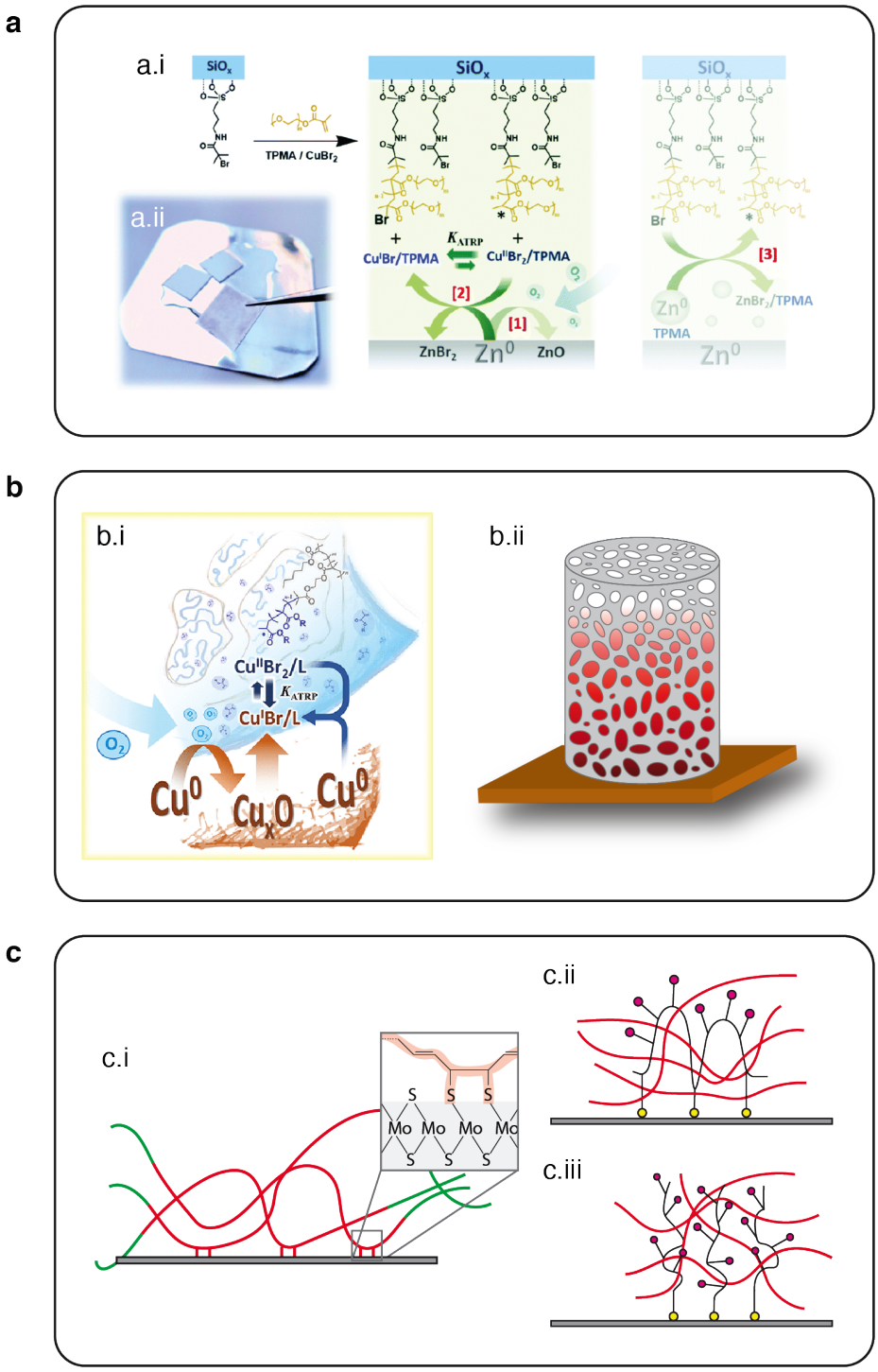


**Figure 1.1.** Organization of the thesis. (a) Understanding the mechanism of $Zn^0$ SI-ATRP (a.i) through functionalization of $SiO_x$ controlled substrates (a.ii) and application of the method to modify cotton-based wound dressings; (b) Exploring $Cu^0$ SI-ATRP (b.i) to fabricate polymer-based 3D graded materials (b.ii); (c) Modulating the interface of 2D-$MoS_2$ polymer matrix composites through interfacial vulcanization (c.i) and architectured polymers to give interfacial loops (c.ii) and interfacial brushes (c.iii).

## 1.2 SURFACE MODIFICATION WITH POLYMERS

Developing a material to adjust its properties, targeting a specific application often requires the combination of diverse components.[1–3] To achieve an effective combination of such components into a material, scientists have developed several methodologies to modify surfaces with polymers to add functionalities, tailor morphology and modulate properties of the final material, aiming for biomedical,[4] aerospace,[5] textiles,[6] microfluidics,[7] energy[8] and electronic[9] applications.

A surface treatment adds functional groups to the material surface, remodeling its surface energy.[1] The surface of a material can be modified based on physical adsorption or chemical processes, that introduce covalent bonds to the system. Three chemistry synthetic strategies enable the chemical surface modification named "grafting to", "grafting from" and "grafting through", Figure 1.2.[10–12] The "grafting to" strategy consists of synthesizing functional polymers, which can be combined to reactive groups of a substrate, Figure 1.2a; the "grafting from" approach comprises a functionalization of the substrate with initiators prior to the polymerization, Figure 1.2b; and in the "grafting through" methodology the substrate surface contains polymerizable groups, Figure 1.2c. The "grafting through" approach might lead to crosslinked systems depending on the concentration of the polymerization mixture, since the growing chains can incorporate polymerizable groups anchored in different substrates.[10] Due to the poorer control over the system based on the "grafting through" approach, this thesis is based on grafting polymers from controlled $SiO_x$ substrates and textiles (Chapter 2) and elastomeric scaffolds (Chapter 3), as well as grafting polymers to 2D-$MoS_2$ (Chapter 4). The polymers were synthesized through ATRP, a controlled/living radical polymerization (CLRP) method.

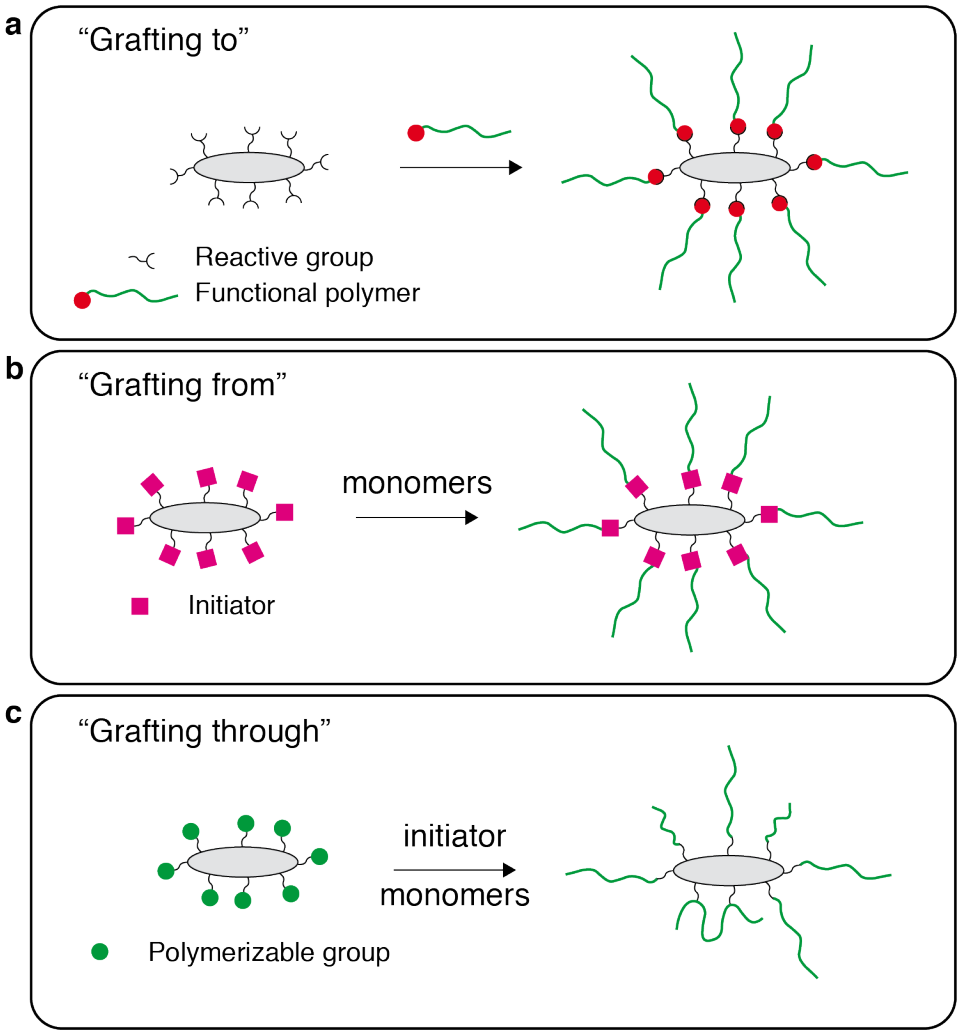


**Figure 1.2.** Schematic representation of the three strategies to chemically modify the surface of a material with polymers, named (a) "grafting to"; (b) "grafting from"; and (c) "grafting through".

## 1.3 CONTROLLED/LIVING RADICAL POLYMERIZATION (CLRP)

FRP is a chain reaction in which unsaturated monomers are added to an active radical specie while transferring the radical to the end of the chain[13] and consists of three steps: initiation, propagation and termination. In the initiation phase, the initiator (I) decomposition is induced by heat, light irradiation or a redox process to form free radical species (R·), Equation 1.1a. In the propagation step, the free radical fragment reacts with a monomer (M) to give an active radical specie (RM·). As long as monomer molecules are added to the active chain, the active polymer chain grows ($RM_n$·), Equation 1.1b. In the termination step, radical species are combined, ending the polymer growth ($RM_{m+n}$), Equation 1.1c.[14]

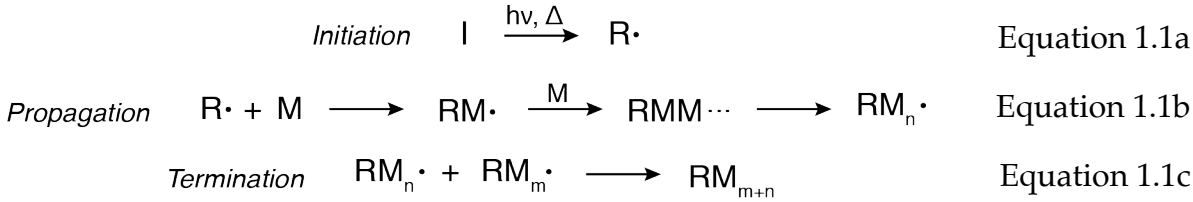


FRP is a widely spread polymerization method, with several well-stablished methodologies to fabricate polymer-based materials in industry due to its satisfactory reproducibility, simple implementation, relative inertia towards functional groups and the possibility to employ water and protic solvents as polymerization medium.[15] However, FRP presents limitations regarding control over molecular weight, chemical composition, chain architecture and functionalities.[16] The development of CLRP methods set aside the constraints of FRP approach, enabling the fabrication of functional polymers with precise architecture. In CLRP methods, the majority of the chains are dormant species and not able to propagate or terminate, while the minority of the chains are actively propagating in a dynamic equilibrium.[16] Among the CLRP methods, NMP, RAFT and ATRP have been widely applied.

NMP method is relatively easy to be performed, does not require a metal-based catalyst and allows the synthesis of colorless and odorless polymers, without the need of purification.[17] However, the polymerization kinetics is slow, demands high temperatures and lengthy polymerization times. Furthermore, side reactions might occur, compromising the molecular weight distribution of the final polymer.[18] As represented in the mechanism of NMP in Figure 1.3a, a radical specie reacts with monomers and either starts chain growth or reacts reversibly with a nitroxide radical (Figure 1.3b), generating a nitroxide-trapped specie.[19,20]

RAFT is a versatile metal-free polymerization method, which enables the polymerization of a wide range of chemically different monomers. Nonetheless, RAFT method requires a RAFT agent, typically a thiocarbonylthio compound that acts as a chain-transfer agent,[21] Figure 1.3c and d. Such RAFT agent is unstable over time, colorful and often presents an unpleasant odor due to the sulfur content, thus purification steps are often needed after RAFT polymerization.[22,23] Next session is dedicated to the discussion of ATRP method.

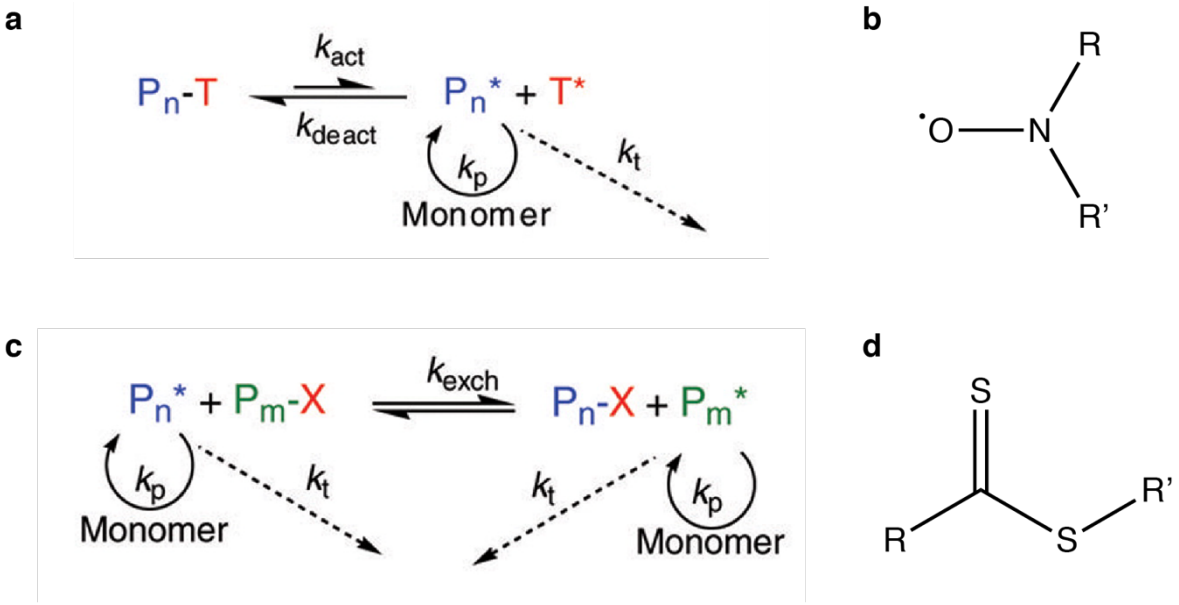


**Figure 1.3.** Schematic representation of the mechanism of two of the most applied CLRP approaches. (a) NMP, where T is a nitroxide group; (b) Chemical structure of a nitroxide radical; (c) RAFT, where X is a RAFT agent; (d) Chemical representation of a RAFT agent. Adapted from Spanswick, 2005.[16]

## 1.4 ATOM TRANSFER RADICAL POLYMERIZATION (ATRP)

ATRP is a CLRP method mediated by a transition metal complex catalyst, Figure 1.4. The mechanism of ATRP involves a reversible homolytic transfer of the halogen from an alkyl halide dormant specie ($P_n$-X), either an initiator or a dormant polymer chain, to a transition metal complex at a lower oxidation state ($Mt^n$/L, activator specie), with a rate constant for activation $k_{act}$. A transition metal complex at a higher oxidation state coordinating the halide (X-$Mt^{n+1}$/L, deactivator specie) and a radical specie ($P_n$*) are generated. The radical specie $P_n$* can either react with monomers, triggering polymer growth in a propagation step, with a rate constant for propagation $k_p$, and be deactivated with a constant rate for deactivation $k_{deact}$ or terminate with a constant rate for termination $k_t$. Because of the Persistent Radical Effect (PRE),[24] the concentration of radicals $P_n$* is low, the probability of radical-radical termination reactions is reduced as the polymerization proceeds and the equilibrium is shifted towards the dormant species ($k_{deac}$ >>> $k_{act}$).[16,25]

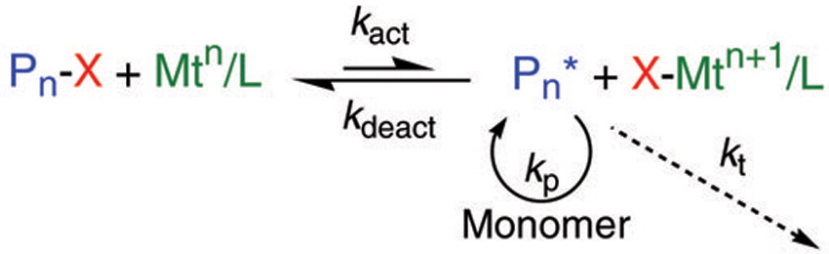


**Figure 1.4.** Schematic representation of ATRP mechanism. The alkyl halide specie ($P_n$-X) undergoes homolytic transfer of the halogen from an alkyl halide dormant specie ($P_n$-X) to the transition metal complex at a lower oxidation state ($Mt^n$/L, activator specie) with rate constant for activation $k_{act}$, generating a radical specie ($P_n$*) and a transition metal complex at a higher oxidation state coordinating the halide (X-$Mt^{n+1}$/L, deactivator specie). The radical specie $P_n$* either react with monomers at $k_p$ propagation rate and is deactivated with rate constant for deactivation $k_{deac}$ or terminate, with termination rate $k_t$. The equilibrium is shifted towards the dormant species and $k_{act}$ <<< $k_{deact}$. Adapted from Spanswick, 2005.[16]

Reaction parameters such as temperature, pressure, solvent, the catalyst and the alkyl halide influence the kinetics of ATRP.[25] Since ATRP is a complex reaction, these parameters have to be carefully chosen accordingly to the final target architecture of the polymer. ATRP allows the fabrication of polymers and copolymers with high control over chemical composition, polydispersity, topology and site specific functionality,[26] Figure 1.5.

In ATRP, the chains are early initiated and grow simultaneously, thus a change in the instantaneous composition due to relative concentration of monomers is replicated along all chains. Such feature can be explored to tune the chemical composition of polymers, for example using monomers with different reactivity ratios leading to statistical/random, periodic or gradient copolymers. Besides, the activated alkyl halide attached to the end of the polymer chain allows additional polymerization steps and the fabrication of copolymers,[26] Figure 1.5a.

The topology of the polymer can be controlled through "grafting from", "grafting through" and "grafting onto" approaches. Graft copolymers can be manufactured through "grafting from" when polymers are grafted from a functional-group-pending macroinitiator, a polymer containing at least one initiator site; "grafting through", with the polymerization of a macromonomer, a macromolecule containing a polymerizable group; or "grafting onto", when a polymer chain is attached to a polymer backbone. Such approaches can be explored to give linear, star/multi-armed, comb, network and (hyper)branched polymers,[26] Figures 1.5b.

Functionalities can be added to the polymers through monomers, initiator fragments or polymer termini. Monomers can either directly introduce a functionality to the material or a protected group, which can be unprotected and modified after the polymerization step. The initiator fragment can add functionalities to the end of the polymer chain, multiple alkyl halide groups can generate multifunctional star-like polymers and the halide at the end of the chain can also be replaced after polymerization, Figure 1.5c. Furthermore, functional polymers fabricated through ATRP approach allows the manufacture of molecular composites such as hybrid materials with inorganic components or biopolymers, functional colloids and modified surfaces,[26] Figure 1.5d.

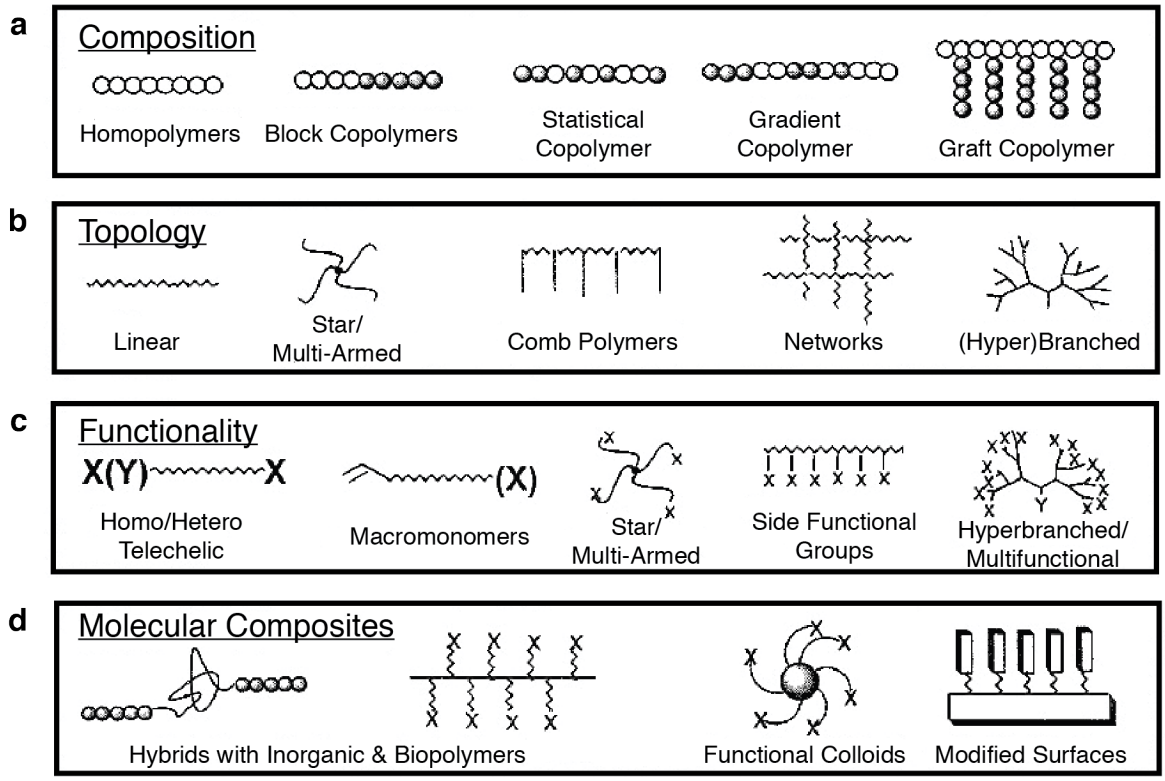


**Figure 1.5.** Schematic representation of architectured polymers prepared through ATRP, tuning (a) Composition; (b) Topology; (c) Functionality; and the fabrication of (d) Molecular Composites. Adapted from Xia, 2001.[26]

ATRP enables the fabrication of polymers with low polydispersity, high control over chemical composition, functionalities and topology, with no side products. However, such methodology is sensitive to oxygen and employs a metal-based catalyst, usually a complex of copper halide and amine ligands. Such drawbacks have limited the use of ATRP in the industrial sector in the past years.[25] However, scientists have been developing strategies to perform ATRP under ambient conditions and using alternative transition metal-based catalyst,[27–30] as reported in Chapter 2. The advances

of ATRP methodologies performed under ambient conditions to modify 2D substrates sets the scene for the fabrication of polymer-based 3D graded materials,[30–32] as reported in Chapter 3. And although the conventional ATRP method requires lengthy freeze-pump-thaw cycles to deoxygenate the system, it allows the creation of architectured polymers that can be grafted to surfaces. Thus, conventional ATRP approach was explored to fabricate architectured polymers and modulate the interface of polymer matrix 2D-$MoS_2$ composites, as reported in Chapter 4.

## 1.5 REFERENCES


1. Nemani, S. K.; Annavarapu, R. K.; Mohammadian, B.; Raiyan, A.; Heil, J.; Haque, M. A.; Abdelaal, A.; Sojoudi, H. Surface Modification of Polymers: Methods and Applications. Adv. Mater. Interfaces 2018, 5 (24), 1–26.
2. Eitan, A.; Jiang, K.; Dukes, D.; Andrews, R.; Schadler, L. S. Surface Modification of Multiwalled Carbon Nanotubes: Toward the Tailoring of the Interface in Polymer Composites. Chem. Mater. 2003, No. 15, 3198–3201.
3. Rong, M. Z.; Zhang, M. Q.; Ruan, W. H. Surface Modification of Nanoscale Fillers for Improving Properties of Polymer Nanocomposites: A Review. Mater. Sci. Technol. 2006, 22 (7), 787–796.
4. Bose, S.; Robertson, S. F.; Bandyopadhyay, A. Surface Modification of Biomaterials and Biomedical Devices Using Additive Manufacturing. Acta Biomater. 2018, 66, 6–22.
5. Kaysser, W. Surface Modifications in Aerospace Applications. Surf. Eng. 2001, 17 (4), 305–312.
6. Hu, J.; Meng, H.; Li, G.; Ibekwe, S. I. A Review of Stimuli-Responsive Polymers for Smart Textile Applications. Smart Mater. Struct. 2012, 21 (5).
7. Hu, S.; Ren, X.; Bachman, M.; Sims, C. E.; Li, G. P.; Allbritton, N. Surface Modification of Poly(Dimethylsiloxane) Microfluidic Devices by Ultraviolet Polymer Grafting. Anal. Chem. 2002, 74 (16), 4117–4123.
8. Yu, Z.; Li, L.; Zhang, Q.; Hu, W.; Pei, Q. Silver Nanowire-Polymer Composite Electrodes for Efficient Polymer Solar Cells. Adv. Mater. 2011, 23 (38), 4453–4457.
9. Yu, X.; Prévot, M. S.; Sivula, K. Multiflake Thin Film Electronic Devices of Solution Processed 2D $MoS_2$ Enabled by Sonopolymer Assisted Exfoliation and

Surface Modification. Chem. Mater. 2014, 26 (20), 5892–5899.

10. Macchione, M. A.; Biglione, C.; Strumia, M. Design, Synthesis and Architectures of Hybrid Nanomaterials for Therapy and Diagnosis Applications. Polymers (Basel). 2018, 10 (5), 1–34.
11. Wu, L.; Glebe, U.; Böker, A. Surface-Initiated Controlled Radical Polymerizations from Silica Nanoparticles, Gold Nanocrystals, and Bionanoparticles. Polym. Chem. 2015, 6 (29), 5143–5184.
12. Ribeiro, J. P. M.; Mendonça, P. V.; Coelho, J. F. J.; Matyjaszewski, K.; Serra, A. C. Glycopolymer Brushes by Reversible Deactivation Radical Polymerization: Preparation, Applications, and Future Challenges. Polymers (Basel). 2020, 12 (6).
13. Morris, B. A. Commonly Used Resins and Substrates in Flexible Packaging. In The Science and Technology of Flexible Packaging; Morris, B. A., Ed.; William Andrew Publishing, 2017; pp 69–119.
14. Selimis, A.; Farsari, M. Laser-Based 3D Printing and Surface Texturing; Elsevier Ltd., 2017; Vol. 3–3.
15. Nesvadba, P. Radical Polymerization in Industry. In Encyclopedia of Radicals in Chemistry, Biology and Materials; 2012 John Wiley & Sons, Ltd., 2012.
16. Matyjaszewski, K.; Spanswick, J. Controlled/Living Radical Polymerization. Mater. Today 2005, 8 (3), 26–33.
17. Sciannamea, V.; Jérôme, R.; Detrembleur, C. In-Situ Nitroxide-Mediated Radical Polymerization (NMP) Processes: Their Understanding and Optimization. Chem. Rev. 2008, 108 (3), 1104–1126.
18. Grubbs, R. B. Nitroxide-Mediated Radical Polymerization: Limitations and Versatility. Polym. Rev. 2011, 51 (2), 104–137.
19. Fischer, A.; Brembilla, A.; Lochon, P. Nitroxide-Mediated Radical Polymerization of 4-Vinylpyridine: Study of the Pseudo-Living Character of the Reaction and Influence of Temperature and Nitroxide Concentration. Macromolecules 1999, 32, 6069–6072.
20. Wang, J.; Matyjaszewski, K. Controlled /“ Living ” Radical Polymerization . Atom Transfer Radical Polymerization in the Presence of Transition-Metal Complexes 1995 American Chemical Society Cl-CunLxj Pi-Cl. 1995, No. 6, 5614–5615.

21. Tian, X.; Ding, J.; Zhang, B.; Qiu, F.; Zhuang, X.; Chen, Y. Recent Advances in RAFT Polymerization: Novel Initiation Mechanisms and Optoelectronic Applications. Polymers (Basel). 2018, 10 (3).

22. Perrier, S. 50th Anniversary Perspective: RAFT Polymerization - A User Guide. Macromolecules 2017, 50 (19), 7433–7447.

23. Nothling, M. D.; Fu, Q.; Reyhani, A.; Allison-Logan, S.; Jung, K.; Zhu, J.; Kamigaito, M.; Boyer, C.; Qiao, G. G. Progress and Perspectives Beyond Traditional RAFT Polymerization. Adv. Sci. 2020, 7 (20), 1–12.

24. Fischer, H. The Persistent Radical Effect: A Principle for Selective Radical Reactions and Living Radical Polymerizations. Chem. Rev. 2001, 101 (12), 3581–3610.

25. Matyjaszewski, K. Atom Transfer Radical Polymerization (ATRP): Current Status and Future Perspectives. Macromolecules 2012, 45 (10), 4015–4039.

26. Matyjaszewski, K.; Xia, J. Atom Transfer Radical Polymerization. Chem. Rev. 2001, 101 (9), 2921–2990.

27. Faggion Albers, R.; Yan, W.; Romio, M.; Leite, E. R.; Spencer, N. D.; Matyjaszewski, K.; Benetti, E. M. Mechanism and Application of Surface-Initiated ATRP in the Presence of a $Zn^0$ plate. Polym. Chem. 2020, 11 (44), 7009–7014.

28. Layadi, A.; Kessel, B.; Yan, W.; Romio, M.; Spencer, N. D.; Zenobi-Wong, M.; Matyjaszewski, K.; Benetti, E. M. Oxygen Tolerant and Cytocompatible Iron(0)-Mediated ATRP Enables the Controlled Growth of Polymer Brushes from Mammalian Cell Cultures. J. Am. Chem. Soc. 2020, 142 (6), 3158–3164.

29. Yan, W.; Fantin, M.; Spencer, N. D.; Matyjaszewski, K.; Benetti, E. M. Translating Surface-Initiated Atom Transfer Radical Polymerization into Technology: The Mechanism of $Cu^0$-Mediated SI-ATRP under Environmental Conditions. ACS Macro Lett. 2019, 8 (7), 865–870.

30 Yan, W.; Fantin, M.; Ramakrishna, S.; Spencer, N. D.; Matyjaszewski, K.; Benetti, E. M. Growing Polymer Brushes from a Variety of Substrates under Ambient Conditions by $Cu^0$-Mediated Surface-Initiated ATRP. ACS Appl. Mater. Interfaces 2019, 11 (30), 27470–27477.

31. Zhang, T.; Benetti, E. M.; Jordan, R. Surface-Initiated Cu(0)-Mediated CRP for the Rapid and Controlled Synthesis of Quasi-3D Structured Polymer Brushes.

ACS Macro Lett. 2019, 8 (2), 145–153.

32. Albers, R. F.; Magrini, T.; Romio, M.; Leite, E. R.; Libanori, R.; Studart, A. R.; Benetti, E. M. Fabrication of Three-Dimensional Polymer Brush Gradients Within Elastomeric Supports by $Cu^0$-Mediated Surface-Initiated ATRP. ACS Macro Lett. 2021, No. 10, 1099–1106.

# Chapter 2

## MECHANISM AND APPLICATION OF SURFACE-INITIATED ATRP IN THE PRESENCE OF A $Zn^0$ PLATE

Rebecca Faggion Albers,[a,b,c,d] Wenqing Yan,[b] Matteo Romio,[b,c] Edson R. Leite,[d,e]

Nicholas D. Spencer,[b] Krzysztof Matyjaszewski,[f] Edmondo M. Benetti*[b,c]

[a]*Complex Materials, Department of Materials, ETH Zürich, Vladimir-Prelog-Weg 1-5/10, CH-8093 Zurich, Switzerland*

[b]*Laboratory for Surface Science and Technology, Department of Materials, ETH Zürich, Vladimir-Prelog-Weg 1-5/10, CH-8093 Zurich, Switzerland.*

[c]*Swiss Federal Laboratories for Materials Science and Technology (Empa), Lerchenfeldstrasse 5, CH-9014 St. Gallen, Switzerland*

[d]*Department of Chemistry, Federal University of São Carlos, 13565-905 São Carlos, SP, Brazil*

[e]*Brazilian Nanotechnology National Laboratory (LNNano), Brazilian Center for Research in Energy and Materials (CNPEM), 13083-970 Campinas, Brazil*

[f]*Department of Chemistry, Carnegie Mellon University, 4400 Fifth Avenue, Pittsburgh, USA*

This chapter was published in:

*Polymer Chemistry*, **2020**, *11* (44), 7009-7014

Supplementary Information is attached in Appendix A in Chapter 6.

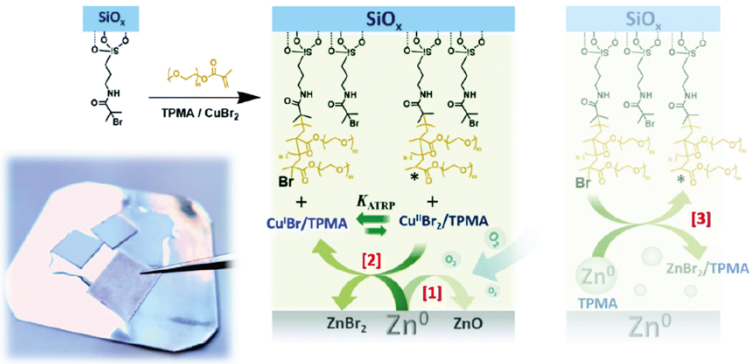

## ABSTRACT

Surface-initiated atom transfer radical polymerization in the presence of a $Zn^0$ plate (SI-$Zn^0$-ATRP) enables the rapid synthesis of chemically diverse polymer brushes from both planar inorganic supports, and fabrics made of natural fibers. This process enables the controlled formation of polymer-brush layers on a variety of substrates, without the need for either inert conditions or lengthy deoxygenation procedures of the reaction mixtures.

## 2.1 INTRODUCTION

The development of oxygen-tolerant, surface-initiated, controlled radical polymerization (SI-CRP) methods has paved the way for the accessible synthesis of polymer-brush coatings on large substrates, circumventing the need for lengthy deoxygenation of reaction mixtures. Following closely the recent advances in the development of oxygen-tolerant CRPs in solution,[1] the application of analogous processes to solid surfaces has offered the possibility to translate the synthesis of polymer brushes from fundamental studies into technologically relevant processes.

Similarly to solution-based approaches, the successful and controlled fabrication of polymer brushes under ambient conditions has been accomplished by employing oxygen scavengers. For instance, in the presence of appropriate reducing agents, Cu-based catalysts efficiently consume oxygen through complexation and can still trigger the growth of compositionally different brushes during surface-initiated activators regenerated by electron transfer atom transfer radical polymerization (SI-ARGET ATRP).[2–7] Alternatively, in the presence of visible or UV light, oxygen can be consumed by organic or organometallic photocatalysts that are typically employed during photoinduced SI-ATRP,[8,9] or photoinduced electron-transfer surface-initiated reversible addition fragmentation chain transfer polymerization (SI-PET RAFT),[10] enabling the rapid fabrication of polymer brushes without degassing the reaction mixtures, while keeping polymerization setups exposed to air.

Besides scavengers present in solution, oxygen can be alternatively consumed by applying zerovalent metal ($Mt^0$)-coated plates, which consume oxygen to form oxide layers, and simultaneously act as source of transition-metal catalyst for ATRP when placed on initiator-bearing surfaces previously covered by a thin layer of monomer/ligand mixtures.[11–18]

Following this strategy, Jordan and co-workers introduced $Cu^0$-mediated SI-ATRP, demonstrating how this process can be applied for the modification of extremely large substrates, by simply keeping them on a lab bench, and using just microliter volumes of polymerization mixtures.[11,19] This process enabled the extremely rapid synthesis of compositionally different polymer brushes[20] from a variety of inorganic and organic supports.[16,21]

Relevantly, when $Cu^0$-coated plates were replaced with $Fe^0$-coated surfaces thick brush films could be grown in a biocompatible process – even from supports pre-seeded with mammalian cells, without altering their viability.[18]

Motivated by the possibility to expand this method to alternative, readily accessible and inexpensive $Mt^0$ plates, in this work we explore the applicability of $Zn^0$ plates to favor the fast and oxygen–tolerant fabrication of thick brush films.

## 2.2 EXPERIMENTAL SECTION

### 2.2.1 MATERIALS

Silicon wafers (P/B⟨100⟩ were purchased from Si-Mat Silicon Wafers (Germany), Zn plates were purchased from Mayitr. 3-(Aminopropyl)triethoxysilane (APTES, ≥98%, Sigma-Aldrich), 2-bromoisobutyryl bromide (BiBB, 98%, Sigma-Aldrich), tri-ethylamine (TEA, ≥99.5%, Sigma-Aldrich), dichloromethane (DCM, dry, ≥99.8%, Acros), cotton fabrics (100%, Rhena® Ideal), tris(2-pyridylmethyl)amine (TPMA, 98%, Sigma Aldrich), 2,2′-bipyridyl (bipy, ≥, Sigma-Aldrich), tris(2-di-methylaminoethyl)amine ($Me_6$TREN, 99%, ABCR), $Cu^{II}Br_2$ (99%, Sigma Aldrich), 2-methacryloyloxyethyl phosphorylcholine (MPC, 97%, Sigma-Aldrich), [2-(methacryloyloxy)ethyl]trimethylammonium chloride solution (METAC, 80% in water, Sigma-Aldrich), and tetrahydrofuran (dry THF, 99.5%, Acros), were used as received. Water used in all experiments was from Millipore Milli-Q. Oligo(ethylene glycol)methacrylate (OEGMA, Mn ~ 500, Sigma-Aldrich), methyl methacrylate (MMA, 99%, Sigma-Aldrich), styrene (99.5%, Acros Organics) and butyl acrylate (BA, 99%, Acros Organics) were purified by passing them through a basic alumina column. N-Isopropylacrylamide (NIPAM, >98.0%, Tokyo Chemical Industry) was recrystallized from toluene to remove inhibitors.

### 2.2.2 METHODS

#### 2.2.2.1 FUNCTIONALIZATION OF SIOX SUBSTRATES

Silicon substrates (Si-Mat Silicon Wafers, Germany) were cleaned with piranha solution (3 : 1 $H_2SO_4$ : $H_2O_2$) for 30 min, and subsequently washed extensively with ultra-pure water. The substrates were first functionalized with APTES, through vapor deposition, and they were subsequently washed with dry toluene and ultra-pure water. Later on, $SiO_x$-APTES substrates were placed in a flask kept under $N_2$ atmosphere, in which dry DCM, BIBB (1 v%) and TEA (1 v%) were added. The reaction was carried out for one hour, and the substrates were finally washed with chloroform and ethanol, yielding ATRP initiator-functionalized $SiO_x$ surfaces.

#### 2.2.2.2 $Zn^0$ PLATE PREPARATION

$Zn^0$ plates were first grinded with Struers SiC foils, presenting grit sizes of 320, 500, 800, 1200, 2000 and 4000 (FEPA). Later on, they were polished with a cloth-coated disc (MD-Mol) using a diamond suspension with a grain size of 3 $\mu$m, and finally washed twice with 2-propanol in an ultrasonic bath for 15 min.

#### 2.2.2.3 SI-$Zn^0$-ATRP

A polymerization mixture was placed dropwise on a polished $Zn^0$ plate, and ATRP initiator-functionalized substrates were placed on top of that, with a dead weight producing a pressure of 6 $g.cm^{-2}$ to hold the substrate against the $Zn^0$ plate. After the polymerization, the substrates were washed with ethanol (POEGMA), water and methanol (PMPC and PMETAC), toluene and dichloromethane (PS and PBA), finally dried with a $N_2$ flux and analyzed by VASE.

#### 2.2.2.4 GRAFTING FROM COTTON

Cotton fabrics were dried under vacuum overnight in a two-neck round-bottom flask and later on functionalized with ATRP initiator. Namely, 2.0 g of cotton, 100 mL of dry THF, 5 mL of TEA and 0.6 g of DMAP were added to the flask, the system was cooled down to 0 °C and 2.2 mL of BIBB were added dropwise. The suspension was stirred at 0 °C for 2 h, and at room temperature for 24 h.[28] The cotton was washed extensively with THF, water and ethanol and dried under vacuum. The resulting ATRP initiator-functionalized cotton was soaked in the polymerization mixture and sandwiched between a $Zn^0$ plate and an inert glass slide.

Following polymerization, brush-modified cotton fabrics were subjected to Soxhlet extraction with ethanol as solvent to remove any unreacted monomer/unbound polymer.

#### 2.2.2.5 VARIABLE-ANGLE SPECTROSCOPIC ELLIPSOMETER (VASE)

The dry thickness of polymer brush films was determined using a M-2000F John Woollam variable angle spectroscopic ellipsometer (VASE, SENTECH Instruments GmbH), equipped with a He–Ne laser source ($\lambda$ = 633 nm, J.A. Woollam Co., Lincoln, NE). The values of amplitude ($\Psi$) and phase ($\Delta$) were acquired by focusing lenses at 70° from the surface normal as a function of wavelength (350–800 nm). Raw data were fitted with a three-layer model, using bulk dielectric functions for Si and $SiO_2$ (software WVASE32, LOT Oriel GmbH, Darmstadt, Germany). The polymer-brush layers were

analyzed based on a Cauchy model: $n = A + B\lambda^{-2}$, where n is the refractive index, $\lambda$ is the wavelength, and A and B are assumed to be 1.45 and 0.01, respectively, as values for transparent organic films. The values of dry thickness of polymer brushes were obtained from 4 different substrates analyzed after SI-$Zn^0$-ATRP. At least 3 different points on each substrate were measured by VASE.

#### 2.2.2.6 ATTENUATED TOTAL REFECTION FOURIER-TRANSFORM INFRARED SPECTROSCOPY (ATR-FTIR).

The ATR-FTIR spectra were recorded using an Alpha, Bruker spectrometer, equipped with a diamond crystal. The material was pressed onto the crystal and 64 scans were acquired with a resolution 4 $cm^{-1}$.

#### 2.2.2.7 SCANNING ELECTRON MICROSCOPY (SEM)

Cotton fabrics were sputter-coated with 5 nm of Pt to avoid charging effects during analysis (CCU-010, Safematic). The micrographs were acquired using a scanning electron microscope (SEM, LEO 1530, Zeiss GmbH, Germany).

## 2.3 RESULTS AND DISCUSSION

As previously demonstrated in the case of polymerizations performed in solution, $Zn^0$ powder efficiently acts as reducing agent for $Cu^{II}$ during supplemental activator and reducing agent (SARA) ATRP,[22–24] showing a very high reducing activity when compared to $Fe^0$ or $Mg^0$.[25]

In the case of the synthesis of polymer brushes from planar substrates, polymerization mixtures including monomer, ligand, $Cu^{II}Br_2$ and solvent are sandwiched between an ATRP initiator-modified $SiO_x$ substrate, and a $Zn^0$ plate.

The metallic plate was polished just before the experiment (Scheme 1) in order to remove the native oxide layer, and to generate a homogeneous metal surface (Appendix A). After this process, a reaction volume of ~1 $\mu L.cm^{-2}$ is generated between the two opposing surfaces, and the vertical spacing between the initiator-bearing substrate and the $Zn^0$ plate (d) corresponds to ~10 μm.[17]

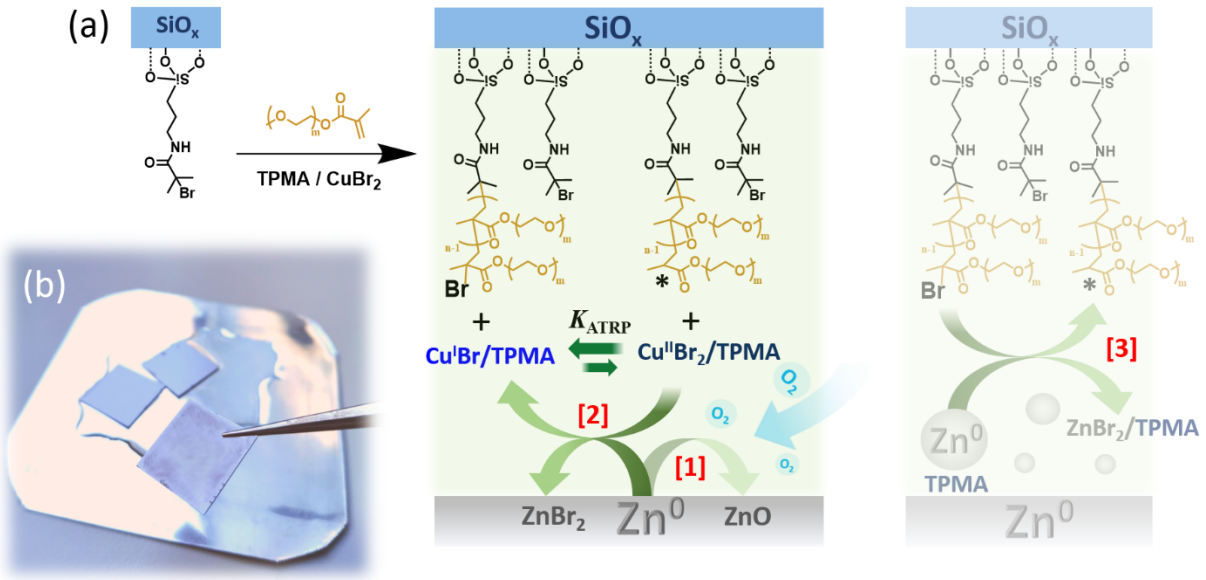


**Scheme 2.1.** (a) Mechanism of SI-$Zn^0$-ATRP. A polymerization mixture comprising monomer, solvent, ligand, and $Cu^{II}Br_2$ is placed in between an ATRP-initiator-functionalized $SiO_x$ substrate and a $Zn^0$ plate. The metallic surface consumes oxygen through the formation of $Zn^{II}O$ [1]. Simultaneously, it acts as reducing agent for $Cu^{II}Br_2$/L, generating $Cu^{I}Br$/L activators which diffuse through the reaction mixture and trigger the controlled growth of polymer grafts [2]. $Zn^0$ particles leaching from the metal plate can act as supplemental activators in the presence of ligand [3], initiating polymerization from the surface and simultaneously providing $Zn^{II}Br_2$/L species. (b) Polymer brush films can be grafted from $SiO_x$ substrates previously functionalized with ATRP initiator.

Under these conditions, oxygen dissolved in the polymerization solution is rapidly consumed through oxidation of $Zn^0$ to $Zn^{II}O$ (Scheme 2.1a [1]),[26,27] while $Cu^{II}Br_2$/L species are simultaneously reduced to $Cu^{I}Br$/L adducts. These can diffuse in the medium and reach the initiator-functionalized surface, triggering the controlled growth of polymer chains according to the ATRP equilibrium (Scheme 2.1a [2]).

Surface-initiated $Zn^0$-mediated ATRP (SI-$Zn^0$-ATRP) of (oligoethylene glycol)methacrylate (OEGMA) was exemplarily investigated. A 50% (v/v) solution of OEGMA in dimethyl-formamide (DMF) containing 10 mM $Cu^{II}Br_2$ and 10 mM tris(2-pyridylmethyl)amine (TPMA) was poured on a freshly polished $Zn^0$ plate, and subsequently covered by a $SiO_x$ substrate, which had previously been functionalized with a silane-based ATRP initiator. Variable-angle spectroscopic ellipsometry (VASE) was employed to monitor the increment in POEGMA-brush dry thickness (Tdry) *ex situ*, providing an insight into brush-growth kinetics. As reported in Figure 2.1a, SI-$Zn^0$-ATRP enabled the rapid and progressive growth of POEGMA brushes, which reached more than 270 nm of dry thickness after 90 min of reaction. No induction time was recorded, suggesting a very fast reduction of $Cu^{II}Br_2$/L species by $Zn^0$,[26] and a rapid diffusion of activators to the initiator sites at the substrate.

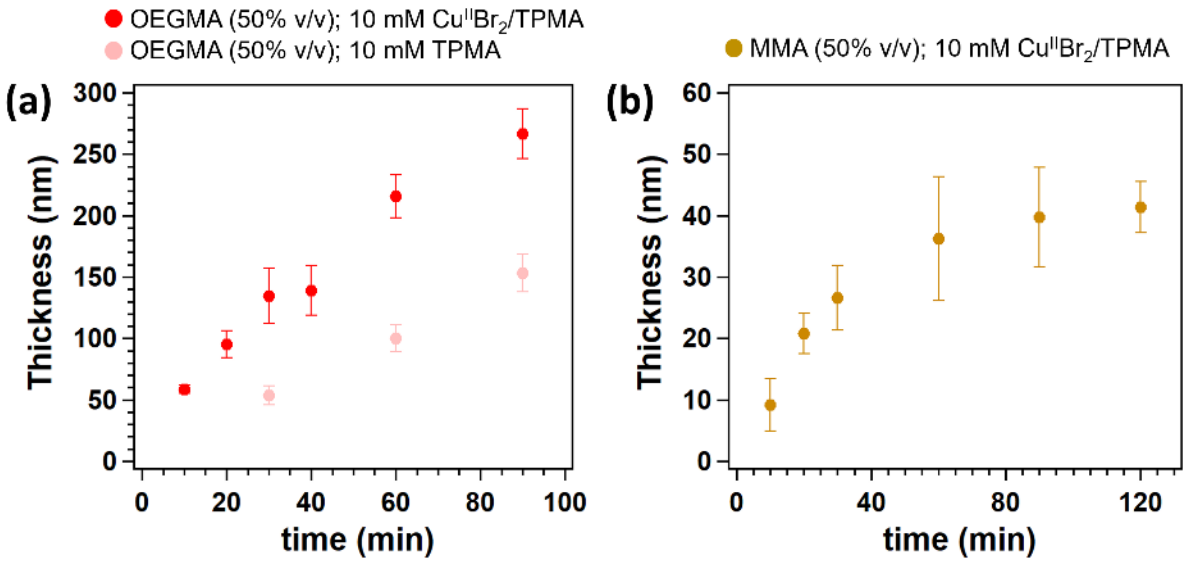


**Figure 2.1.** Dry thickness of polymer brushes synthesized by SI-Zn$^0$-ATRP and measured by VASE. (a) Dry thickness of POEGMA brushes after different polymerization times, using a 50% OEGMA (v/v) solution in DMF, 10 mM TPMA, with and without 10 mM Cu$^{II}$Br$_2$. (b) Dry thickness of PMMA brushes synthesized by using a mixture of 50% MMA (v/v) in DMF, and 10 mM Cu$^{II}$Br$_2$/TPMA.

It is important to emphasize that the preparation of Zn$^0$ plates by polishing is a standard procedure for treating metal surfaces and requires just 15–20 minutes, and (rather cheap) sandpaper. After this process, 20 × 20 cm$^2$ activated Zn$^0$ plates (typical cost ~2 €) are obtained. These can be used multiple times and for grafting brushes on a relatively large number of substrates. Similarly to POEGMA analogues, the growth of poly(methylmethacrylate) (PMMA) brushes by SI-Zn$^0$-ATRP (50% v/v in DMF, with 10 mM Cu$^{II}$Br$_2$/TPMA) followed an initially fast kinetics, without an induction period (Figure 2.1b). However, the rate of PMMA-brush thickening significantly slowed down after ~60 min, and PMMA films reached a dry thickness of ~40 nm after two hours of reaction.

Interestingly, when SI-Zn$^0$-ATRP was performed in the absence of Cu$^{II}$Br$_2$ but in the presence of ligand, significant brush growth could still be recorded. As shown in Figure 2.1a, POEGMA brushes reached nearly 150 nm of dry thickness when a mixture including 50% OEGMA and 10 mM TPMA was sandwiched between a Zn$^0$ plate and an ATRP initiator-bearing substrate for 90 min.

This result suggests that Zn$^0$ can act as supplemental activator during the growth of polymer brushes by SI-Zn$^0$-ATRP, in agreement with the mechanism of SARA ATRP studied in solution in the presence of Zn$^0$ particles.[25]

Considered the physical distance between the Zn$^0$ plate and the ATRP initiator-functionalized substrate within an ideal polymerization setup, we hypothesize that

$Zn^0$ micro/nano-particles produced during the polishing process (Figure A.1, Appendix A) might diffuse within the polymerization medium and in the presence of ligand can activate surface-bound initiators, triggering brush growth (Scheme 2.1a [3]). In particular, $Zn^0$/L adducts can act as supplemental activators reacting with alkyl halides and generating radicals that can initiate polymerization from the surface. However, this process simultaneously produces $Zn^{II}Br_2$/L species, which are very poor deactivators, presumably leading to a redox-initiated free radical surface-initiated polymerization process.[25]

Hence, $Cu^{II}$-based species added in solution are fundamental to guarantee a controlled and steady growth of polymer brushes. The role of $Cu^{II}Br_2$/L during SI-$Zn^0$-ATRP can be elucidated by measuring the dry thickness of POEGMA and PMMA brushes obtained after a fixed polymerization time of 30 min, while varying [$Cu^{II}Br_2$/L] initially added in the mixture. As reported in Figure 2.2a, both POEGMA- and PMMA-brush thicknesses significantly increase with [$Cu^{II}Br_2$/L] until a maximum in $T_{dry}$ is reached, in correspondence to a value of [$Cu^{II}Br_2$/L] ~ 10 mM. When [$Cu^{II}Br_2$/L] is further increased, the values of $T_{dry}$ progressively decrease, indicating that an "optimum" concentration of $Cu^{II}$-based species enables the fastest growth of polymer brushes through SI-$Zn^0$-ATRP.

On the one hand, an initial increment in [$Cu^{II}Br_2$/L] results in a concomitant increase in [$Cu^{I}Br$/L] through the rapid reduction by $Zn^0$, determining a faster polymerization and thus the formation of thicker brushes. On the other hand, a further increase in [$Cu^{II}Br_2$/L] beyond 10 mM presumably causes accumulation of deactivators, which necessarily slows down the grafting process and lead to the formation of thinner films.

Hence, the balance between generation of activator species by $Zn^0$-mediated reduction and accumulation of $Cu^{II}$-based deactivators, determines the brush-growth kinetics during SI-$Zn^0$-ATRP.

Under optimized conditions, SI-$Zn^0$-ATRP enabled the synthesis of chemically different polymer brushes by simply performing the grafting process on a Petri dish exposed to air and placed on a lab bench, using just few microliter volumes of reaction solutions, and without the need for their deoxygenation. In this way, poly(methacrylate), poly(acrylate), poly(acrylamide) and poly(styrene) brushes could be fabricated and under full ambient conditions (Figure 2.2b). In particular poly(N-isopropylacrylamide) (PNIPAM), poly(2-methacrylolyloxyethyl-trimethylammonium chloride) (PMETAC) and poly(2-methacryloyloxyethyl

phosphorylcholine) (PMPC) brushes with thicknesses ≥ 30 nm were synthesized following relatively short reaction times. In contrast, poly(styrene) (PS) and poly(butyl acrylate) (PBA) brushes showed just ~10 nm of dry thickness, presumably due to the relatively low temperature applied during the grafting process.

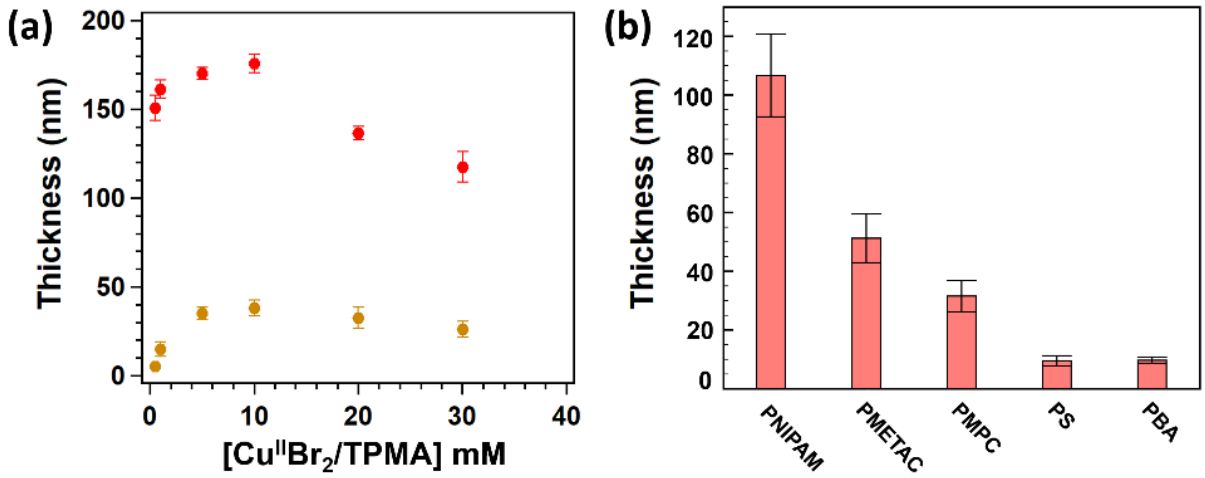


**Figure 2.2:** (a) Dry thickness of POEGMA and PMMA brushes synthesized by SI-Zn$^0$-ATRP keeping a constant polymerization time of 30 min, and by varying [Cu$^{II}$Br$_2$/TPMA]. (b) Dry thickness of chemically different polymer brushes synthesized by SI-Zn$^0$-ATRP. Poly(N-isopropylacrylamide) (PNIPAM) (conditions: 3 M NIPAM, 10 mM TPMA, 10 mM Cu$^{II}$Br$_2$ in DMSO for 30 min); poly(2-methacrylolyloxyethyltrimethylammonium chloride) (PMETAC) (1.5 M METAC, 10 mM TPMA, 10 mM Cu$^{II}$Br$_2$, 10 mM NaBr in H$_2$O for 120 min); poly(2-methacryloyloxyethyl phosphorylcholine) (PMPC) (1.5 M MPC, 20 mM 2-2'-bipyridyl, 10 mM Cu$^{II}$Br$_2$ in methanol, for 180 min); poly(styrene) (PS) (20% v/v styrene, 10 mM TPMA, 10 mM Cu$^{II}$Br$_2$, in DMF, for 180 min); poly(butyl acrylate) (PBA) (20% v/v BA, 10 mM tris[2-(dimethylamino)ethyl]amine, 10 mM Cu$^{II}$Br$_2$ in DMF, for 180 min).

It is also important to emphasize that with respect to the corresponding grafting process employing Cu$^0$ plates, SI-Zn$^0$-ATRP enables the controlled grafting of polymer brushes while applying reaction environments that could virtually display relatively low toxicity. In order to confirm this hypothesis, besides Cu$^{II}$/Cu$^{I}$ species, the rapid growth of POEGMA brushes could be accomplished by applying a Fe-based catalyst. In particular, Fe$^{III}$Br$_3$/tetrabutylammonium bromide (TBABr) is readily reduced to Fe$^{II}$Br$_2$/TBABr activators by the Zn$^0$ surface, triggering the growth of more than 30 nm-thick POEGMA brushes in just 60 min of reaction (Figure A.2, Appendix A). Relevantly, a similar result was previously accomplished by using Fe$^0$ plates as reducing agent for Fe$^0$-mediated SI-ATRP (SI-Fe$^0$-ATRP).[19] However, in contrast to SI-Fe$^0$-ATRP, in SI-Zn$^0$-ATRP the grafting process is mediated by metallic plates based on Zn$^0$, which are much cheaper (2 vs. 60 € for a 20 × 20 cm$^2$ plate) and more readily available with respect to Fe$^0$ or Fe$^0$-coated analogues.

In order to demonstrate the applicability of SI-$Zn^0$-ATRP for the modification of a variety of supports, we subsequently investigated the growth of polymer brushes from cotton-based wound dressings, which had previously been modified with ATRP initiator moieties. 100%-cotton fabrics functionalized with $\alpha$-bromoisobutyrate functions were initially soaked in a polymerization mixture comprising 50% (v/v) OEGMA in DMF and 10 mM $Cu^{II}Br_2$/TPMA, and subsequently sandwiched between a $Zn^0$ plate and an inert glass slide. Attenuated total reflection Fourier-transform infrared spectroscopy (ATR-FTIR) confirmed the successful grafting of POEGMA brushes from the cotton fibers after 2 and 8 hours of reaction (Figure 2.3a), through the appearance of the C=O stretching band at 1717 $cm^{-1}$, the C–H band at 2869 $cm^{-1}$ and the C–O signals at 1248 and 1102 $cm^{-1}$. In addition, the decrease in the values of transmittance of the C=O band with polymerization time suggested the progressive growth of POEGMA grafts (Figure 2.3b). The formation of brush layers on the cotton fibers was additionally confirmed by scanning electron microscopy (SEM). As reported in Figure 2.3c–f, the surface morphology of cotton fibers did not show a significant variation after functionalization with ATRP initiator. However, following SI-$Zn^0$-ATRP, a uniform brush film became visible on the cotton structures, and grew thicker after relatively long polymerization times (Figure 2.3g-j).

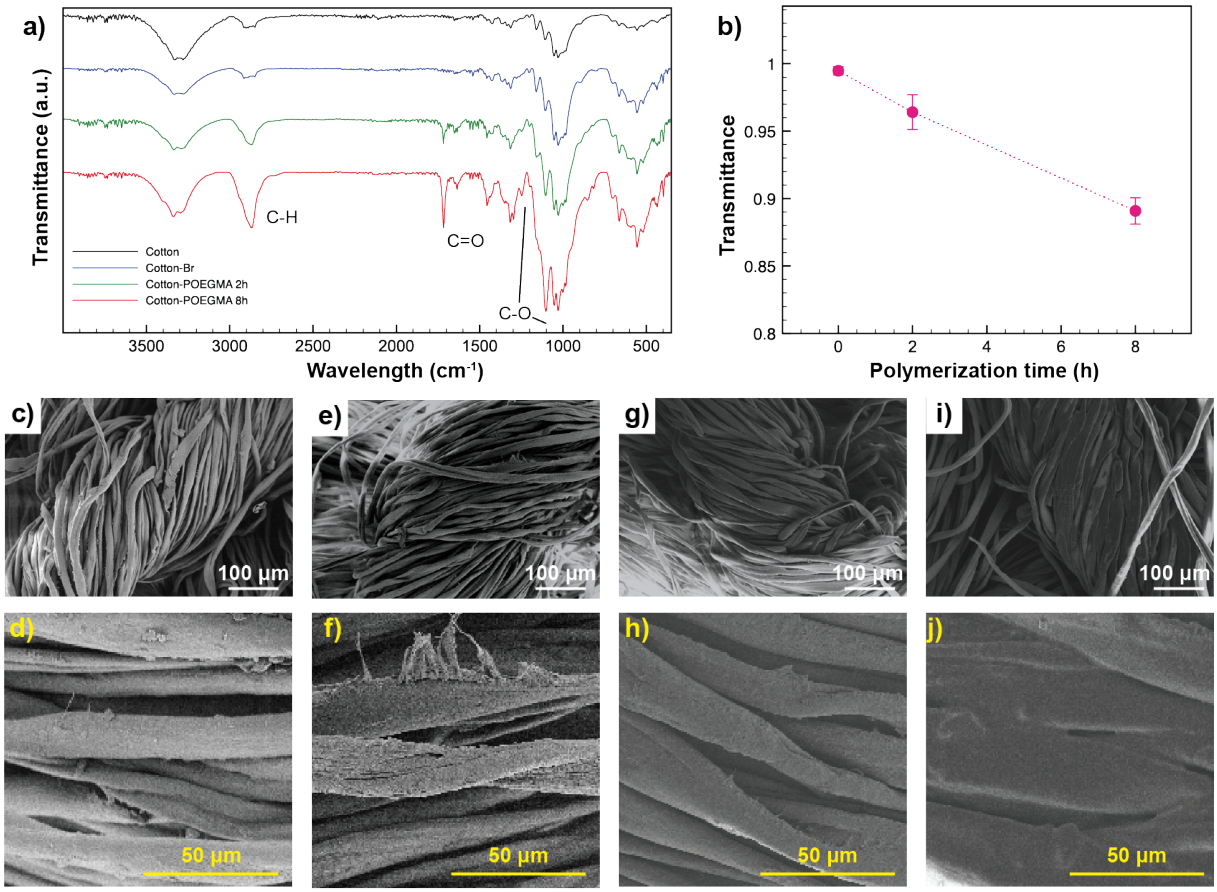


**Figure 2.3.** (a) ATR-IR spectra from unmodified cotton fabrics (Cotton), ATRP-initiator-functionalized cotton (Cotton-Br), POEGMA brush-functionalized cotton after 2 h (Cotton-POEGMA 2h) and 8 h (cotton-POEGMA 8h) of SI-$Zn^0$-ATRP. (b) Values of transmittance of C=O band as a function of polymerization time. Scanning electron micrographs recorded on unmodified Cotton (c, d), Cotton-Br (e, f), Cotton-POEGMA 2h (g, h), and Cotton-POEGMA 8h (i, j).

## 2.4 CONCLUSIONS

SI-$Zn^0$-ATRP represents an extremely versatile method to synthesize chemically different polymer brushes under full ambient conditions, using just microliter volumes of reaction solutions, and without the need for their previous deoxygenation. When a polymerization mixture including $Cu^{II}$ salts, ligand and monomer is sandwiched between a $Zn^0$ plate and a $SiO_x$ substrate functionalized with ATRP initiators oxygen is rapidly consumed via the formation of $Zn^{II}O$. Simultaneously, $Cu^{II}$-based species are reduced by the $Zn^0$ plate, yielding $Cu^I$ activators that in the presence of ligand diffuse to the initiator-bearing substrate, and lead to the rapid growth of polymer grafts, which proceeds according to the ATRP equilibrium. $Zn^0$ micro/nanoparticles leaching from the metallic surface can additionally act as supplemental activators while diffusing through the polymerization mixture. In the absence of $Cu^{II}$ species, $Zn^0$/L centers trigger a redox-initiated, free-radical

polymerization process, through the simultaneous generation of poor deactivators based on $ZnBr_2$/L adducts.

Under optimized experimental conditions, SI-$Zn^0$-ATRP enables the rapid polymerization of different monomer species (acrylates, methacrylates, acrylamides and styrene), it is compatible with both Cu- and Fe-based catalysts, and it could be applied from model inorganic substrates as well as for the modification of three-dimensional fabrics, such as in the case of cotton-based wound dressings.

## 2.5 ACKNOWLEDGMENTS

We thank Prof André R. Studart, Dr Rafael Libanori (ETH Zürich) and Prof. Katharina Maniura (EMPA) for the fruitful scientific discussions. We acknowledge the funding Brazilian agency Fundação de Amparo à Pesquisa do Estado de São Paulo – FAPESP (2016/14493-7 and 2017/22304-2) and EMPA for the financial support.

## 2.6 REFERENCES

1. J. Yeow, R. Chapman, A. J. Gormley and C. Boyer, Chem. Soc. Rev., 2018, 47, 4357–4387.
2. K. Matyjaszewski, H. C. Dong, W. Jakubowski, J. Pietrasik and A. Kusumo, Langmuir, 2007, 23, 4528–4531.
3. G. J. Dunderdale, C. Urata, D. F. Miranda and A. Hozumi, ACS Appl. Mater. Interfaces, 2014, 6, 11864–11868.
4. T. Sato, G. J. Dunderdale, C. Urata and A. Hozumi, Macromolecules, 2018, 51, 10065–10073.
5. N. Li, T. Li, X. Y. Qiao, R. Li, Y. Yao and Y. K. Gong, ACS Appl. Mater. Interfaces, 2020, 12, 12337–12344.
6. D. Hong, H. C. Hung, K. Wu, X. J. Lin, F. Sun, P. Zhang, S. J. Liu, K. E. Cook and S. Y. Jiang, ACS Appl. Mater. Interfaces, 2017, 9, 9255–9259.
7. H. Kang, W. Jeong and D. Hong, Langmuir, 2019, 35, 7744– 7750.
8. B. Narupai, Z. A. Page, N. J. Treat, A. J. McGrath, C. W. Pester, E. H. Discekici, N. D. Dolinski, G. F. Meyers, J. R. de Alaniz and C. J. Hawker, Angew. Chem., Int. Ed., 2018, 57, 13433–13438.
9. W. Q. Yan, S. Dadashi-Silab, K. Matyjaszewski, N. D. Spencer and E. M. Benetti, Macromolecules, 2020, 53, 2801–2810.

10. M. Li, M. Fromel, D. Ranaweera, S. Rocha, C. Boyer and C. W. Pester, ACS Macro Lett., 2019, 8, 374–380.

11. T. Zhang, Y. Du, F. Muller, I. Amin and R. Jordan, Polym. Chem., 2015, 6, 2726–2733.

12. E. S. Dehghani, Y. H. Du, T. Zhang, S. N. Ramakrishna, N. D. Spencer, R. Jordan and E. M. Benetti, Macromolecules, 2017, 50, 2436–2446.

13. Y. J. Che, T. Zhang, Y. H. Du, I. Amin, C. Marschelke and R. Jordan, Angew. Chem., Int. Ed., 2018, 57, 16380–16384.

14. T. Zhang, E. M. Benetti and R. Jordan, ACS Macro Lett., 2019, 8, 145–153.

15. M. Fantin, S. N. Ramakrishna, J. J. Yan, W. Q. Yan, M. Divandari, N. D. Spencer, K. Matyjaszewski and E. M. Benetti, Macromolecules, 2018, 51, 6825–6835.

16. W. Q. Yan, M. Fantin, S. Ramakrishna, N. D. Spencer, K. Matyjaszewski and E. M. Benetti, ACS Appl. Mater. Interfaces, 2019, 11, 27470–27477.

17. W. Q. Yan, M. Fantin, N. D. Spencer, K. Matyjaszewski and E. M. Benetti, ACS Macro Lett., 2019, 8, 865–870.

18. A. Layadi, B. Kessel, W. Yan, M. Romio, N. D. Spencer, M. Zenobi-Wong, K. Matyjaszewski and E. M. Benetti, J. Am. Chem. Soc., 2020, 142, 3158–3164.

19. T. Zhang, Y. H. Du, J. Kalbacova, R. Schubel, R. D. Rodriguez, T. Chen, D. R. T. Zahn and R. Jordan, Polym. Chem., 2015, 6, 8176–8183.

20. W. Q. Yan, M. Fantin, N. D. Spencer, K. Matyjaszewski and E. M. Benetti, ACS Macro Lett., 2019, 8, 865–870.

21. K. H. Zhang, W. Q. Yan, R. Simic, E. M. Benetti and N. D. Spencer, ACS Appl. Mater. Interfaces, 2020, 12, 6761– 6767.

22. K. F. Augustine, T. G. Ribelli, M. Fantin, P. Krys, Y. Cong and K. Matyjaszewski, J. Polym. Sci., Part A: Polym. Chem., 2017, 55, 3048–3057.

23. D. Konkolewicz, Y. Wang, M. Zhong, P. Krys, A. A. Isse, A. Gennaro and K. Matyjaszewski, Macromolecules, 2013, 46, 8749–8772.

24. D. Konkolewicz, Y. Wang, P. Krys, M. J. Zhong, A. A. Isse, A. Gennaro and K. Matyjaszewski, Polym. Chem., 2014, 5, 4396–4417.

25. Y. Zhang, Y. Wang and K. Matyjaszewski, Macromolecules, 2011, 44, 683–685.

26. A. Anastasaki, V. Nikolaou, G. Nurumbetov, P. Wilson, K. Kempe, J. F. Quinn, T. P. Davis, M. R. Whittaker and D. M. Haddleton, Chem. Rev., 2016, 116, 835–877.

27. E. Liarou, R. Whitfield, A. Anastasaki, N. G. Engelis, G. R. Jones, K. Velonia and D. M. Haddleton, Angew. Chem., Int. Ed., 2018, 57, 8998–9002.

28. X. Dong, H. Bao, K. Ou, J. Yao, W. Zhang and J. He, Fibers Polym., 2015, 16, 1478–1486.

# Chapter 3

## Fabrication of Three-Dimensional Polymer Brush Gradients Within Elastomeric Supports by $Cu^0$-Mediated Surface-Initiated ATRP

Rebecca F. Albers,[a,b,c,d,e] Tommaso Magrini,[a] Matteo Romio,[b,c] Edson R. Leite,[d,e] Rafael Libanori,[a] André R. Studart,[a] Edmondo M. Benetti*[b,c,f]

[a]*Complex Materials, Department of Materials, ETH Zürich, Vladimir-Prelog-Weg 1-5/10, CH-8093 Zurich, Switzerland*

[b]*Laboratory for Surface Science and Technology, Department of Materials, ETH Zürich, Vladimir-Prelog-Weg 1-5/10, CH-8093 Zurich, Switzerland.*

[c]*Swiss Federal Laboratories for Materials Science and Technology (Empa), Lerchenfeldstrasse 5, CH-9014 St. Gallen, Switzerland*

[d]*Department of Chemistry, Federal University of São Carlos, 13565-905 São Carlos, SP, Brazil*

[e]*Brazilian Nanotechnology National Laboratory (LNNano), Brazilian Center for Research in Energy and Materials (CNPEM), 13083-970 Campinas, Brazil*

[f]*Department of Chemical Sciences, University of Padova, 35131 Padova, Italy*

This chapter was published in:

*ACS Macro Letters*, **2021**, *XXX* (10), 1099-1106

Supplementary Information is attached in Appendix B in Chapter 7.

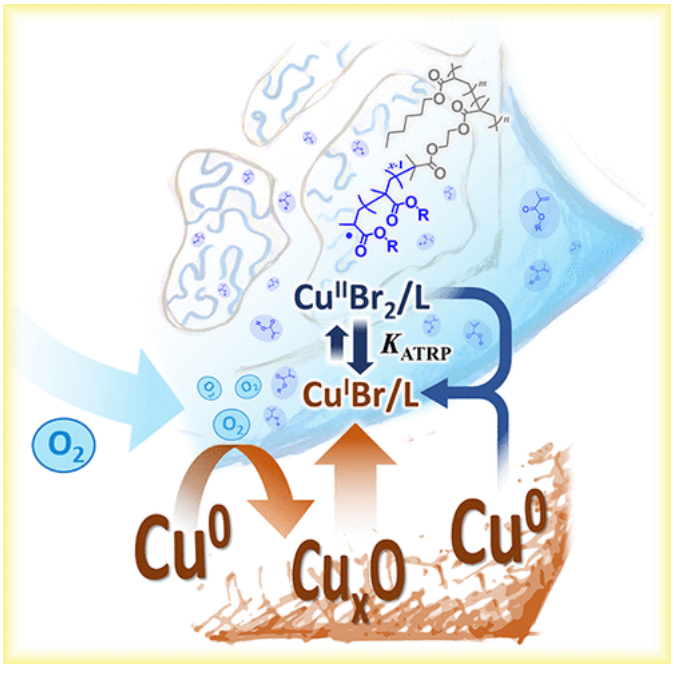

## ABSTRACT

$Cu^0$-mediated surface-initiated ATRP ($Cu^0$ SI-ATRP) emerges as a versatile, oxygen-tolerant process to functionalize three-dimensional (3D), microporous supports forming single and multiple polymer-brush gradients with a fully tunable composition. When polymerization mixtures are dispensed on a $Cu^0$-coated plate, this acts as oxygen scavenger and source of active catalyst. In the presence of an ATRP initiator-bearing microporous elastomer placed in contact with the metallic plate, the reaction solution infiltrates by capillarity through the support, simultaneously triggering the controlled growth of polymer brushes. The polymer grafting process proceeds with kinetics that are determined by the progressive infiltration of the reaction solution within the microporous support and by the continuous diffusion of catalyst regenerated at the $Cu^0$ surface. The combination of these effects enables the accessible generation of 3D polymer-brush gradients extending across the microporous scaffolds used as supports, finally providing materials with a continuous variation of interfacial composition and properties.

## 3.1 INTRODUCTION

The development of surface-initiated reversible deactivation radical polymerization (SI-RDRP) techniques that are tolerant to oxygen has enabled the translation of the synthesis of polymer brushes into fabrication processes that could potentially lead to industrial applications.[1]

SI-RDRP methods that are compatible with ambient conditions typically encompass the application of oxygen scavengers. These prevent the need for performing long and tedious deoxygenation processes prior to the application of polymerization mixtures on initiator-bearing supports, and thus permit the syntheses of polymer brushes from extremely large substrates.[2–4] Recently applied oxygen scavengers include transition metal complexes coupled to visible/UV light[5] or appropriate reducing agents,[6] enzymes,[7,8] photosensitizers,[9,10] or zerovalent-metal surfaces.[11–14]

The application of zerovalent-metal ($Mt^0$) plates for surface-initiated atom transfer radical polymerization ($Mt^0$ SI-ATRP) has been recently demonstrated to enable the rapid fabrication of polymer-brush coatings, on both inorganic and organic surfaces under ambient conditions, and to employ just microliter volumes of reaction mixtures.[15–17]

During $Cu^0$-mediated SI-ATRP ($Cu^0$ SI-ATRP), the most widely applied $Mt^0$ SI-ATRP, a polymerization mixture, including monomer (M), solvent, and transition metal complex-based catalyst in its highest oxidation state ($Cu^{II}$/L, where L is a generic ligand), is sandwiched between an initiator-bearing substrate and a $Cu^0$-coated plate. The $Cu^0$- coated surface consumes oxygen dissolved in the polymerization medium, generating a $Cu_xO$ layer that acts as the source of $Cu^{II}$/L and $Cu^{I}$/L species. Simultaneously, $Cu^{II}$/L species diffusing from the $Cu_xO$ layer and those that were externally added constantly (re)generate $Cu^{I}$-based activators through comproportionation with $Cu^0$. When the catalyst diffusing from the metallic plate reaches the ATRP initiator-functionalized substrate, the growth of polymer brushes according to the ATRP equilibrium is eventually triggered.[18]

Following this general mechanism, SI-ATRPs mediated by $Cu^0$ and, recently, $Zn^0$ plates were used to fabricate compositionally diverse brushes from model, flat substrates, and different organic supports, including microporous cellulose, elastomers, and hydrogels.[16,17,19] In addition, the growth of polymer brushes under cytocompatible conditions was demonstrated in the case of $Fe^0$-mediated SI-ATRP.[20]

Through a comprehensive understanding of its mechanism, the groups of Jordan and Benetti demonstrated that $Mt^0$ SI-ATRP can be additionally applied to fabricate structured coatings across large substrates. For instance, by continuously varying the vertical distance between an ATRP initiator-bearing surface and a $Mt^0$-coated plate (i.e., by tilting the $Mt^0$- coated plate), coatings featuring multiple gradients in brush composition and properties could be obtained.[13,14,18] Moreover, micropatterned brush films presenting different polymer compositions could be synthesized with the aid of microfluidics.[21]

Motivated by the versatility and the widespread applicability of $Mt^0$ SI-ATRP for the chemical and morphological structuring of polymer brush coatings on two-dimensional (2D) substrates, in this work, we concentrated on applying this technique for functionalizing three-dimensional (3D) supports in a spatially controlled fashion.

## 3.2 EXPERIMENTAL SECTION

### 3.2.1 MATERIALS

Silicon wafers were purchased from SiMat (Landsberg, Germany) and coated with $Cu^0$ through reactive magnetron sputtering (Paul Scherrer Institute, Villigen, Switzerland), yielding 200 nm-thick layer of $Cu^0$. 2-bromoisobutyryl bromide (BIBB, 98%, Sigma-Aldrich), triethylamine (TEA, ≥99.5%, Sigma-Aldrich), dichloromethane (DCM, dry, ≥99.8%, Acros Organics), polyethylene glycol sorbitan monooleate (TWEEN® 80, Sigma Aldrich), potassium persulfate (KPS, ≥99%, Sigma-Aldrich), calcium chloride anhydrous ($CaCl_2$, ≥93%, Sigma-Aldrich), methanol (MeOH, ≥99.8%, AnalaR NORMAPUR), hydrochloric acid (HCl, 37%, VWR Chemicals), acetone (>99.8%, AnalaR NORMAPUR), N,N-dimethylformamide (DMF, >99%, Sigma-Aldrich), tris(2- pyridylmethyl)amine (TPMA, 98%, Sigma-Aldrich), Copper(II) bromide ($Cu^{II}Br_2$, 99%, Sigma Aldrich), 2,2'-Azobis(2-methylpropionitrile) (AIBN, 98%, Sigma Aldrich) were all used as received. 2-Hydroxyethyl methacrylate (HEMA, ≥99%, Sigma-Aldrich), hexyl methacrylate (HMA, 98%, Sigma Aldrich), ethylene glycol dimethacrylate (EGDMA, ≥ 97%, Fluka-Chemie AG), and oligo(ethylene glycol) methacrylate (OEGMA, Mn ~ 500, Sigma-Aldrich) were purified by passing them through a column with basic alumina. N-isopropylacrylamide (NIPAM, >98.0%, Tokyo Chemical Industry) was recrystallized from n-hexane prior to use.

## 3.2.2 METHODS

### 3.2.2.1 SYNTHESIS OF ATRP INIMER 2-(2-BROMOISOBUTYRYLOXY)ETHYL METHACRYLATE (BIEM)

BIEM was synthesized by a coupling reaction between BIBB and HEMA. BIBB (0.024 mol, 0.096 M) was added dropwise to a solution of HEMA (0.023 mol, 0.092 M) and TEA (0.115 mol, 0.46 M) in dry DCM at 0 °C. The mixture was subsequently left stirring at room temperature overnight. Subsequently, solvent and excess of TEA were removed under reduced pressure, ethyl acetate was added, and the mixture was filtrated to remove triethylammonium bromide. The filtrate was washed with brine, and ultrapure water, dried over $MgSO_4$, and the solvent was finally removed under reduced pressure.

### 3.2.2.2 PREPARATION OF ATRP INITIATOR-BEARING POLYHIPE

A high internal phase emulsion was prepared by adding an apolar phase (10 vol%) in an aqueous mixture (90 vol%). The apolar (or oil) phase contained HMA (63 mol%), BIEM (17 mol%), EGDMA (4 mol%) and poly(ethylene glycol) sorbitan monooleate (16 mol%). The aqueous phase included KPS (7.4 mM) and $CaCl_2$ (90 mM). $N_2$ was bubbled separately in both the aqueous and oil phases by $N_2$ bubbling for 20 min, after which the system was emulsified using a vortex (~10 min). The emulsion was polymerized at 80 °C in an oven overnight. The nonreacted chemicals were eliminated through Soxhlet extraction with acetone overnight. Thereafter, the polyHIPE was swollen in ultra-pure water and finally freeze-dried, yielding microporous with cylindrical shape.

### 3.2.2.3 $Cu^0$ SI-ATRP

POEGMA brushes were grown from ATRP initiator-bearing polyHIPEs using a polymerization mixture containing 25 % v/v OEGMA in DMF, 10 mM TPMA and 10 mM $Cu^{II}Br_2$. PNIPAM brushes were grown using a polymerization mixture containing 3 M NIPAM in DMF, 10 mM TPMA and 10 mM $Cu^{II}Br_2$. PHEMA brushes were fabricated using a mixture of 25 % v/v HEMA in DMF, 10 mM TPMA and 10 mM $Cu^{II}Br_2$. Each polymerization mixture was dispensed on a freshly activated $Cu^0$ plate and a polyHIPE was placed on the surface. The solution infiltrated the polyHIPE by capillary forces, and the system was incubated inside a desiccator coupled to an Ar-filled balloon. After brush growth, unreacted chemicals were eliminated through

Soxhlet extraction with acetone overnight, the functionalized polyHIPE was swollen in ultra-pure water for at least 4 hours, and finally freeze-dried.

#### 3.2.2.4 ACTIVATION OF $Cu^0$ PLATE

The surface of the $Cu^0$ plate was chemically activated through a solution of 2 MeOH : 1 HCl for 10 min, rinsed with MeOH and dried prior to functionalization of the ATRP initiator-bearing polyHIPE.

#### 3.2.2.5 CALIBRATION OF ATR-IR

To the mixture used to prepare the polyHIPEs 1, 10 and 50 wt% of POEGMA were added, which was previously synthesized by free radical polymerization. ATR-IR spectra of samples with different contents of POEGMA revealed distinct absorbance of the band at 1109.4 $cm^{-1}$ (Figure B.3a, Appendix B), from the C-O stretching of POEGMA. All the ATR-IR spectra were normalized with respect to the band at 1728 $cm^{-1}$ corresponding to stretching of C=O groups. The normalized values of absorbance were then used to build a calibration curve (Figure B.3, Appendix B).

Following a similar procedure, polyHIPEs were mixed with 1, 10 and 50 wt% of PNIPAM, which was synthesized by FRP. The resulting ATR-IR spectra were normalized with respect to the band at 1728 $cm^{-1}$, corresponding to stretching of C=O groups. The normalized absorbance values of the band at 1636 $cm^{-1}$, correlated to the C=O stretching from the amide groups were used to estimate the content of PNIPAM (Figure B.4a, Appendix B), and were used to build a calibration curve (Figure B.4b, Appendix B).

## 3.3 RESULTS AND DISCUSSION

The 3D supports used as starting platforms for the growth of chemically different brushes are microporous elastomers obtained by cross-linking poly(high internal phase emulsion)s (polyHIPEs).[22] These were obtained by vigorously mixing an apolar phase, which contained the ATRP inimer 2-(2- bromoisobutyryloxy)ethyl methacrylate (BIEM; 17 mol %),[23] hexyl methacrylate (HMA, 63 mol %), ethylene glycol dimethacrylate (EGDMA, 4 mol %), and poly(ethylene glycol) sorbitan monooleate (PEGSM, 16 mol %), with an aqueous phase containing $CaCl_2$ (90 mM) and the free radical initiator potassium persulfate (KPS, 7.4 mM; Figure 3.1a).

Free radical polymerization (FRP) and cross-linking of the generated emulsion were induced by heating at 80 °C overnight to yield a highly porous, elastomeric 3D

structure (Figure 3.1a), which included ATRP initiator functions (Figure B.2, Appendix B).

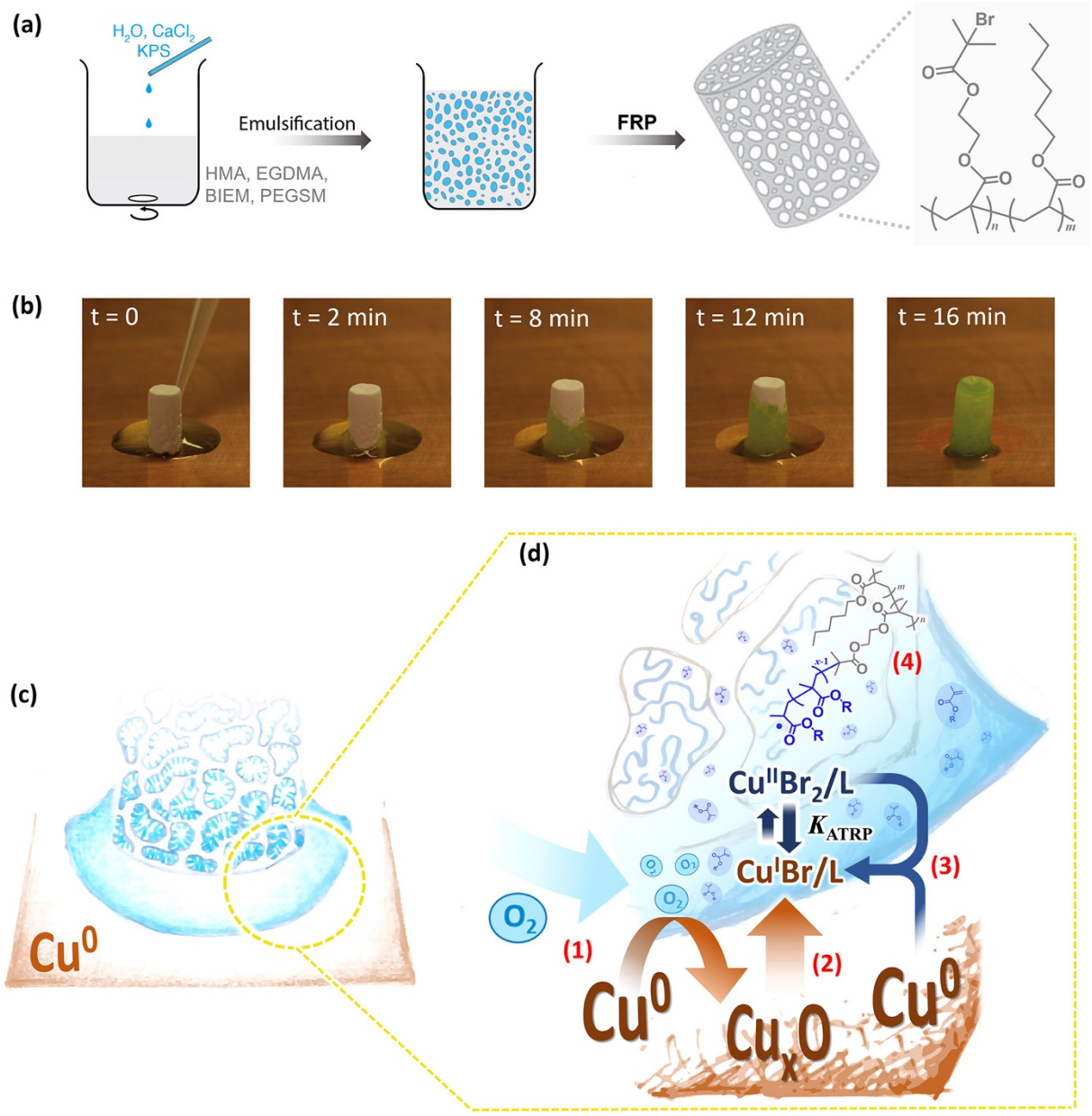


**Figure 3.1.** (a) Fabrication of an ATRP initiator-bearing polyHIPE. The HIPE was prepared by mixing an apolar (oil) phase containing HMA (63 mol %), EGDMA (4 mol %), BIEM (17 mol %), and PEGSM (16 mol %), with an aqueous phase including $CaCl_2$ (90 mM) and the free radical initiator KPS (7.4 mM). The ATRP initiator-bearing polyHIPE was obtained through FRP and cross-linking of the HIPE, followed by Soxhlet extraction with acetone, solvent exchange to water, and freeze-drying. (b) A polymerization mixture containing monomer (M), solvent, ligand (L), and $Cu^{II}Br_2$ was dispensed on an activated $Cu^0$-coated surface, and the polyHIPE was placed in contact with it. Complete infiltration of the polymerization mixture through the polyHIPE required ~16 min. (c, d) Mechanism of $Cu^0$ SI-ATRP from ATRP initiator-bearing polyHIPEs. (1) Oxygen is consumed by the $Cu^0$ surface through the formation of a $Cu_xO$ layer, which acts (2) as the source of catalyst; (3) $Cu^I/L$ activators are continuously (re)generated by comproportionation between $Cu^0$ and $Cu^{II}/L$ species; the growth of polymer grafts (4) within the pores proceeds according to the ATRP equilibrium.

The obtained polyHIPEs were subsequently used as supports for $Cu^0$ SI-ATRP. Following a typical polymer grafting process, which is depicted in Figure 3.1b,c, 125 μL of a polymerization mixture containing ligand, $Cu^{II}Br_2$, monomer, and solvent was dispensed on a $Cu^0$ plate, which was previously "activated" by chemically removing the oxide layer that spontaneously formed on it. A cylindrical polyHIPE with a height of 8 mm and a base of 13 $mm^2$ was subsequently placed in contact with the polymerization solution, and the whole $Cu^0$ SI-ATRP setup was immediately positioned within a closed desiccator connected to a balloon full of Ar, in this way, generating an environment presenting a limited amount of oxygen. The polymerization mixture rapidly infiltrated into the microporous structure of the polyHIPE due to capillary forces.[24] Simultaneously, direct contact between the reaction mixture and the $Cu^0$ plate led to the consumption of $O_2$ and the concomitant formation of a $Cu_xO$ layer on the metallic surface.

Within this setup (Figure 3.1c,d), $Cu^I$/L-based activators are generated both by diffusion of $Cu^I$ species from the newly formed oxide layer in the presence of complexing L[15,18] and due to comproportionation between $Cu^{II}$/L species and $Cu^0$.[25–28] $Cu^I$/L species are transported with the polymerization solution through the microporous scaffold and trigger the growth of polymer brushes from initiator sites that are exposed on the surface of pores, which proceeds according to the ATRP equilibrium (Figure 3.1d).

Generally, two main parameters are expected to regulate the formation of a brush gradient within the 3D supports via $Cu^0$ SI-ATRP. On the one hand, the progressive and relatively quick infiltration of the reaction mixture determines different polymerization times within a polyHIPE. On the other hand, the presence of a $Cu^0$ plate that is left in contact with one side of the microporous support triggers the formation of $Cu^I$/L activators and their slow diffusion, as it was described in detail previously.[18]

The vertical distance between a specific pore and the $Cu^0$ plate (where the reaction mixture is initially dispensed) determines the contact time between the mixture and the reactive sites. Hence, ATRP initiators that are closer to the plate are in contact for longer times with the polymerization solution and, thus, can generate brushes with relatively higher molar masses compared to those grown from sites further away from the bottom of the microporous scaffold.

Simultaneously, the concentration of $Cu^I$/L activators progressively decreases with the distance from the metallic plate, where these are constantly (re)generated

through comproportionation. This phenomenon induces a local increase of $[Cu^I/L]/[Cu^{II}/L]$ close to the metallic surface and, thus, an increment in the polymerization rate,[29] which is expected to follow a progressive decay across the polyHIPE when this is fully infiltrated by the mixture.

The combined effects of progressive variations in polymerization time and rate resulted in the formation of a polymer-brush gradient across the polyHIPE. However, it is important to emphasize that the infiltration of polyHIPEs by the reaction mixtures and the diffusion of $Cu^I/L$ species continuously (re)generated at the $Cu^0$ plate are phenomena taking place at different time scales. In the first case, complete infiltration requires just minutes. In the second case, diffusion of the catalyst within the already infiltrated polyHIPEs is much slower, typically occurring at rates <1 $mm.h^{-1}$.[18]

Hence, considering that at the typical polymerization rates attained by $Cu^0$ SI-ATRP in organic solvents, brush growth proceeds at 10−20 nm $h^{-1}$, the relatively fast infiltration process is expected to play a non-negligible, but minor role in determining the formation of brush gradients. In contrast, diffusion of activators, which occurs at time scales similar to those relevant for brush growth, is expected to be the major determinant for the formation of graded brushes across the supports.

The formation of a single 3D gradient of poly-[(oligoethylene glycol) methacrylate] (POEGMA) brushes within an ATRP initiator-bearing polyHIPE is exemplarily described.

A polymerization mixture (125 μL) containing OEGMA (25% v/v) in dimethylformamide (DMF), 10 mM tris(2-pyridylmethyl)amine (TPMA), and 10 mM $Cu^{II}Br_2$ was poured on a freshly activated $Cu^0$ plate. A polyHIPE presenting a cylindrical shape was immediately placed on the drop of this reaction mixture, and the entire setup was closed inside a desiccator connected with a balloon filled with Ar. The progressive infiltration of the polymerization mixture, which presented a pale green color, within the colorless, microporous structure could be clearly visualized, and it was typically quick, with the entire support getting filled up within just ~16 min (Figure 3.1b). To generate a POEGMA brush gradient, the polyHIPE was incubated on the $Cu^0$ plate for an overall time of 5 h, after which the support was extensively rinsed by Soxhlet extraction in acetone, later swollen in ultra-pure water, and finally freeze-dried.

The formation of a 3D POEGMA-brush gradient was verified by attenuated total reflection infrared (ATR-IR) spectroscopy, which was used to record the

composition of the microporous elastomer at different positions along its main axis, namely, 1, 3, 5, and 7 mm away from the contact area with the $Cu^0$ plate (Figure 3.2a).

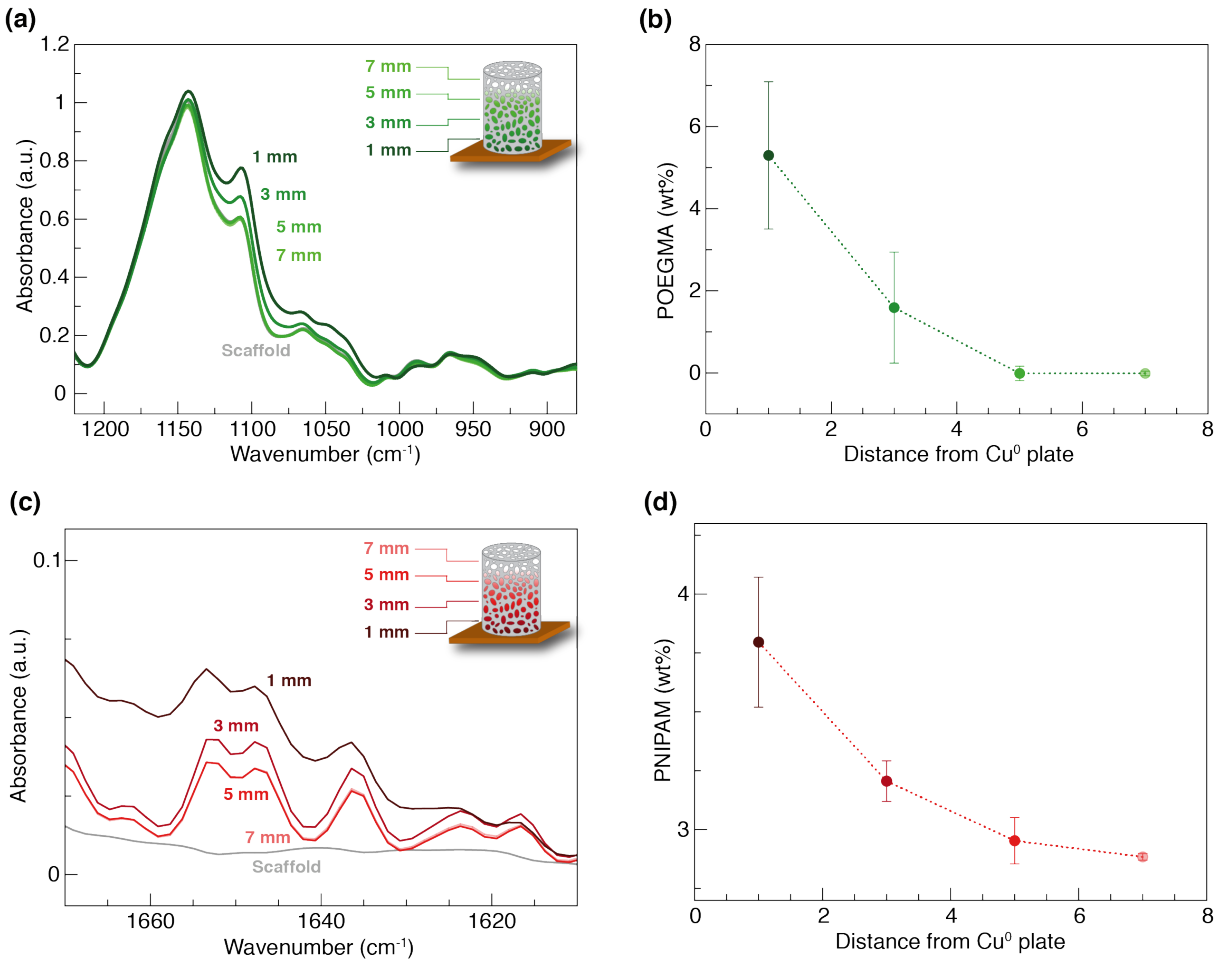


**Figure 3.2.** (a) ATR-IR spectra of polyHIPE recorded at positions that were kept at different distances (1, 3, 5, and 7 mm) from the $Cu^0$ plate during $Cu^0$ SI-ATRP of OEGMA. (b) Relative content (wt %) of POEGMA brushes recorded at different positions across the polyHIPE following $Cu^0$ SIATRP. (c) ATR-IR spectra recorded at different positions across a polyHIPE (1, 3, 5, and 7 mm) from the $Cu^0$ surface during $Cu^0$ SI-ATRP of NIPAM. (d) Relative content (wt %) of PNIPAM brushes across a brush-functionalized polyHIPE.

All ATR-IR spectra were normalized with respect to the band at 1728 $cm^{-1}$ correlated to the stretching of C=O groups, which are included both in the repeating units of the polymer forming the support and in POEGMA brushes.

Following $Cu^0$ SI-ATRP, the appearance of the band at 1109.4 $cm^{-1}$, corresponding to the C-O stretching of the ether moieties along the OEGMA side chains, confirmed the successful growth of POEGMA brushes. The relative intensity of this specific signal gradually decreased with increasing the distance from the $Cu^0$ plate, indicating that the pores closer to the metallic plate were functionalized with higher-molar-mass brushes compared to those further away from it (Figure 3.2a) and, thus, confirming the formation of a brush gradient across the elastomer. Calibration of

the ATR-IR data (Figure B.3, Appendix B) enabled to quantitatively estimate the relative amount of POEGMA brushes across the polyHIPE, which varied between 0 and 7 wt % across 7 mm of distance from the $Cu^0$ plate (Figure 3.2b).

Chemically different 3D brush gradients could be easily fabricated by varying the composition of the polymerization mixture. Following a similar procedure as the one reported above, poly(N-isopropylacrylamide) (PNIPAM) brush gradients were obtained by placing an ATRP initiator-bearing polyHIPE on a $Cu^0$ plate previously wetted with 125 μL of a mixture comprising 3 M NIPAM in DMF, 10 mM TPMA, and 10 mM $Cu^{II}Br_2$.

After 4 h, during which the infiltrated support was left in contact with the $Cu^0$ plate, the functionalized elastomer was thoroughly rinsed by Soxhlet extraction in acetone, swollen in ultra-pure water, and freeze-dried. ATR-IR revealed the presence of PNIPAM grafts, through the appearance of a clear band at 1646 $cm^{-1}$, which originated from the C=O stretching of the amide groups of the polymer. Opportune calibration (Figure B.4, Appendix B) enabled the quantification of the relative content of PNIPAM brushes, which varied between 2 and 4 wt % across the functionalized support. The amount of PNIPAM brushes progressively decreased between the portion of the elastomer that had been in contact with the metallic plate and the volumes that had been at ~7 mm of vertical distance from it during $Cu^0$ SI-ATRP.

The generation of POEGMA and PNIPAM brush gradients within polyHIPEs was further confirmed by analyzing scanning electron microscopy (SEM) images recorded across functionalized supports at positions that were kept at different distances from the metallic surface during $Cu^0$ SI-ATRP. Because $Cu^0$ SI-ATRP induced the growth of brushes within the pores, the formation of brush gradients could be monitored through a simultaneous, gradual variation in the pore-size distributions across the supports.

As reported in Figure 3.3a, both POEGMA and PNIPAM brushes almost completely filled the pores of the elastomeric structures where these were in direct contact with the $Cu^0$ plates (positions 0 mm, as indicated in Figure 3.3a).

Assuming that any change in porosity after $Cu^0$ SI-ATRP was exclusively due to the growth of polymer grafts, the presence of brushes at a given vertical distance from the $Cu^0$ plate > 0 mm could be recorded as a change in pore size with respect to the pristine, unfunctionalized support.

As reported in Figure 3.3, following $Cu^0$ SI-ATRP, pore-size distributions progressively shifted toward a greater relative incidence of small pores due to the growth of POEGMA (Figure 3.3b) and PNIPAM (Figure 3.3c) brushes. The presence of smaller pores is especially highlighted in positions that were close to the metallic plate during $Cu^0$ SI-ATRP (2 and 4 mm of vertical distances), while the porosity of functionalized polyHIPEs gradually approximated that recorded on pristine supports at a distance of 6 mm.

In the case of POEGMA, the brush gradient extended within the scaffold across ~4 mm from the contact with the $Cu^0$ plate. In contrast, the PNIPAM brush gradient seemed to develop through the whole volume of the polyHIPE, with pores relatively far away from the $Cu^0$ surface still being functionalized with PNIPAM grafts.

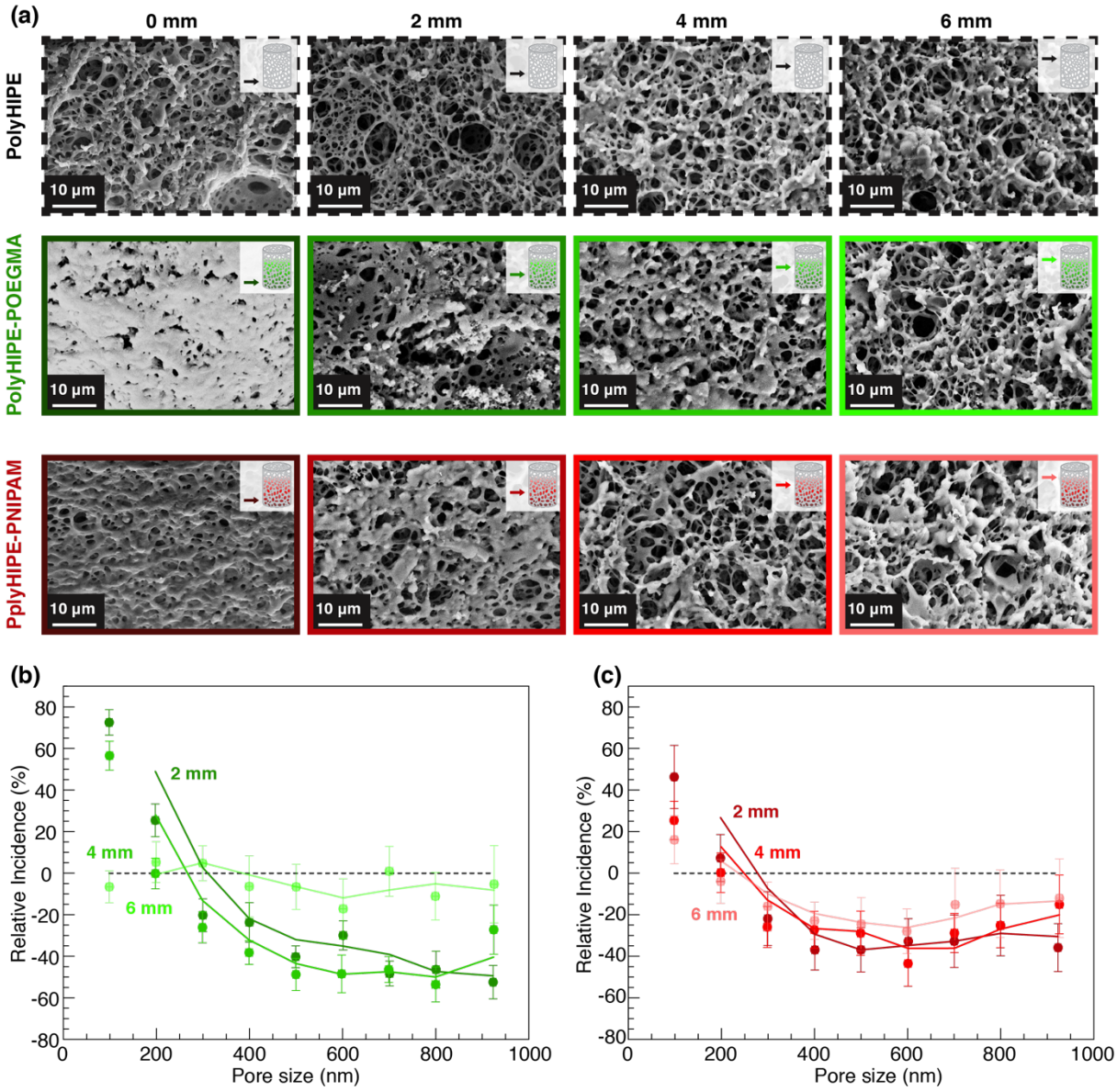


**Figure 3.3.** (a) SEM micrographs of the polyHIPE before (dashed black frame) and after functionalization with POEGMA (green frame) and PNIPAM (red frame) brushes. The micrographs

were recorded at different positions across the main axis of the supports, namely, at 0, 2, 4, and 6 mm of the distance from the $Cu^0$ plate. Pore size distributions within polyHIPEs following the growth of (b) POEGMA and (c) PNIPAM brushes.

Hence, the combination of ATR-IR and SEM analyses demonstrated the formation of POEGMA- and PNIPAM-brush gradients within microporous polyHIPEs. In the former case, brush gradients presented a "steeper" morphology, with a more marked variation in brush-molar mass across relatively small distances. In the latter case, PNIPAM brush gradients showed a less pronounced variation in brush properties, and extended across the entire support. This phenomenon was presumably due to the faster kinetics of $Cu^0$ SI-ATRP of NIPAM, which determined the formation of high-molar-mass grafts already after relatively short incubation times in the reaction mixture.[15]

The application of $Cu^0$ SI-ATRP on initiator-bearing polyHIPEs additionally enabled the fabrication of multiple brush gradients within the same support. This is especially relevant, as 3D polymeric matrices including brushes featuring graded variations in functionalities and properties could be employed as suitable supports for a variety of applications, including cell-culture platforms, tissue engineering supports, and fully synthetic prostheses.[30]

Multiple brush gradients could be easily generated if the general functionalization procedure described for a single brush gradient was repeated, for example, by turning upside down a brush-functionalized polyHIPE after a first $Cu^0$ SI ATRP step and subjecting it to the diffusion of a reaction mixture containing a different monomer.

For instance, a polyHIPE featuring a POEGMA brush 3D gradient (polyHIPE-POGEMA) was subjected to an additional $Cu^0$ SI-ATRP step to generate a second brush gradient of poly(2-hydroxylethyl methacrylate) (PHEMA) in the opposite direction along the main axis of the elastomeric support (yielding polyHIPE-POEGMA-PHEMA; Figure 3.4).

Following a similar protocol as that reported above, 125 μL of polymerization mixture containing 25% v/v HEMA in DMF, 10 mM TPMA, and 10 mM $Cu^{II}Br_2$ was dispensed on an activated $Cu^0$ surface. A previously prepared polyHIPE-POEGMA was turned upside down and placed on the dropped solution, with the side that was left unfunctionalized during the first $Cu^0$ SI-ATRP step now facing the metallic plate. The new reaction mixture was left diffusing inside the polyHIPE-POEGMA for 2 h,

after which the support was rinsed by Soxhlet extraction in acetone, swollen in ultrapure water, and again freeze-dried.

ATR-IR and SEM confirmed the formation of a double brush gradient. As reported in Figure 3.4a, following $Cu^0$ SI-ATRP of OEGMA, the appearance of a strong band at 1109.4 $cm^{-1}$, corresponding to C-O stretching, confirmed the presence of high-molar-mass POEGMA grafts at one side of the polyHIPE. This was confirmed by SEM (Figure 3.4d), which highlighted how POEGMA brushes nearly completely filled the pores of the polyHIPE where this was contacting the $Cu^0$ plate. After $Cu^0$ SI-ATRP of HEMA, the ATR-IR spectrum recorded on the opposite side of the polyHIPE showed the appearance of the bands at 1074.7 $cm^{-1}$ from C-O stretching and 3480 $cm^{-1}$ from O-H stretching, confirming the successful growth of PHEMA brushes (Figure 3.4b). This result was corroborated by the SEM micrographs recorded on the same areas of the polyHIPE, which suggested the presence of brushes covering the pores of the support (Figure 3.4e).

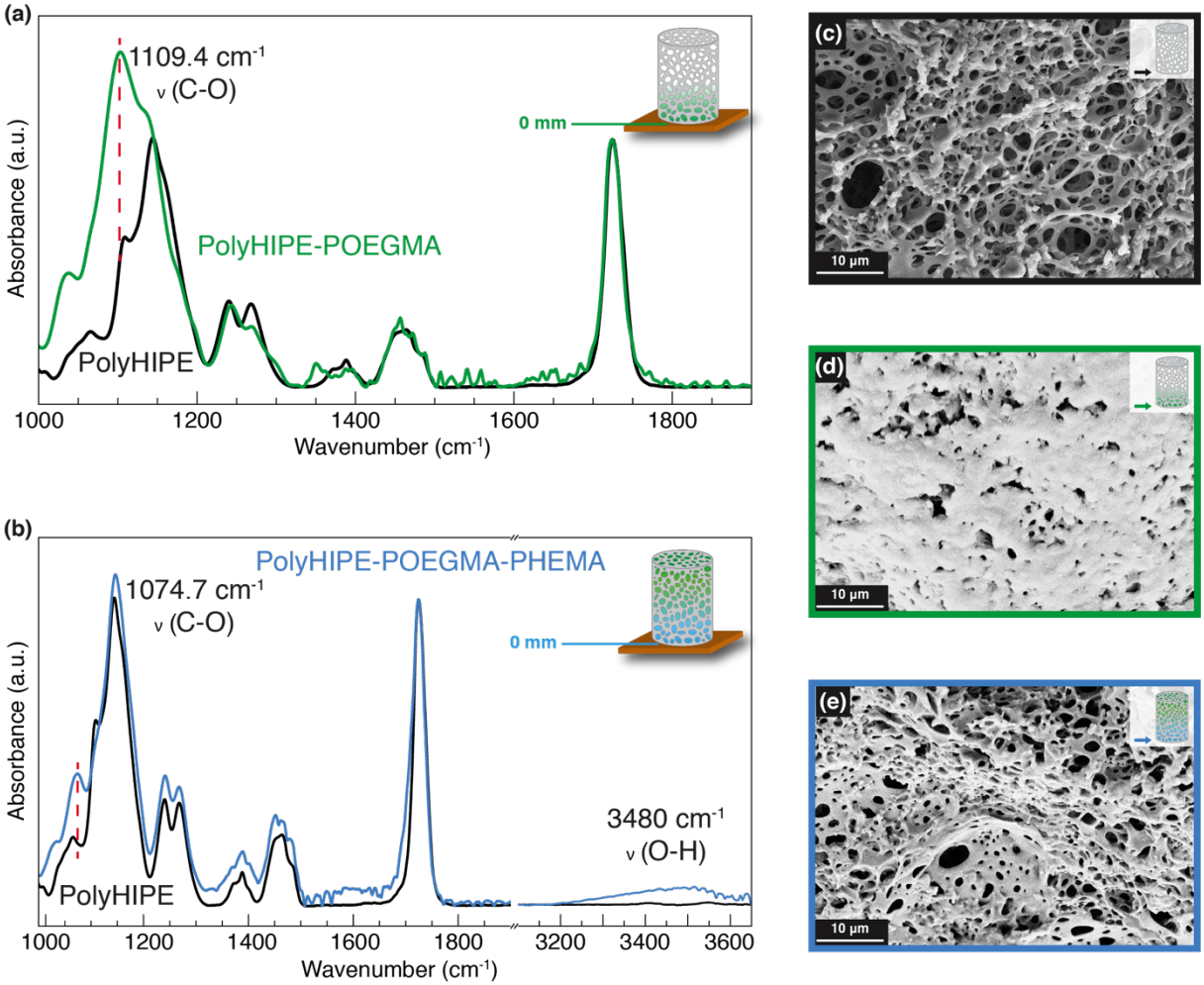


**Figure 3.4.** (a) ATR-IR spectra of polyHIPE before (black trace) and after (green trace) the growth of POEGMA brushes (yielding polyHIPE-POEGMA). The spectrum of polyHIPE-POEGMA was recorded on the side of the elastomer that was in contact with the $Cu^0$ plate during $Cu^0$ SI-ATRP.

(b) ATR-IR spectra of polyHIPE-POEGMA before (black trace) and after (blue trace) $Cu^0$ SI-ATRP of HEMA (which yielded polyHIPE-POEGMA-PHEMA). (c) SEM micrograph of unfunctionalized polyHIPE. (d) SEM micrograph of polyHIPE-POEGMA, recorded on the side of the elastomer that was in contact with the $Cu^0$ plate during $Cu^0$ SI-ATRP of OEGMA. (e) SEM micrograph of polyHIPE-POEGMA-PHEMA, recorded on the portion of the elastomer that was in contact with the $Cu^0$ plate during $Cu^0$ SI-ATRP of HEMA.

## 3.4 CONCLUSION

These results demonstrated that $Cu^0$ SI-ATRP represents an efficient process not only to generate structured polymer brushes from 2D substrates[31] but also to functionalize 3D supports in a controlled fashion, forming single and multiple brush gradients with a fully tunable composition. It is important to emphasize that even when applied on 3D supports, $Cu^0$ SI-ATRP could be performed without the need for deoxygenation of the polymerization mixtures and enabled the controlled growth of brushes also in the presence of a limited content of oxygen. These attractive features further confirmed the versatility of this polymerization process for the synthesis of polymer brush coatings from multidimensional materials and the possibility to translate it into upscalable functionalization techniques.

## 3.5 ACKNOWLEDGEMENTS

We thank Prof. Katharina Maniura (EMPA) for the fruitful scientific discussions. We acknowledge Empa and the Brazilian agency Fundação de Amparo à Pesquisa do Estado de São Paulo-FAPESP (2016/14493-7 and 2017/22304-2) for the financial support.

## 3.6 REFERENCES

1. Yeow, J.; Chapman, R.; Gormley, A. J.; Boyer, C. Up in the Air: Oxygen Tolerance in Controlled/Living Radical Polymerisation. Chem. Soc. Rev. 2018 , 47, 4357−4387.

2. Dunderdale, G. J.; Urata, C.; Miranda, D. F.; Hozumi, A. Large-Scale and Environmentally Friendly Synthesis of PH-Responsive Oil-Repellent Polymer Brush Surfaces under Ambient Conditions. ACS Appl. Mater. Interfaces 2014, 6, 11864−11868.

3. Dunderdale, G. J.; England, M. W.; Urata, C.; Hozumi, A. Polymer Brush Surfaces Showing Superhydrophobicity and Air-Bubble Repellency in a Variety of Organic Liquids. ACS Appl. Mater. Interfaces 2015 , 7, 12220−12229.

4. Sato, T.; Dunderdale, G. J.; Urata, C.; Hozumi, A. Sol-Gel Preparation of Initiator Layers for Surface-Initiated ATRP: Large-Scale Formation of Polymer Brushes Is Not a Dream. Macromolecules 2018 , 51, 10065−10073.

5. Yan, W.; Dadashi-Silab, S.; Matyjaszewski, K.; Spencer, N. D.; Benetti, E. M. Surface-Initiated Photoinduced ATRP: Mechanism, Oxygen Tolerance, and Temporal Control during the Synthesis of Polymer Brushes. Macromolecules 2020, 53, 2801.

6. Matyjaszewski, K.; Dong, H.; Jakubowski, W.; Pietrasik, J.; Kusumo, A. Grafting from Surfaces for "Everyone": ARGET ATRP in the Presence of Air. Langmuir 2007 , 23, 4528−4531.

7. Navarro, L. A.; Enciso, A. E.; Matyjaszewski, K.; Zauscher, S. Enzymatically Degassed Surface-Initiated Atom Transfer Radical Polymerization with Real-Time Monitoring. J. Am. Chem. Soc. 2019, 141, 3100−3109.

8. Divandari, M.; Pollard, J.; Dehghani, E.; Bruns, N.; Benetti, E. M. Controlling Enzymatic Polymerization from Surfaces with Switchable Bioaffinity. Biomacromolecules 2017 , 18, 4261−4270.

9. Narupai, B.; Page, Z. A.; Treat, N. J.; McGrath, A. J.; Pester, C. W.; Discekici, E. H.; Dolinski, N. D.; Meyers, G. F.; Read de Alaniz, J.; Hawker, C. J. Simultaneous Preparation of Multiple Polymer Brushes under Ambient Conditions Using Microliter Volumes. Angew. Chem., Int. Ed. 2018 , 57, 13433−13438.

10. Li, M.; Fromel, M.; Ranaweera, D.; Rocha, S.; Boyer, C.; Pester, C. W. SI-PET-RAFT Surface-Initiated Photoinduced Electron Transfer-Reversible Addition-Fragmentation Chain Transfer Polymerization. ACS Macro Lett. 2019, 8, 374−380.

11. Mohamadnia, Z.; Ahmadi, E.; Ghasemnejad, M.; Hashemikia, S.; Doustgani, A. Surface Modification of Mesoporous Nanosilica with [3-(2-Aminoethylamino) Propyl] Trimethoxysilane and Its Application in Drug Delivery. Mater. Sci. Eng., C 2015 , 11, 167−177.

12. Zhang, T.; Du, Y.; Kalbacova, J.; Schubel, R.; Rodriguez, R. D.; Chen, T.; Zahn, D. R. T.; Jordan, R. Wafer-Scale Synthesis of Defined Polymer Brushes under Ambient Conditions. Polym. Chem. 2015 , 6, 8176−8183.

13. Dehghani, E. S.; Du, Y.; Zhang, T.; Ramakrishna, S. N.; Spencer, N. D.; Jordan, R.; Benetti, E. M. Fabrication and Interfacial Properties of Polymer Brush

Gradients by Surface-Initiated Cu(0)-Mediated Controlled Radical Polymerization. Macromolecules 2017, 50, 2436−2446.

14 Zhang, T.; Du, Y.; Müller, F.; Amin, I.; Jordan, R. Surface-Initiated Cu(0) Mediated Controlled Radical Polymerization (SICuCRP) Using a Copper Plate. Polym. Chem. 2015 , 6 (14), 2726−2733.

15. Yan, W.; Fantin, M.; Spencer, N. D.; Matyjaszewski, K.; Benetti, E. M. Translating Surface-Initiated Atom Transfer Radical Polymerization into Technology: The Mechanism of $Cu^0$-Mediated SI-ATRP under Environmental Conditions. ACS Macro Lett. 2019, 8, 865−870.

16. Yan, W.; Fantin, M.; Ramakrishna, S.; Spencer, N. D.; Matyjaszewski, K.; Benetti, E. M. Growing Polymer Brushes from a Variety of Substrates under Ambient Conditions by $Cu^0$-Mediated Surface-Initiated ATRP. ACS Appl. Mater. Interfaces 2019, 11, 27470−27477.

17. Zhang, K.; Yan, W.; Simic, R.; Benetti, E. M.; Spencer, N. D. Versatile Surface Modification of Hydrogels by Surface-Initiated, $Cu^0$-Mediated Controlled Radical Polymerization. ACS Appl. Mater. Interfaces 2020, 12, 6761−6767.

18. Fantin, M.; Ramakrishna, S. N.; Yan, J.; Yan, W.; Divandari, M.; Spencer, N. D.; Matyjaszewski, K.; Benetti, E. M. The Role of $Cu^0$ in Surface-Initiated Atom Transfer Radical Polymerization: Tuning Catalyst Dissolution for Tailoring Polymer Interfaces. Macromolecules 2018 , 51, 6825−6835.

19. Faggion Albers, R.; Yan, W.; Romio, M.; Leite, E. R.; Spencer, N. D.; Matyjaszewski, K.; Benetti, E. M. Mechanism and Application of Surface-Initiated ATRP in the Presence of a $Zn^0$ plate. Polym. Chem. 2020, 11, 7009−7014.

20. Layadi, A.; Kessel, B.; Yan, W.; Romio, M.; Spencer, N. D.; Zenobi-Wong, M.; Matyjaszewski, K.; Benetti, E. M. Oxygen Tolerant and Cytocompatible Iron(0)-Mediated ATRP Enables the Controlled Growth of Polymer Brushes from Mammalian Cell Cultures. J. Am. Chem. Soc. 2020, 142, 3158−3164.

21. Li, W.; Sheng, W.; Wegener, E.; Du, Y.; Li, B.; Zhang, T.; Jordan, R. Capillary Micro Fluidic-Assisted Surface Structuring. ACS Macro Lett. 2020, 9, 328−333.

22 Kimmins, S. D.; Cameron, N. R. Functional Porous Polymers by Emulsion Templating: Recent Advances. Adv. Funct. Mater. 2011, 21, 211−225.

23 Matyjaszewski, K.; Pyun, J.; Gaynor, S. G. Preparation of Hyperbranched Polyacrylates by Atom Transfer Radical Polymerization, 4: The Use of Zero-Valent Copper. Macromol. Rapid Commun. 1998 , 19, 665−670.

24 Gunnewiek, M. K.; Di Luca, A.; Bollemaat, H. Z.; van Blitterswijk, C. A.; Vancso, G. J.; Moroni, L.; Benetti, E. M. Creeping Proteins in Microporous Structures: Polymer Brush-Assisted Fabrication of 3D Gradients for Tissue Engineering. Adv. Healthcare Mater. 2015 , 4 (8), 1169−1174.

25. Konkolewicz, D.; Wang, Y.; Zhong, M.; Krys, P.; Isse, A. A.; Gennaro, A.; Matyjaszewski, K. Reversible-Deactivation Radical Polymerization in the Presence of Metallic Copper. A Critical Assessment of the SARA ATRP and SET-LRP Mechanisms. Macromolecules 2013, 46, 8749−8772.

26. Augustine, K. F.; Ribelli, T. G.; Fantin, M.; Krys, P.; Cong, Y.; Matyjaszewski, K. Activation of Alkyl Halides at the $Cu^0$ Surface in SARA ATRP: An Assessment of Reaction Order and Surface Mechanisms. J. Polym. Sci., Part A: Polym. Chem. 2017 , 55, 3048− 3057.

27. Konkolewicz, D.; Wang, Y.; Krys, P.; Zhong, M.; Isse, A. A.; Gennaro, A.; Matyjaszewski, K. SARA ATRP or SET-LRP. End of Controversy? Polym. Chem. 2014, 5, 4409−4417.

28. Konkolewicz, D.; Krys, P.; Góis, J. R.; Mendonça, P. V.; Zhong, M.; Wang, Y.; Gennaro, A.; Isse, A. A.; Fantin, M.; Matyjaszewski, K. Aqueous RDRP in the Presence of $Cu^0$: The Exceptional Activity of $Cu^I$ Confirms the SARA ATRP Mechanism. Macromolecules 2014, 47, 560−570.

29. Jeyaprakash, J. D.; Samuel, S.; Dhamodharan, R.; Rühe, J. Polymer Brushes via ATRP: Role of Activator and Deactivator in the Surface-Initiated ATRP of Styrene on Planar Substrates. Macromol. Rapid Commun. 2002, 23, 277−281.

30. Benetti, E. M.; Gunnewiek, M. K.; Van Blitterswijk, C. A.; Julius Vancso, G.; Moroni, L. Mimicking Natural Cell Environments: Design, Fabrication and Application of Bio-Chemical Gradients on Polymeric Biomaterial Substrates. J. Mater. Chem. B 2016 , 4, 4244− 4257.

31. Zhang, T.; Benetti, E. M.; Jordan, R. Surface-Initiated Cu(0)-Mediated CRP for the Rapid and Controlled Synthesis of Quasi-3D Structured Polymer Brushes. ACS Macro Lett. 2019, 8, 145−153.

# Chapter 4

## FABRICATION OF 2D-$MoS_2$-REINFORCED COMPOSITES WITH INTERFACIAL LOOP-CHAIN ENTANGLEMENTS THROUGH SELECTIVE VULCANIZATION OF INTERFACES

Rebecca F. Albers,[a,b,c,d,e] Tommaso Magrini,[a] Andrea Arcifa,[f] Edson R. Leite,[d,e] Edmondo Benetti,[b,c,g] André R. Studart,[a] Rafael Libanori*[a]

[a]*Complex Materials, Department of Materials, ETH Zürich, Vladimir-Prelog-Weg 1-5/10, CH-8093 Zurich, Switzerland*

[b]*Laboratory for Surface Science and Technology, Department of Materials, ETH Zürich, Vladimir-Prelog-Weg 1-5/10, CH-8093 Zurich, Switzerland.*

[c]*Swiss Federal Laboratories for Materials Science and Technology (Empa), Lerchenfeldstrasse 5, CH-9014 St. Gallen, Switzerland*

[d]*Department of Chemistry, Federal University of São Carlos, 13565-905 São Carlos, SP, Brazil*

[e]*Brazilian Nanotechnology National Laboratory (LNNano), Brazilian Center for Research in Energy and Materials (CNPEM), 13083-970 Campinas, Brazil*

[f]*Surface Science & Coating Technologies, Swiss Federal Laboratories for Materials Science and Technology (Empa), Überlandstrasse 129, CH-8600 Dübendorf, Switzerland*

[g]*Department of Chemical Sciences, University of Padova, 35131 Padova, Italy*

To be submitted in 2021

Supplementary Information is attached in Appendix C in Chapter 8.

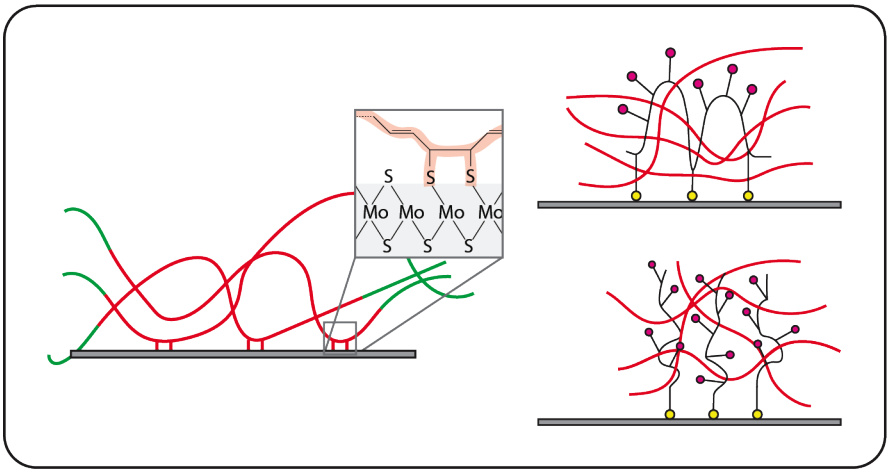

## ABSTRACT

Chemical compatibility between matrix and reinforcing elements enhances mechanical properties of composites, however interfacial architecture also influences the mechanical response of the final material. Quasi-static mechanical tests after thermal treatment at 150 $^{o}$C suggest an interfacial vulcanization process occurring between the sulfur of 2D-$MoS_2$ and the polybutadiene block of PSBS. The reaction of 2D-$MoS_2$ with a rubbery matrix might lead to the formation of polymer loops that entangle with polymer chains from the matrix at the interface. To understand the transference of stress in such composites, architectured interface composites were fabricated with interfacial brushes and loops and cyclic tested in tensile mode. The molecular mechanical interlocking due to loop-chain entanglements experimented at the interface of the composites suppresses chain sliding during loading-unloading cycles, leading to higher elastic recovery, lower plastic deformation and lower energy dissipation of interfacial loops composites when compared to interfacial brushes composites.

## 4.1 INTRODUCTION

Improving chemical compatibility between matrix and reinforcing elements is known to enhance the mechanical behavior of polymer matrix composites.[1–3] Theoretically, stiff and brittle reinforcing elements can be combined with ductile polymers to give composites with a range of toughness and strength for biomedical,[4] aerospacial[5] and civil construction[6] applications. Nonetheless, the mechanical response of the composite is often not enhanced just by mixing the two components, due to the poor interfacial bonding between them.[7] When matrix and filler present very different surface energy, the filler tends to agglomerate within the matrix rather than forming a well-dispersed system. The mechanical loading of such composites with low interfacial bonding leads to non-effective stress transfer from the matrix to the filler and, consequently, impairment of their mechanical response as compared to the expected mechanical properties.[8,9] Even in well-dispersed composites, since the reinforcing elements and the polymer matrix present a discrepancy of elastic modulus, upon applied strain the matrix undergoes greater deformation than the filler. Such mismatch of mechanical behavior leads to shear stresses at the interface, which are responsible for transferring mechanical loads from the matrix to the reinforcing elements. Enlarging chemical compatibility between the composite building blocks increases interfacial strength, improves the stress transfer at the interface and enhances the composite performance.

Many strategies have been developed to chemically modify the filler surface, according to the chemical nature of both components.[10] Chemical functionalization of the filler disfavors the interaction filler/filler while favors the interface filler/matrix, enhancing the homogeneity of the composite.[8] Besides, chemical modification is a tool to design the interface of composites and enhance stress transfer mechanisms. Improving the filler dispersion in the matrix and introducing effective stress transfer mechanisms from the matrix to the reinforcing elements lead to enhanced mechanical properties of the final material. Chemical compatibility through surface modification of the reinforcing elements is not the only feature that drives the mechanical response of the material. Interfacial architecture is also expected to play a role in the stress-transfer mechanism and has been explored by Libanori et al.[11] and Xia et al.[12] in alumina platelets composites with controlled roughness at the interface. The authors have reported inorganic nanoasperities on the surface of the reinforcing elements led to toughening mechanisms based on mechanical interlocking that enhanced the mechanical response of such composites. Interfacial design achieved through

anchoring inorganic nanoasperities on the surface of alumina platelets sets the scene for modulating the interface architecture of organic molecules at the interface of polymer matrix composites through chemical functionalization of the reinforcing elements.

The mechanism through which organic polymer chains from the matrix and brushes from chemical functionalization rub at the interface of composites and how this friction contributes to the mechanical response of the composite has never been explored. Understanding the stress-transfer mechanism at the interface polymer/polymer in composites paves the way to control the mechanical behavior of such composites, allowing tailoring properties according to the target application.

This paper gives insights on how the architecture of 2D-$MoS_2$ surface changes the friction of polymer chains at the interface of the composite during mechanical loading and unloading, inducing different mechanisms of energy dissipation. The presence of sulfur in the nanosheets can lead to a confined interfacial vulcanization in rubber-like matrices. Since the polymer chains of the matrix are already entangled, such vulcanization process might lead to the formation of polymer loops on the surface of the nanosheets. The entanglements between these interfacial loops and polymer chains are expected to induce an efficient transference of stress from the matrix to the reinforcing elements as well as an increased energy dissipation and improved elastic recovery through molecular mechanical interlocking. To investigate the formation of loops at the interface of the 2D-$MoS_2$ composites, we have modified the surface of nanosheets with linear brushes and loop-forming polymer chains. Both brushes and loops enhance the chemical compatibility of the 2D-$MoS_2$ with the rubbery matrix as the chemical composition of the backbone of both functionalization polymers is identical. However, the mechanical response in cyclic tests revealed distinctive energy dissipation mechanisms, as a consequence of the interfacial architecture.

## 4.2 EXPERIMENTAL SECTION

### 4.2.1 MATERIALS

Ethyl $\alpha$-bromoisobutyrate (EBIB, Sigma Aldrich, 98%); 2-Hydroxyethyl 2-bromoisobutyrate (HEBIB, Sigma Aldrich, 95%); 2-Phenoxyethyl acrylate (PEA, Tokyo Chemical Industry, 90%), tert-Butyl acrylate (t-BA, Sigma Aldrich, 98%), N,N,N′,N″,N″-Pentamethyldiethylenetriamine (PMDETA, Sigma Aldrich, 99%), Copper(I) bromide ($Cu^{I}Br$, Sigma Aldrich, 99.999%), Copper(II) bromide ($Cu^{II}Br_2$, Sigma Aldrich, 99%), Tris-[2-(dimethylamino)-ethyl]-amine ($Me_6$TREN, ABCR, 99%);

Dichloromethane (DCM, Sigma Aldrich, 99%); Trifluoroacetic acid (TFA, Fluka, >98%); Piperazine (Sigma Aldrich, 99%); O-(1H-Benzotriazol-1-yl)-N,N,N',N'-tetramethyluronium hexaflorophosphate (HBTU, AlfaAesar, 98%); 1H-Benzo[d][1,2,3]triazol-1-ol (HOBt); N,N-Diisopropylethylamine (DIPEA, Sigma Aldrich, 99.5%); dry DMF (Acros, 99.8%); N,N'-Dicyclohexylcarbodiimide (DCC, Fluka, >99%); N,N-Dimethylpyridin-4-amine (DMAP, Fluka, >98%); (±)-α-Lipoic acid (LA, Sigma Aldrich, >98%); dry DCM (Acros, 99.8%). Molybdenum disulfide ($MoS_2$, Sigma Aldrich, <2 μm, 98%); Tetrahydrofuran (THF, Sigma Aldrich, >99.5%), Polystyrene-block-polybutadiene-block-polystyrene (PSBS, Sigma Aldrich, styrene 30 wt. %, average Mw ~140,000). Monomers were purified through chromatography column with basic alumina prior to use. Water used in the experimental procedure was from Millipore Milli-Q.

### 4.2.2 METHODS

#### 4.2.2.1 POLYMER SYNTHESIS

Both linear brushes and loop-forming polymers are linear polymer chains, containing disulfide functionalities that can be attached to the 2D-$MoS_2$ through reaction with sulfur vacancies of the 2D-$MoS_2$. The linear brushes are disulfide-terminated poly(2-Phenoxyethyl acrylate) and the loop-forming polymer is a disulfide pending copolymer poly(2-Phenoxyethyl acrylate-co-1-(4-acryloylpiperazin-1-yl)-5-(1,2-dithiolan-3-yl)pentan-1-one). Both linear brushes and loop-forming polymers were synthesized by ATRP, purified and post-modified.

#### 4.2.2.2 LOOP-FORMING POLYMER SYNTHESIS

The polymerization mixture containing 0.26 mmol EBIB, 52 mmol PEA, 2.7 mmol t-BA, 0.27 mmol PMDETA, 5mL acetone and 1g anisole was prepared in a Schlenk flask and deoxygenized through freeze-pump-thaw cycles. Next, 0.26 mg $Cu^{I}Br$, 0.013 mmol $Cu^{II}Br_2$ were added to the Schlenk flask and the polymerization mixture was kept under stirring at 60 °C, in an oil bath. The reaction conversion was tracked through NMR spectra, using the peak of anisole as a reference for the integrals. Within 80% of conversion from monomer to polymer, oxygen was bubbled in the mixture through a needle to stop the reaction. Then the polymer was purified through a chromatography column with basic alumina, precipitated twice in cold hexane and dried under high vacuum overnight. Deliverable: poly(2-Phenoxyethyl acrylate-co-tert-butyl acrylate).

#### 4.2.2.3 LOOP-FORMING POLYMER MODIFICATION

##### 4.2.2.3.1 DEPROTECTION OF T-BUTYL GROUPS

T-butyl groups were deprotected with TFA. Poly(2-Phenoxyethyl acrylate-co-tert-butyl acrylate) was dissolved in DCM (0.15 g of polymer/mL) and TFA (5 eq.) was added to the flask. The mixture was subsequently left under stirring at room temperature overnight. Next, TFA excess and DCM were eliminated through rotary evaporation from the reaction mixture and the polymer was dried under high vacuum overnight. Deliverable: poly(2-Phenoxyethyl acrylate-co-acrylic acid).

##### 4.2.2.3.2 PIPERAZINE COUPLING

Coupling reaction between carboxylic acid groups and piperazine. In a single-neck round-bottom flask, poly(2-Phenoxyethyl acrylate-co-acrylic acid) was dissolved in dry DCM and kept at 0 $^{o}$C. In a second flask, the coupling agents HBTU (1 eq.) and HOBt (1 eq.) and the piperazine (5 eq.) were dissolved in dry DCM. Next, the coupling agents solution was added to the polymer dispersion in dry DCM at 0 $^{o}$C under stirring and DIPEA (1 eq.) was added to the system. The mixture was stirred at 0 $^{o}$C for 2 hours and at room temperature overnight. Then, the polymer was precipitated in ultra-pure water twice, washed with acidic water (pH = 2) and dried under high vacuum overnight. Deliverable: poly(2-Phenoxyethyl acrylate-co-1-(piperazin-1-yl)prop-2-en-1-one).

##### 4.2.2.3.3 LIPOIC ACID COUPLING

Coupling reaction between amine groups with lipoic acid. In a single-neck round-bottom flask, poly(2-Phenoxyethyl acrylate-co-1-(piperazin-1-yl)prop-2-en-1-one) was dissolved in dry DCM. In a second flask, the coupling agent DCC (2 eq.) and the lipoic acid (2 eq.) were dissolved in dry DCM and the system was cooled at 0 $^{o}$C. Subsequently, the polymer dispersion was added to the mixture of DCC and lipoic acid in dry DCM. Then, TEA (2 eq) was added to the system and the mixture was kept under stirring at 0 $^{o}$C for 2 hours and at room temperature overnight. After, the polymer was precipitated in ethanol, centrifuged twice and dried under high vacuum overnight. Deliverable: poly(2-Phenoxyethyl acrylate-co-1-(4-acryloylpiperazin-1-yl)-5-(1,2-dithiolan-3-yl)pentan-1-one).

#### 4.2.2.4 LINEAR BRUSHES POLYMER SYNTHESIS

The polymerization mixture containing 0.26 mmol HEBIB, 52 mmol PEA, 0.13 mmol $Me_6$TREN, 5 mL of acetone and 1g of anisole was prepared in a Schlenk flask and deoxygenized through freeze-pump-thaw cycles. Next, 0.13 mmol $Cu^{I}Br$, 0.00065 mmol $Cu^{II}Br_2$ were added to the system. The polymerization mixture was kept under stirring in an oil bath at 60 ºC. Using the integral of the NMR peak of anisole as a reference to calculate the conversion rate of monomers into polymer, the polymerization was interrupted after 53 % of conversion through $O_2$ bubbling in the polymerization mixture. The polymer was purified through a chromatography column with basic alumina and precipitated twice in cold hexane. Deliverable: poly(2-Phenoxyethyl acrylate).

#### 4.2.2.5 LINEAR BRUSHES POLYMER MODIFICATION

##### 4.2.2.5.1 LIPOIC ACID COUPLING

Coupling reaction between hydroxy groups (from HEBIB) and lipoic acid. In a single-neck round-bottom flask, poly(2-Phenoxyethyl acrylate) was dissolved in dry DCM. In a second flask, DCC (2 eq.), DMAP (2 eq) and lipoic acid (2 eq.) were dissolved in dry DCM and kept at 0 ºC. Next, the polymer dispersion was added to the DCC, DMAP and lipoic acid in dry DCM at 0 ºC. The system was kept under stirring 0 ºC for 2 hours and at room temperature overnight. The polymer was precipitated in ethanol twice and centrifuged. Deliverable disulfide-poly(2-Phenoxyethyl acrylate).

#### 4.2.2.6 $MoS_2$ EXFOLIATION

A Schott bottle containing 4g of $MoS_2$ and sealed with a septum was degassed under high vacuum and fulfilled with Ar three times. 25 mL of butyl-lithium solution (1.6 M in hexane) were added to the Schott bottle and the system was kept under stirring for 72 hours. Next, stirring was interrupted and the $MoS_2$ flakes were decanted. The excess of butyl-lithium solution was removed from the system through a syringe and neutralized in a solution of 2-propanol in heptane at 0 ºC, under inert atmosphere. The Schott bottle was unsealed and the hexane residue was evaporated. Next, 100 mL of ultra-pure water were added to the system and the $MoS_2$ intercalated with $Li^+$ was exfoliated in a ultrasonication bath for 1.5 hours. Finally, the material was centrifuged and washed twice with water and once with ethanol. Deliverable: 2D-$MoS_2$.

#### 4.2.2.6 2D-$MoS_2$ FUNCTIONALIZATION

In a single-neck round-bottom flask, 1g of polymer (linear brushes or loop-forming polymers) was dissolved in 50 mL of THF. Subsequently, 1g of 2D-$MoS_2$ was added to the system, which was kept under stirring for 24 hours. Next, the product (2D-$MoS_2$-interfacial brushes or 2D-$MoS_2$-interfacial loops) was centrifuged, washed three times with THF and dried under vacuum.

#### 4.2.2.7 COMPOSITE FABRICATION

The filler (2D-$MoS_2$ or 2D-$MoS_2$-interfacial brushes or 2D-$MoS_2$-interfacial loops) was added to a dispersion of 20 wt% of PSBS in THF to obtain 2.5 v% composites (considering filler density as 5.06 $g.cm^{-1}$). The dispersion was defoamed for 1 min at 2000 rpm in a planetary mixer (Thinky) and casted on a teflon mold. After drying, the composite films were submitted to a thermal treatment at 60, 100 or 150 $^oC$ for 1, 3 or 4.5 hours in a ventilated oven (Memmert).

#### 4.2.2.8 CHARACTERIZATION

DRIFTS spectra were recorded using a Bruker Tensor 27 equipment, with sample powders diluted in KBr (5 wt%). 2D-$MoS_2$/PSBS sample preparation for DRIFTS analysis: 2D-$MoS_2$ was added to a single-neck round-bottom flask, containing PSBS dissolved in DMF. The mixture was kept under stirring at 150 $^oC$ for 3 hours in an oil bath. Next, the reaction mixture was centrifuged and washed with THF three times. Finally, the powder 2D-$MoS_2$/PSBS was dried under vacuum overnight.

XPS analysis were carried out in a Quantera equipment, 200 μm spot, 55 eV PE. 2D-$MoS_2$/PSBS sample preparation for XPS analysis: 2D-$MoS_2$ (16 vol%, considering filler density 5.06 $g.cm^{-1}$) was added to a PSBS dispersion in THF (20 wt%). The solvent was evaporated and the composite was heat treated at 150 $^oC$ for 3 hours.

Mechanical tests were performed using a Shimadzu universal testing machine AGS-X, with a 10 N load cell. Dog bones were cut with $L_0$ of 16 mm.

Quasi-static tensile tests: dog bones were loaded at 30 $mm.min^{-1}$ until failure. Cyclic tensile tests up to 2 MPa: samples were loaded up to 2 MPa engineering stress at a loading rate of 30 $mm.min^{-1}$ and unloaded to 0.01 MPa engineering stress at unloading rate of 5 $mm.\ min^{-1}$. Incremental cyclic tensile tests: samples were loaded increasing 0.1 MPa engineering stress each cycle at loading rate of 30 $mm.min^{-1}$ and unloaded to 0.1 MPa engineering stress every cycle at unloading rate of 5 $mm.min^{-1}$.

1H-NMR spectra were recorded using a 300 MHz Bruker Avance III spectrometer.

## 4.3 RESULTS AND DISCUSSION

Exfoliated 2D-$MoS_2$ particles are obtained by wet chemical intercalation of bulk $MoS_2$ particles with $Li^+$ ions in a butyl-lithium/hexane solution under inert atmosphere followed by solvent removal and ultrasonication treatment in water (Figure 4.1a). Such wet chemical intercalation process is widely employed to prepare few-layer 2D-$MoS_2$ particles and result in the formation of sulfur vacancies that can be explored for surface functionalization with sulfur-containing organic molecules that allows for modulation of their chemical properties.[13–17] The highly electron donating nature of Li provides the driving force for the intercalation through a charge transfer reaction that overcomes the van der Waals interactions between the layers.[18] Effective exfoliation of bulk $MoS_2$ into few-layer 2D-$MoS_2$ takes place through the generation of $H_2$ bubbles during the hydrolysis when $Li^+$ ions are in contact with water in the ultrasonic bath.[18–22] The exposed sulfur atoms on the surface of the 2D-$MoS_2$ can be explored to form C-S bonds with organic molecules through a local vulcanization reaction, as illustrated in Figure 4.1b.[23,24] By casting a mixture of 2D-$MoS_2$ particles dispersed in a polystyrene-block-polybutadiene-block-polystyrene (PSBS) solution in THF into a mold, followed by drying and thermal treatment at 150 $^oC$ (Figure 4.1c), we expect that the PSBS chains attach covalently on the surface of the 2D-$MoS_2$ through an interfacial vulcanization process resulting from the reaction of the double bonds of the polybutadiene block with the sulfur atoms of the 2D-$MoS_2$. Such interfacial vulcanization process might lead to the formation of polymer loops on the surface of the 2D-$MoS_2$ that can entangle with PSBS chains of the polymer matrix, as depicted in Figure 4.1b. The formation of these interfacial loop-chain entanglements ensures an efficient transference of stresses from the matrix to the reinforcing elements and can potentially generate additional mechanisms of energy dissipation and elastic recovery through molecular friction when the composite material is subjected to mechanical loads.

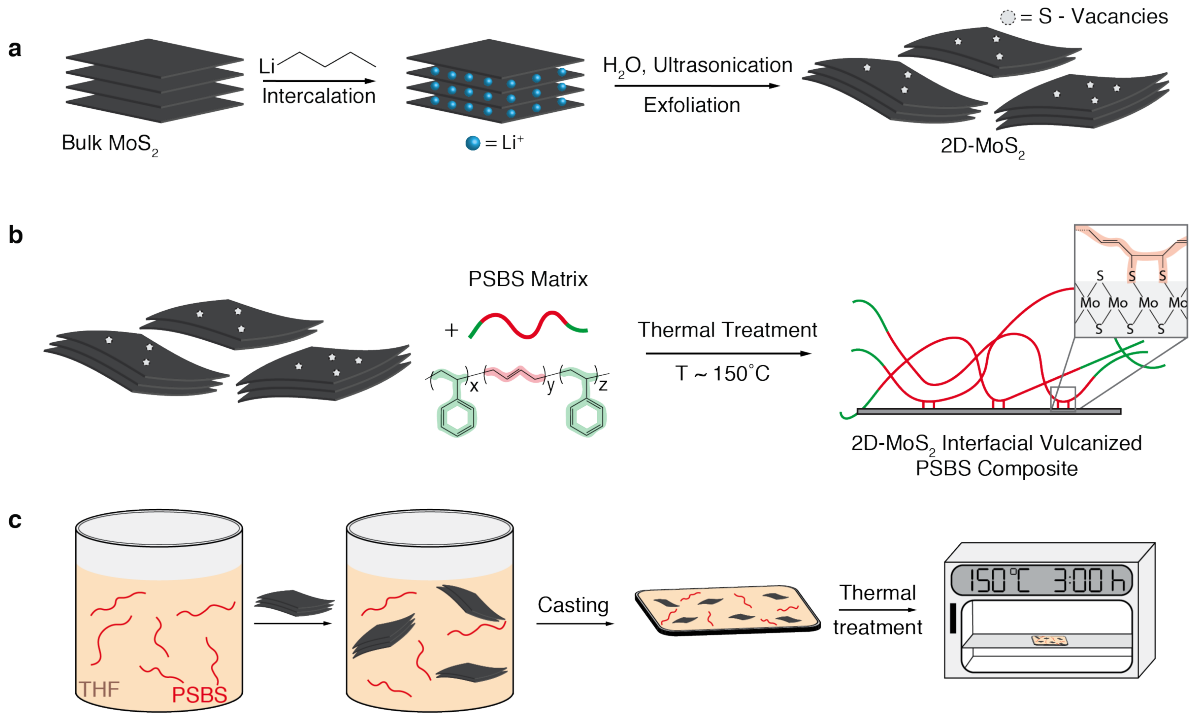


**Figure 4.1.** (a) Bulk $MoS_2$ is chemically exfoliated by $Li^+$ intercalation and ultrasonication in water to yield few-layer 2D-$MoS_2$; (b) 2D-$MoS_2$ reacts with double bonds of the polybutadiene block of PSBS in a thermally-activated interfacial vulcanization; (c) Schematics illustrating the process to obtain 2D-$MoS_2$-composites with interfacial vulcanization: 2D-$MoS_2$ addition to a dispersion of PSBS in THF, casting into a mold and solvent evaporation and thermal treatment in an oven at 150 °C for 3 hours.

Evidence for the covalent attachment of PSBS chains on the surface of the 2D-$MoS_2$ through the formation of C-S bonds is revealed by Diffuse Reflectance Infrared Fourier Transform Spectroscopy (DRIFTS) and shown in Figure 4.2. Given the relatively low concentration of 2D-$MoS_2$ particles dispersed within the composite (2.5 vol%) and to enhance the radiation absorption of chemical bonds formed at the interface, we have functionalized 2D-$MoS_2$ particles with PSBS in solution (2D-$MoS_2$/PSBS sample preparation for DRIFTS analysis, section 4.2.2.8). After heat treatment in solution at 150 °C for 3h and solvent removal, the resulting powder was diluted in KBr (5 wt%) and the DRIFTS spectrum acquired. The appearance of the IR absorption bands at 700 $cm^{-1}$ and 1020 $cm^{-1}$ for the sample exposed to PSBS indicates the formation of the C-S bond that results from the interfacial vulcanization process (Figure 4.2a and b).[25] Strikingly, X-ray Photoelectron Spectroscopy (XPS) analysis carried out on composites containing 16 vol% 2D-$MoS_2$ (2D-$MoS_2$/PSBS sample preparation for XPS analysis, section 4.2.2.8) does not indicate significant changes in the chemical state of sulfur atoms after heat treatment at 150 °C for 3 hours (Figure C.7, Appendix C). Similar XPS and FT-IR results were obtained by Gonçalves and co-workers for the functionalization of 2D-$MoS_2$ with polybutadiene.[24] Although XPS analysis appears to not corroborate the results obtained by FT-IR, the authors observed

the formation of a 30 nm-thick layer on the disulfide-rich edges of 2D-$MoS_2$, which suggests the covalent attachment of polybutadiene chains on the surface of the 2D-$MoS_2$ through the formation of C-S bonds.

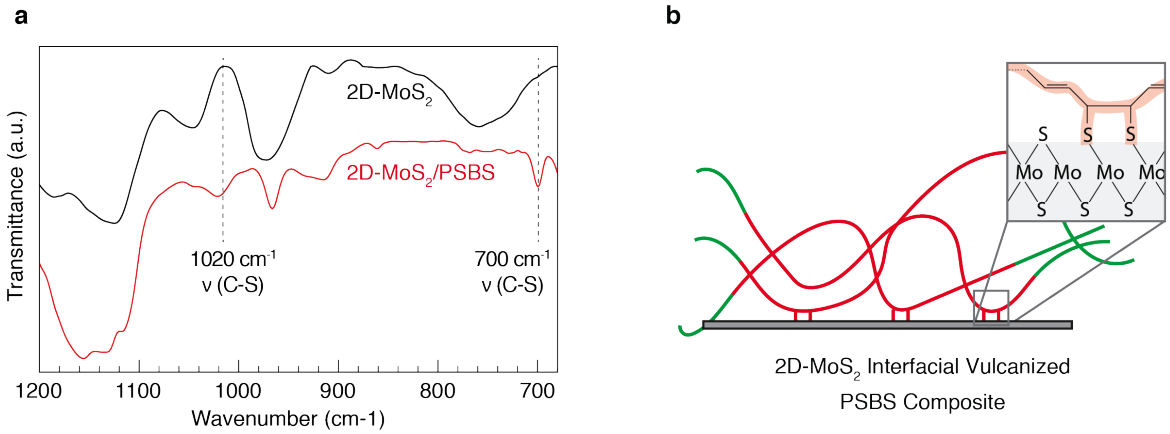


**Figure 4.2.** (a) DRIFTS spectra of 2D-$MoS_2$ and 2D-$MoS_2$/PSBS showing the appearance of the bands at 1020 $cm^{-1}$ and 700 $cm^{-1}$ after thermal treatment, suggesting the C-S bond formation; (b) Schematic representation of interfacial vulcanization process that takes place between exposed S atoms from the 2D-$MoS_2$ and C=C bonds from the polybutadiene block from PSBS.

The effective reinforcement of the continuous PSBS phase with 2D-$MoS_2$ particles requires a strong interfacial bonding between the polymer matrix and the reinforcing particles. Such strong bonding enables stress transfer from the continuous polymeric phase to the discontinuous reinforcing elements during mechanical loading. The formation of the C-S covalent bond through an interfacial vulcanization process is expected to enhance the stress transfer at the interface and improve the mechanical performance of the 2D-$MoS_2$-reinforced-PSBS. Vulcanization of rubber-based materials using elemental sulfur is a thermally-activated chemical process that usually occurs with reasonably fast curing rates at temperatures starting at 140 °C.[26] The mechanical performance under quasi-static loading condition of PSBS composites reinforced with 2.5 vol% of 2D-$MoS_2$ is summarized in Figure 4.3. Despite the addition of reinforcing elements to the PSBS matrix, composites that are heat treated at 60 °C do not show a significant increase in mechanical properties (Figure 4.3a). This is a clear evidence of the weak interfacial bonding between the 2D-$MoS_2$ particles and the PSBS matrix. In contrast, enhanced mechanical performance due to stronger interfacial bonding is evident for composites that are vulcanized at 150 °C as compared to the pure PSBS matrix (Figure 4.3b, Figures C.8 and C.9, Appendix C). The elastic modulus of such vulcanized composites increases 56% and 14% as compared to that of the PSBS matrix heat treated at the same temperature (150 °C) and the composite heat treated at 60 °C, respectively (Figure 4.3c). However, as the interfacial vulcanization process

leads to the formation of crosslinking points between the continuous PSBS matrix and the 2D-$MoS_2$ particles, the stress and the strain at failure reduces from 31.6 MPa and 16.9 in composites heat treated at 60 °C to 10.0 MPa and 11.4, respectively, for those heat treated at 150 °C (Figure 4.3a, b and c). Remarkably, the modulus of toughness and the stress at failure of the composites increase concomitantly, reaching values that are 1.5-fold and 1.2-fold higher than those of the PSBS matrix when heat treated at 60 °C and 3.7-fold and 3.4-fold higher when heat treated ate 150 °C (Figure 4.3d). Such concomitant increase in strength and toughness is not typically observed in reinforced composites[27] and might have its origins on the molecular friction generated during mechanical loading in the interfacial loop-chain entanglements.

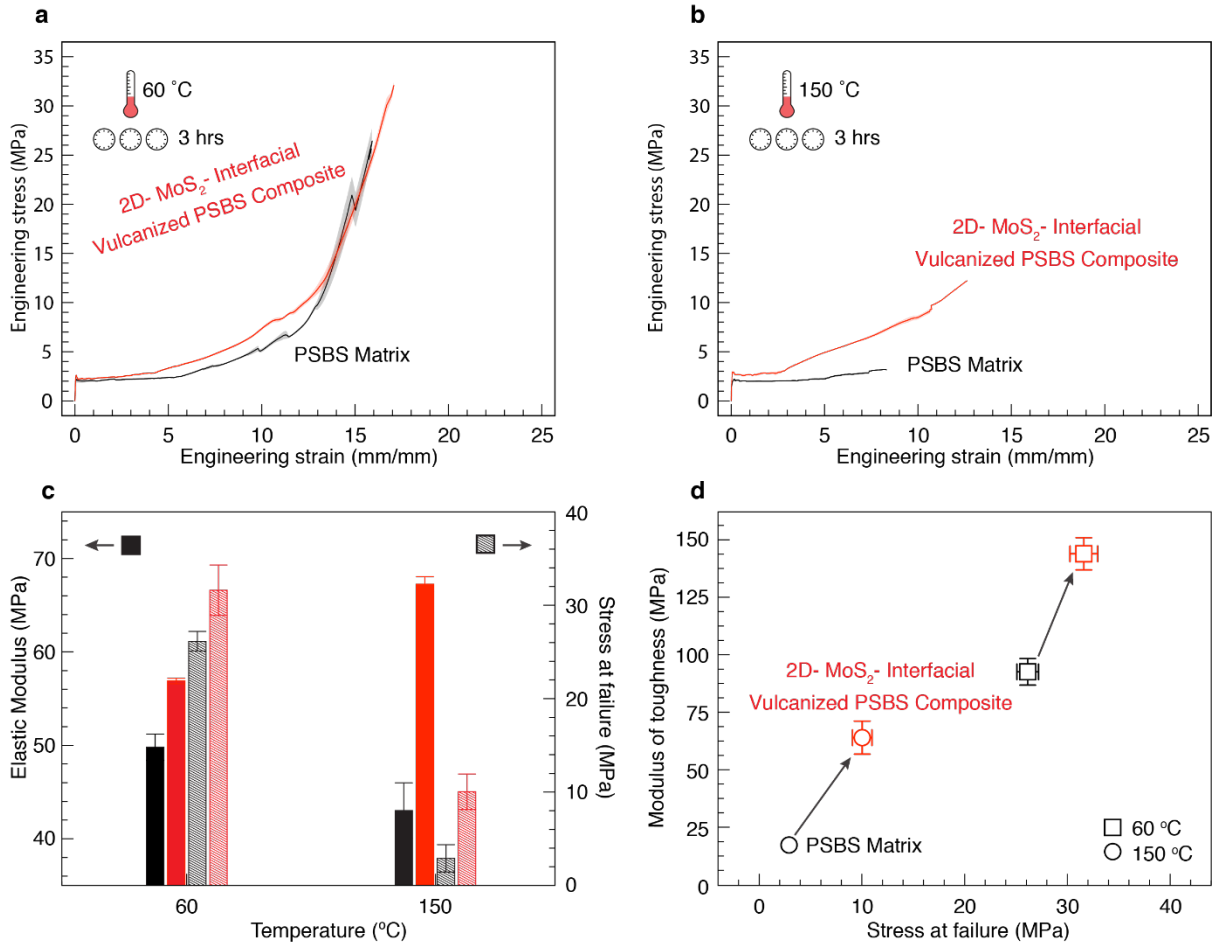


**Figure 4.3.** Quasi-static engineering stress versus engineering strain curves of PSBS matrix (black) and 2D-$MoS_2$-vulcanized PSBS composite (red) after thermal treatment for three hours at (a) 60 °C and (b) 150 °C; (c) Elastic modulus (full bars) and stress at failure (slashed bars) of PSBS matrix and 2D-$MoS_2$-vulcanized PSBS composite after thermal treatment at 60 °C and 150 °C for three hours; (d) Modulus of toughness versus stress at failure of PSBS matrix and 2D-$MoS_2$-vulcanized PSBS composite after heat treatment at 60 °C and 150 °C.

To obtain additional evidences for the enhancement of the mechanical performance of composites through architectural control of interfaces, we designed

and synthesized polymers bearing disulfide moieties with controlled molecular architectures (Figure 4.4a and b). These disulfide groups can react with the sulfur vacancies generated during the wet chemical exfoliation to yield functionalized 2D-$MoS_2$ particles, as illustrated in Figure 4.4c and d.[13–16] To induce the formation of interfacial loops similar to those that might be generated in the 2D-$MoS_2$-reinforced PSBS composites through interfacial vulcanization, a random block copolymer containing disulfide and 2-phenoxyethyl pending groups (Figure 4.4a; 5 mol% in disulfide pending groups) was synthesized by Atom Transfer Radical Polymerization (ATRP). A second polymer containing only 2-phenoxyethyl pending groups and functionalized in one of the chain ends with lipoic acid (disulfide group) was also prepared and characterized (Figure 4.4b). Details about polymers synthesis, purification, modification and structural elucidation by NMR spectroscopy can be found in the Experimental Section and in the Appendix C (Figures C.1, C.2, C.3, C.4, C.5 and C.6). While the block-copolymer containing disulfide pending groups is expected to yield interfacial loops similar to those obtained through interfacial vulcanization of PSBS in the presence of 2D-$MoS_2$ particles (Interfacial Loops, Figure 4.4c), the polymer functionalized with disulfide group at one of the chain ends is expected to form an interfacial architecture in which the polymer chains extend linearly away from the 2D-$MoS_2$ particles surface (Interfacial Brushes, Figure 4.4d). The surface functionalization is carried out by dispersing 2D-$MoS_2$ particles in a mixture containing excess of the architectured polymer in THF for 24 hours followed by washing and drying. As shown in Figure 4.4e, DRIFTS spectra acquired after surface functionalization reveal the appearance of an absorption band at 1732 $cm^{-1}$, which is characteristic of stretching of the C=O bond present in the molecular structure of the architectured polymers. These results indicate that functionalization of 2D-$MoS_2$ particles with both architectured polymers is achieved through the reaction between the disulfide groups in the polymer chain and the sulfur vacancies on the surface of 2D-$MoS_2$ particles.

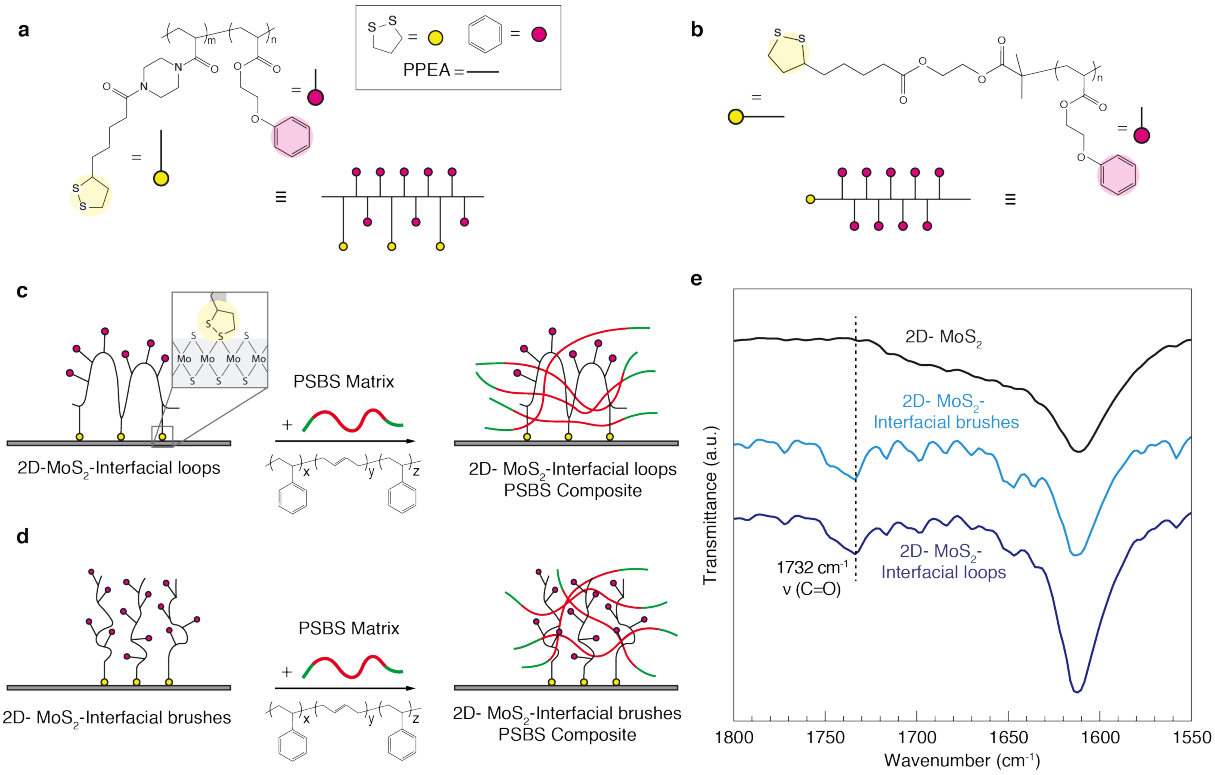


**Figure 4.4.** Architectural control of interfaces. (a) Random block copolymer containing disulfide and 2-phenoxyethyl pending groups; (b) Polymer containing 2-phenoxyethyl pending groups and a disulfide group in one of the chain ends; (c) Disulfide pending groups react with sulfur vacancies, forming interfacial loops on the surface of 2D-$MoS_2$; (d) Disulfide-ended polymer reacts with sulfur vacancies, yielding interfacial brushes on the surface of 2D-$MoS_2$; (e) DRIFTS spectra of 2D-$MoS_2$ and 2D-$MoS_2$ functionalized with architectured polymers.

Although both architectured polymers are expected to increase the interfacial interactions between 2D-$MoS_2$ particles and the PSBS matrix, we hypothesize that the loop and linear interfacial architectures might result in distinct mechanical behavior when the composites are subjected to cyclic mechanical tests. Provided that loops are indeed formed at the interface and entangle with the polymer chains of the bulk PSBS, molecular events such as suppressed chain sliding and mechanical interlocking between entangled chains that derives from the interfacial stress transfer during mechanical loading can potentially dissipate more energy and enhance elastic recovery as compared to those of the linear interfacial architecture. As a result, composites with loop-chain interfacial entanglements are expected to exhibit enhanced energy dissipation and elastic recovery during loading-unloading events in cyclic tests, as compared to those in which chain-chain entanglements dominates the interfacial interactions. To quantify the energy dissipation and elastic recovery of the composites exhibiting different interfacial architectures, we carried out two cyclic tests (Figure 4.5). First, samples are subjected to multiple loading-unloading cycles to a maximum applied stress of 2 MPa (Figure 4.5a, b and c). The residual strain after each

cycle as a function of the number of cycles is presented in Figure 4.5b and the accumulated dissipated energy is calculated by adding the individual integrals of the areas under the loading-unloading cycles and is plotted as a function of the number of cycles in Figure 4.5c. In the second cyclic test, loading and unloading cycles with increasing increments of stress of 0.1 MPa are applied in tensile mode until the failure of the sample (Figure 4.5d, e and f). The residual strain and the accumulated dissipated energy are plotted as a function of number of cycles in Figure 4.5 e and f, respectively.

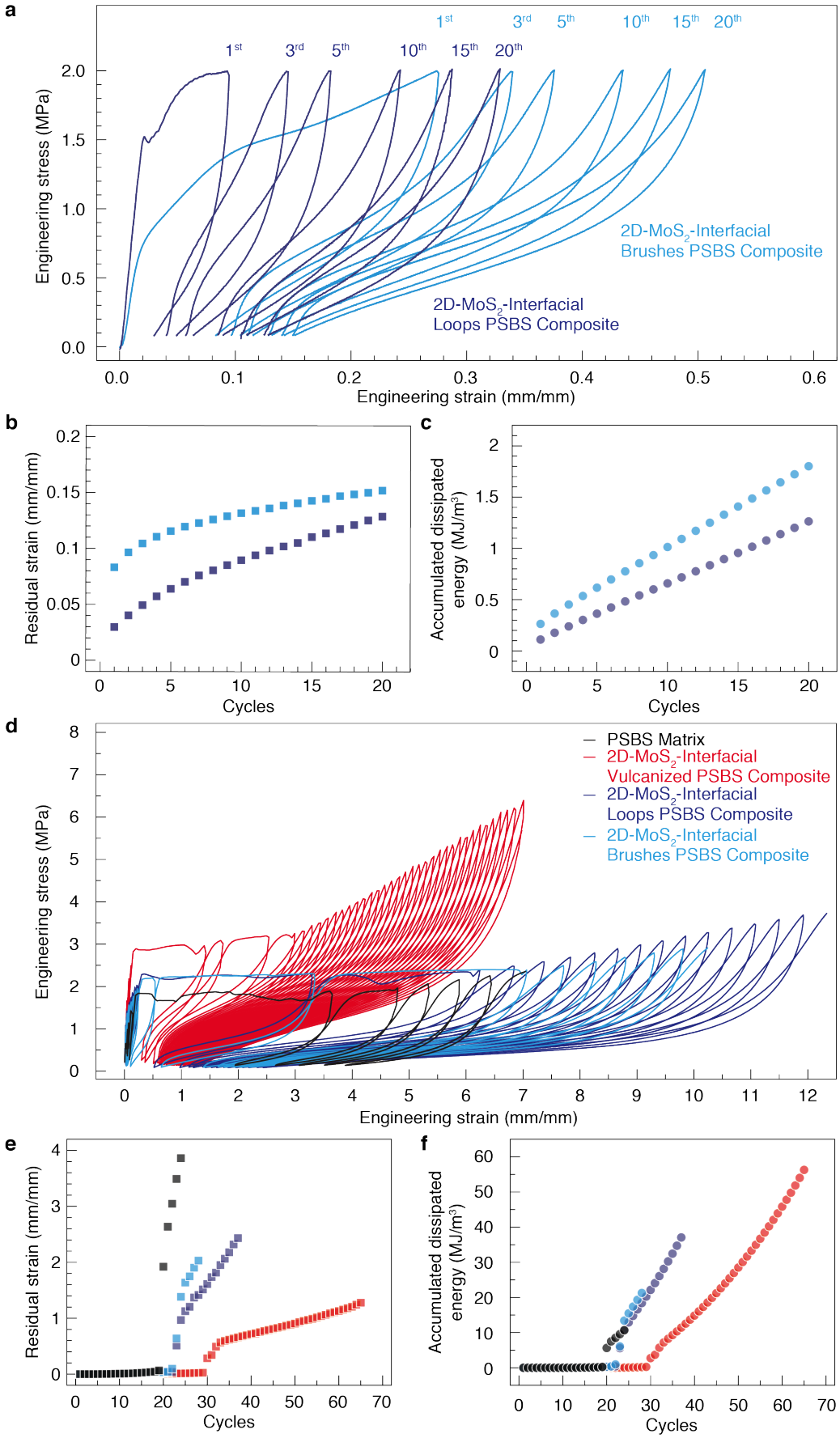


**Figure 4.5.** Cyclic tensile tests up to 2 MPa and incremental cyclic tensile tests. (a) Engineering stress versus engineering strain curves; (b) Residual strain versus number of cycles; and (c) Accumulated

dissipated energy versus number of cycles of cyclic tensile tests up to 2 MPa; (d) Engineering stress versus engineering strain curves; (e) Residual strain versus number of cycles; and (f) Accumulated dissipated energy versus number of cycles of incremental cyclic tensile tests, increasing engineering stress by 0.1 MPa every cycle.

The effective formation of loop-chain entanglements at the interface between the bulk PSBS matrix and the 2D-$MoS_2$ particles is expected to affect the mechanical behavior of the composites. Surprisingly, composites modified with interfacial brushes and loops exhibit very similar stress-strain curves when tested in quasi-static mode (Figure C.10, Appendix C). This observation suggests that the interfacial shear strength resulting from the coupling between the chains of the PSBS matrix with the modified 2D-$MoS_2$ surfaces exhibits comparable values for loop-chain and chain-chain entanglements. Given the predominant composition of both surface modifiers with 2-phenoxyethyl acrylate monomers, one can expect comparable molecular interactions occurring at the interfaces formed by loop-chain and chain-chain entanglements. However, the elastic recoverability of composites functionalized with polymer loops (purple curve, Figure 4.5a and b) is markedly increased as compared to those containing polymer brushes when tested in cyclic mode (light blue curve, Figure 4.5a and b). In this series of cyclic tests, the composites are subjected to a sequence of loading-unloading events with a maximum stress that is close to their yield point (2 MPa). As illustrated in Figure 4.5b, the formation of interfacial loop-chain entanglements (purple curve) leads to a significant reduction in the residual strain after each loading-unloading cycle when compared to chain-chain entanglements (light blue curve). The relative reduction in residual strain starts at 64% in the first cycle and decreases to 15% in cycle $20^{th}$. This surprising increase in elastic recovery probably results from the enhanced molecular mechanical interlocking provided by the loop-chain entanglements, which suppresses chain sliding and, thus, decreases the interfacial plastic deformation. The higher is the number of loading-unloading cycles applied to the material, the higher is the number of ruptured loop-chain entanglements, which leads to the asymptotic reduction in relative residual strain with increasing number of cycles when comparing the composites functionalized with polymer brushes and loops. Because of the enhanced elastic recovery and decreased plastic deformation in the interfacial loop composite (purple curve) due to mechanical interlocking and suppress of chain sliding, the dissipated energy of such composite in the $1^{st}$ cycle corresponds to 42% of the dissipated energy of the interfacial brush composite (light blue curve), Figure 4.5c. However, as a consequence of the loop-chain entanglement ruptures with increasing number of loading-unloading cycles during

the cyclic tensile test, the accumulated dissipated energy of the interfacial loop composite reaches 70% of the value for interfacial brush composite in the 20$^{th}$ cycle.

The mechanical performance exhibited by both composites during the second type of the loading-unloading tests (incremental cyclic test) reveals similar elastic recovery and energy dissipation behavior with increasing number of cycles (light blue and purple curves shown in Figure 4.5d, e and f). Remarkably, composites functionalized with interfacial loops (purple curve) withstand a number of cycles before failure that is 32% higher than the maximum number of cycles exhibited by composites presenting interfacial brushes (light blue curve). The residual strain as a function of the number of cycles shows the loop-chain entanglements lead to an improved elastic recovery also for the interfacial vulcanized composites (red curve), Figure 4.5e. The difference in absolute values of residual strain among interfacial loops (purple curve) and interfacial vulcanized composites (red curve) might reside on the concentration of loop-chain entanglements and the chemistry nature of the polymers at the interface. In the interfacial vulcanized composites, the PSBS chains entangled during composite preparation prior to heat treatment, presumably leading to a higher entanglement degree. Besides, interfacial vulcanized composite presents loop-chain entanglements of PSBS-PSBS, while in interfacial loops composite the chemical composition of such interfacial architecture is poly(2-phenoxyethyl acrylate)-PSBS.

Despite the similar mechanical performance exhibited by both composites in the initial part of the loading-unloading test, the higher number of cycles before failure observed for composites functionalized with interfacial loops (purple curve) leads to an accumulated dissipated energy that is 0.74-fold higher than that of the composite functionalized with interfacial brushes (light blue curve), Figure 4.5d and f. The similar slopes exhibited by both composites in Figure 4.5f (light blue and purple curves) suggest that interfacial loop-chain entanglements for this specific molecular configuration do not lead to an enhanced mechanism of energy dissipation through molecular friction. However, the formation of loop-chain entanglements at the interface seems to result in a more effective molecular mechanical interlocking than that provided by chain-chain entanglements as evidenced by the higher maximum number of cycles presented by composites functionalized with interfacial loops. As expected, the strong reinforcing effect obtained by the interfacial vulcanization (red curve) process increases even further the accumulated dissipated energy. When compared with the composites functionalized with interfacial brushes and loops, the maximum energy dissipation during the cycling loading increases from 21.3 MJ/m$^3$

and 37.1 $MJ/m^3$, respectively, to 56.3 $MJ/m^3$ for the same volume fraction of reinforcing particles. Interestingly, the composite with vulcanized interfaces presents clear transitions in accumulated dissipated energy curve, which is represented by the changes in the slope of the red curve, Figure 4.5f. Between the yield point (cycle $29^{th}$) and the onset of the strain hardening, the composite exhibits a deformation behavior that resembles that of the PSBS matrix (black curves, Figure 4.5d and f). In this region, the slope seems to slowly reduce as more strain is applied in the material. When the applied strain reaches the strain hardening region (cycle $34^{th}$ onwards), the slope of the curve starts to slowly increase again. These observations suggest that different deformation mechanisms are contributing to the overall energy dissipation during the mechanical loading of these materials. Because the interfacial vulcanization process can lead to covalent anchoring of polymer chains on multiple bonding sites on the surface of the 2D-$MoS_2$ particles, a selective strengthening of the interfacial material might occur due to a localized increase in the apparent crosslinking density. Therefore, during the initial stage of plastic deformation, the bulk polymer matrix can deform at a larger extent as compared to the interfacial material. As more deformation is applied and the onset of the strain hardening is approached, the stresses transferred from the bulk matrix to the interface material through the loop-chain entanglements are sufficiently high to promote the deformation and extension of the interfacial material. At this point, stretching of the polymer loops and efficient molecular mechanical interlocking through loop-chain entanglements starts to contribute to the overall energy dissipation, causing the observed increase in the slope of the red curve in Figure 4.5f. Assuming that the interfacial vulcanization process leads to a higher density of covalent anchoring points of the polymer chains, this deformation model can be used to explain the pronounced strain hardening effect observed in vulcanized composites as compared to those functionalized with interfacial loops. Overall, the cyclic mechanical tests provide evidences that support the formation of loop-chain entanglements both in the composite functionalized with polymer loops as well as in the composite that underwent an interfacial vulcanization process. Such loop-chain entanglements seem to suppress chain sliding and increase elastic recoverability thanks to a more efficient molecular mechanical interlocking between polymer chains.

## 4.4 CONCLUSIONS

The formation of interfacial loop-chain entanglements in PSBS composites reinforced with 2D-$MoS_2$ particles in an interfacial vulcanization process leads to materials with enhanced stiffness, strength and elastic recovery thanks to an effective

molecular mechanical interlocking between the polymer chains present in the matrix and on the surface of 2D-$MoS_2$ particles. FT-IR measurements in DRIFTS mode reveal that the surface of 2D-$MoS_2$ particles is successfully functionalized through the covalent attachment of PSBS chains and surface modifiers capable of forming interfacial brushes and loops. The interfacial vulcanization process occurs between the double-bonds of the polybutadiene block of the PSBS matrix and the exposed sulfur on the surface of the 2D-$MoS_2$ particles whereas the functionalization with model polymer chains takes place by the reaction between disulfide groups and sulfur vacancies that are originated during the wet-chemical exfoliation process. Quasi-static mechanical tests provide evidence of the thermally-activated vulcanization process that occurs at the matrix-reinforcing particle interface. Vulcanized composites obtained through this method exhibit elastic modulus, strength-at-failure and ductility that are 56 %, 244 % and 54 % higher than the PSBS matrix prepared in the same conditions. The heat treatment required to activate the interfacial vulcanization process impairs the ductility of the PSBS matrix, which is reduced from 15.5 mm/mm to 7.4 mm/mm. Such reduction is probably caused by thermo-oxidative degradation that typically occurs in similar materials when subjected to thermal treatment.[28] Cyclic tests performed on model composites functionalized with interfacial brushes and loops reveals that loop-chain entanglements lead to an increased material's elastic recovery. The reduction of residual strain upon cyclic loading exhibited by composites functionalized with interfacial loops reaches values of up to 64% as compared to those containing interfacial brushes. Vulcanized composites seem to undergo a selective strengthening of the interfacial material due to the covalent attachment of PSBS chain on multiple surface binding sites of the 2D-$MoS_2$ particles. Such selective strengthening shields deformation away from the interface at applied strains up to the onset of the strain hardening region. Consequently, the contribution to the energy dissipation upon mechanical loading in the first stage of the deformation process seems to be dominated by the mechanical properties of the polymer matrix. Once the applied strain approaches the strain hardening region, stretching of the interfacial loops through a molecular mechanical interlocking provides an additional contribution to the energy dissipation mechanism. These findings demonstrate the benefits of applying an interfacial design approach as a tool to further enhance the mechanical performance of discontinuous composite materials. We envision that the design of interfacial loop-chain entanglements that can favor chain sliding while still promoting mechanical interlocking at high applied strains can further boost the energy dissipation upon deformation in composite materials.

## 4.5 REFERENCES

1. Pukánsky, B. Influence of Interface Interaction on the Ultimate Tensile Properties of Polymer Composites. Composites 2012, 21 (3), 255–262.

2. Jesson, D. A.; Watts, J. F. The Interface and Interphase in Polymer Matrix Composites: Effect on Mechanical Properties and Methods for Identification. Polym. Rev. 2012, 52 (3–4), 321–354.

3. Samyn, P. Engineering the Cellulose Fiber Interface in a Polymer Composite by Mussel-Inspired Adhesive Nanoparticles with Intrinsic Stress-Sensitive Responsivity. ACS Appl. Mater. Interfaces 2020, 12 (25), 28819–28830.

4. Ramakrishna, S.; Mayer, J.; Wintermantel, E.; Leong, K. Biomedical Applications of Polymer-Composite Materials: A Review. Compos. Sci. Technol. 2001, 61, 1189–1224.

5. Liu, Y.; Du, H.; Liu, L.; Leng, J. Shape Memory Polymers and Their Composites in Aerospace Applications: A Review. Smart Mater. Struct. 2014, 23 (2).

6. Pendhari, S. S.; Kant, T.; Desai, Y. M. Application of Polymer Composites in Civil Construction: A General Review. Compos. Struct. 2008, 84 (2), 114–124.

7. Song, N.; Gao, Z.; Li, X. Tailoring Nanocomposite Interfaces with Graphene to Achieve High Strength and Toughness. Sci. Adv. 2020, 6 (42).

8. Rong, M. Z.; Zhang, M. Q.; Ruan, W. H. Surface Modification of Nanoscale Fillers for Improving Properties of Polymer Nanocomposites: A Review. Mater. Sci. Technol. 2006, 22 (7), 787–796.

9. Bonderer, L. J.; Studart, A. R.; Gauckler, L. J. Bioinspired Design and Assembly of Platelet Reinforced Polymer Films. Science (80-. ). 2008, 319, 1069–1073.

10. Gorga, R. E.; Lau, K. K. S.; Gleason, K. K.; Cohen, R. E. The Importance of Interfacial Design at the Carbon Nanotube/Polymer Composite Interface. J. Appl. Polym. Sci. 2006, 102 (2), 1413–1418.

11. Libanori, R.; Carnelli, D.; Rothfuchs, N.; Binelli, M. R.; Zanini, M.; Nicoleau, L.; Feichtenschlager, B.; Albrecht, G.; Studart, A. R. Composites Reinforced via Mechanical Interlocking of Surface-Roughened Microplatelets within Ductile and Brittle Matrices. Bioinspiration and Biomimetics 2016, 11 (3).

12. Xia, S.; Wang, Z.; Chen, H.; Fu, W.; Wang, J.; Li, Z.; Jiang, L. Nanoasperity: Structure Origin of Nacre-Inspired Nanocomposites. ACS Nano 2015, 9 (2), 2167–2172.

13. Jeong, M.; Kim, S.; Ju, S. Y. Preparation and Characterization of a Covalent Edge-Functionalized Lipoic Acid-$MoS_2$ Conjugate. RSC Adv. 2016, 6 (43), 36248–36255.

14. Chen, X.; McDonald, A. R. Functionalization of Two-Dimensional Transition-Metal Dichalcogenides. Adv. Mater. 2016, 28 (27), 5738–5746.

15. Presolski, S.; Pumera, M. Covalent Functionalization of $MoS_2$. Mater. Today 2016, 19 (3), 140–145.

16. Stergiou, A.; Tagmatarchis, N. Molecular Functionalization of Two-Dimensional MoS Nanosheets 2 Dr. Chem. - A Eur. J. 2018, 24 (69), 18246–18257.

17. Canton-vitoria, R.; Sayed-ahmad-baraza, Y.; Pelaez-fernandez, M.; Arenal, R.; Ewels, C. P.; Tagmatarchis, N. Functionalization of MoS 2 with 1 , 2-Dithiolanes : Toward Donor- Acceptor Nanohybrids for Energy Conversion. npj 2D Mater. Appl. 2017, No. January, 1–8.

18. Zhou, J.; Lin, Z.; Ren, H.; Duan, X.; Shakir, I.; Huang, Y.; Duan, X. Layered Intercalation Materials. Adv. Mater. 2021, 33, 2004557–2004557.

19. Fan, X.; Xu, P.; Zhou, D.; Sun, Y.; Li, Y. C.; Nguyen, M. A. T.; Terrones, M.; Mallouk, T. E. Fast and Efficient Preparation of Exfoliated 2H $MoS_2$ Nanosheets by Sonication-Assisted Lithium Intercalation and Infrared Laser-Induced 1T to 2H Phase Reversion. Nano Lett. 2015, 15 (9), 5956–5960.

20. Jawaid, A.; Nepal, D.; Park, K.; Jespersen, M.; Qualley, A.; Mirau, P.; Drummy, L. F.; Vaia, R. A. Mechanism for Liquid Phase Exfoliation of $MoS_2$. Chem. Mater. 2016, 28 (1), 337–348.

21. Zhang, Q.; Mei, L.; Cao, X.; Tang, Y.; Zeng, Z. Intercalation and Exfoliation Chemistries of Transition Metal Dichalcogenides. J. Mater. Chem. A 2020, 8 (31), 15417–15444.

22. Gordon, R. A.; Yang, D.; Crozier, E. D.; Jiang, D. T.; Frindt, R. F. Structures of Exfoliated Single Layers of WS2, $MoS_2$, and MoSe2 in Aqueous Suspension. Phys. Rev. B - Condens. Matter Mater. Phys. 2002, 65 (12), 1254071–1254079.

23. Stergiou, A.; Tagmatarchis, N. Molecular Functionalization of Two-Dimensional $MoS_2$ Nanosheets. Chem. - A Eur. J. 2018, 24 (69), 18246–18257.

24. Gonçalves, R. H.; Fiel, R.; Soares, M. R. S.; Schreiner, W. H.; Silva, C. M. P.; Leite, E. R. Single-Step Exfoliation and Covalent Functionalization of $MoS_2$Nanosheets by an Organosulfur Reaction. Chem. - A Eur. J. 2015, 21 (44), 15583–15588.

25. Zhou, L.; He, B.; Yang, Y.; He, Y. Facile Approach to Surface Functionalized $MoS_2$ Nanosheets. RSC Adv. 2014, 4 (61), 32570–32578.

26. Kurian, T.; George, K. E. Effect of Vulcanization Temperature on the Technical Properties of NR, SBR, and BR. J. Appl. Polym. Sci. 1989, 37 (4), 987–997.

27. Ritchie, R. O. The Conflicts between Strength and Toughness. Nat. Mater. 2011, 10 (11), 817–822.

28. Guo, L.; Huang, G.; Zheng, J.; Li, G. Thermal Oxidative Degradation of Styrene-Butadiene Rubber (SBR) Studied by 2D Correlation Analysis and Kinetic Analysis. J. Therm. Anal. Calorim. 2014, 115 (1), 647–657.

# Chapter 5

## CONCLUSIONS

Surface modification is a powerful tool to adjust chemical composition, morphology and properties of materials. In this thesis, "grafting from" and "grafting to" approaches were combined with ATRP method to understand the mechanism of $Zn^0$ SI-ATRP and functionalize natural fibers, fabricate polymer-based 3D graded materials through $Cu^0$ SI-ATRP and decorate 2D-$MoS_2$ particles with architectured polymers to modulate the interface of polymer matrix composites.

The mechanism of $Zn^0$ SI-ATRP was explored through the functionalization of $SiO_x$ controlled substrates with POEGMA and PMMA. $Zn^0$ acts as a reducing agent, consuming $O_2$ dissolved in the reaction mixture, forming $Zn^{II}O$. Concomitantly, $Cu^{II}Br_2$/L deactivator species are reduced to $Cu^{I}Br$/L activator species, which diffuse through the reaction medium, reach the initiator and trigger controlled polymerization. Moreover, $Zn^0$ acts as a supplemental activator, combines with the ligand, triggers polymerization and provides $ZnBr_2$/L. $Zn^0$ SI-ATRP is an inexpensive versatile method to modify planar inorganic supports with chemically different polymers such as acrylates, methacrylates, polyamides and styrene, under ambient conditions, using microliters of polymerization mixture and compatible with both Cu- and Fe-based catalysts. Furthermore, $Zn^0$ SI-ATRP enabled the controlled functionalization of cotton-based fabrics with POEGMA brushes, which grew thicker over time, without the need of lengthy deoxygenation procedures. These findings contribute to the development of new strategies to perform oxygen-tolerant ATRP and translates fundamental research into technologically relevant applications.

In $Cu^0$ SI-ATRP approach, the grafting density is a function of the distance between the ATRP initiator and the reducing agent ($Cu^0$). Such feature was explored and $Cu^0$ SI-ATRP successfully enabled the surface modification of 3D elastomeric supports, yielding graded polymer-based materials. A polyHIPE containing ATRP initiator in its structure was fabricated through FRP and used as a scaffold to obtain single and multiple gradients. A polymerization mixture containing monomer, solvent and a Cu-based catalyst was dropped on the surface of a previously activated $Cu^0$ plate and the polyHIPE was placed in contact with it. The polyHIPE acted as a microporous scaffold, with tunable chemical composition and morphology, according to the

monomer used during the functionalization (OEGMA, NIPAM, HEMA). PolyHIPEs were functionalized with single gradients of POEGMA and PNIPAM, and double gradients of POEGMA-PHEMA. ATR-IR and SEM analysis revealed the chemical and morphological gradients extension, which is mainly a function of the ATRP kinetics of each system and the diffusion of Cu-based species through the foam. This work contributes to the development of $Mt^0$ SI-ATRP method to fabricate 3D structures, with single and multiple gradients and high control over chemical composition and morphology in oxygen tolerant systems. Furthermore, these outcomes set the scene for the upscaled production of multidimensional graded materials without the need of deoxygenation procedures in industries.

Interfacial vulcanization was triggered at the interface of 2D-$MoS_2$-reinforced-PSBS composites. The exposed S on the surface of 2D-$MoS_2$ and the double bonds of the polybutadiene block of PSBS undergo vulcanization through a thermal treatment at 150 $^oC$ for three hours, inducing the formation of C-S covalent bond, confirmed by FT-IR measurements in DRIFTS mode. Such process leads to the formation of loop-chain entanglements at the interface of the composite. To investigate how the interfacial architecture influences the mechanical properties of the composite, linear brushes and loop-forming polymers were synthesized through conventional ATRP in solution and grafted to 2D-$MoS_2$ particles. Composites containing decorated 2D-$MoS_2$ were fabricated, yielding composites with interfacial loops and interfacial brushes, and cyclic tested in tensile mode. Cyclic mechanical tests revealed loop-chain entanglements cause molecular mechanical interlocking, which suppresses chain sliding, decreasing plastic deformation and enhancing elastic recovery. These findings demonstrate how the interfacial architecture impacts the mechanical behavior of composites, as well as stablish a way of modulating the interfacial architecture of a polymer matrix composite through surface modification of the reinforcing elements with architectured polymers. Besides, this work throws light on understanding the phenomena occurring at the interface of polymer matrix composites when transferring stress from the matrix to the reinforcing elements during loading and unloading events.

# Chapter 6

## OUTLOOK

The findings regarding surface modification through ATRP developed in the works that compose this thesis could be further explored in innovative directions. Since $Zn^0$ SI-ATRP is a cheap and versatile method to modify silicon substrates with various chemically different polymers and enabled the functionalization of natural fabrics, such approach could be applied to modify textiles adding functionalities for biomedical applications. Because $Zn^0$ SI-ATRP is also compatible with Fe-based catalysts, such approach could be performed to functionalize natural fabrics aiming the fabrication of antibacterial wound dressings. Antimicrobial wound dressings decrease the chance of bacterial colonization and infections, enhancing the healing process.[1] PMPC, one of the polymers grafted from $SiO_x$ through $Zn^0$ SI-ATRP (Chapter 2), was reported to show anti-biofouling properties due to zwitterionic moieties.[2] The mechanism of $Zn^0$ SI-ATRP is currently revealed, the challenges for an industrial application reside on finding the best conditions to functionalize fabrics aiming properties for a target application and the scalability of the process, including the development of strategies to remove catalyst residues through transition metal complex chelation.[3]

$Cu^0$ SI-ATRP is an effective method to prepare 3D polymer-based single and multiple graded materials, with tunable chemical composition and morphology, in a fast and controlled fashion, without the need of lengthy deoxygenation processes. These findings pave the way to fabricate 3D polymer-based materials exhibiting a gradual change in biochemical composition and properties through $Mt^0$ SI-ATRP. 3D graded materials can be employed in biomedical applications such as cell-culture platforms, tissue engineering supports, and synthetic prostheses.[4] Besides, since the scaffold is produced through the polymerization of an emulsion, the system could be adapted to additive manufacture, which would allow the fabrication of on-demand products with low costs.[5] Moreover, the emulsion could be replaced by other 3D printable systems to fabricate the scaffold, such as nanocellulose. Nanocellulose surface provides OH groups, which can be functionalized with ATRP initiator, following the procedure described to modify cotton-based wound dressings (Chapter 2).[6] Combining 3D printing of nanocellulose structures, the functionalization of natural

fibers with ATRP initiator, the possibility of creating multiple gradients through $Cu^0$ SI-ATRP and biocompatible studies already reported applying $Fe^0$ SI-ATRP[7] opens the door for the manufacture of 3D on-demand graded materials for bone and cartilage prosthetics.

Even though we have applied classical ATRP in solution to synthesize architectured polymers, which is expensive, lengthy and complicated to be applied in an industrial level, other approaches can be performed to achieve interfacial architecture, such as vulcanization, a process that was first discovered in 1853 by Charles Goodyear and is widely applied in industrial processes.[8] Since we have a better understanding of the influence of interfacial architecture on mechanical performance of materials, we could use surface modification as a tool to modulate the interfacial architecture of polymer matrix composites, favoring molecular mechanical interlocking or chain sliding, depending on the aimed property. Furthermore, a new route to functionalize 2D-$MoS_2$ through local vulcanization without the need of additional elemental S has not yet been reported prior to the present thesis. Given the importance of 2D-$MoS_2$ for technological applications,[9] this work also contributes to the development of novel strategies to fabricate stretchable materials containing lamellar dichalcogenides.

## REFERENCES

1. Simões, D.; Miguel, S. P.; Ribeiro, M. P.; Coutinho, P.; Mendonça, A. G.; Correia, I. J. Recent Advances on Antimicrobial Wound Dressing: A Review. Eur. J. Pharm. Biopharm. 2018, 127 (February), 130–141.

2. Vales, T. P.; Jee, J. P.; Lee, W. Y.; Cho, S.; Lee, G. M.; Kim, H. J.; Kim, J. S. Development of Poly (2-Methacryloyloxyethyl Phosphorylcholine)-Functionalized Hydrogels for Reducing Protein and Bacterial Adsorption. Materials (Basel). 2020, 13 (4).

3. Ding, M.; Jiang, X.; Zhang, L.; Cheng, Z.; Zhu, X. Recent Progress on Transition Metal Catalyst Separation and Recycling in ATRP. Macromol. Rapid Commun. 2015, 36 (19), 1702–1721.

4. Benetti, E. M.; Gunnewiek, M. K.; Van Blitterswijk, C. A.; Julius Vancso, G.; Moroni, L. Mimicking Natural Cell Environments: Design, Fabrication and Application of Bio-Chemical Gradients on Polymeric Biomaterial Substrates. J. Mater. Chem. B 2016, 4 (24), 4244–4257.

5. Studart, A. R. Additive Manufacturing of Biologically-Inspired Materials. Chem. Soc. Rev. 2016, 45 (2), 359–376.

6. Albers, R. F.; Magrini, T.; Romio, M.; Leite, E. R.; Libanori, R.; Studart, A. R.; Benetti, E. M. Fabrication of Three-Dimensional Polymer Brush Gradients Within Elastomeric Supports by $Cu^0$-Mediated Surface-Initiated ATRP. ACS Macro Lett. 2021, No. 10, 1099–1106.

7. Layadi, A.; Kessel, B.; Yan, W.; Romio, M.; Spencer, N. D.; Zenobi-Wong, M.; Matyjaszewski, K.; Benetti, E. M. Oxygen Tolerant and Cytocompatible Iron(0)-Mediated ATRP Enables the Controlled Growth of Polymer Brushes from Mammalian Cell Cultures. J. Am. Chem. Soc. 2020, 142 (6), 3158–3164.

8. Goodyear, C. Gum-Elastic and Its Varieties : With a Detailed Account of Its Applications and Uses, and of the Discovery of Vulcanization; 1853.

9. Singh, E.; Singh, P.; Kim, K. S.; Yeom, G. Y.; Nalwa, H. S. Flexible Molybdenum Disulfide (MoS 2 ) Atomic Layers for Wearable Electronics and Optoelectronics. ACS Appl. Mater. Interfaces 2019, 11 (12), 11061–11105.

# Chapter 7

## APPENDIX A

**Supplementary Information for "Mechanism and application of surface-initiated ATRP in the presence of a $Zn^0$ plate"**

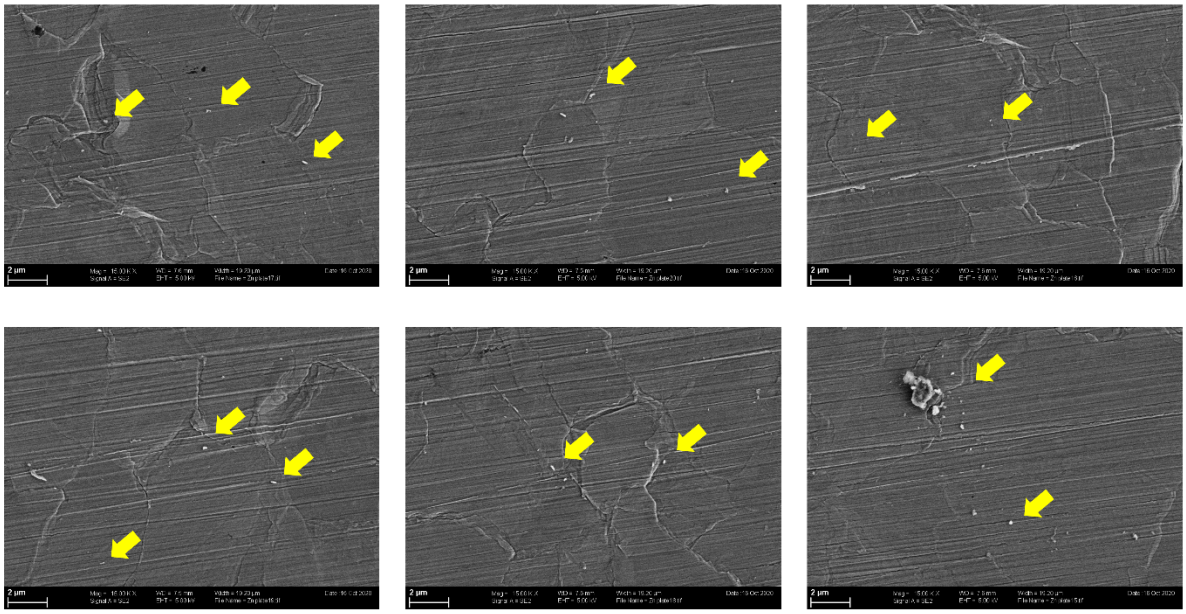

**Figure A.1.** Scanning electron micrographs (SEM) highlighting the formation of $Zn^0$ nano/microparticles after the polishing process.

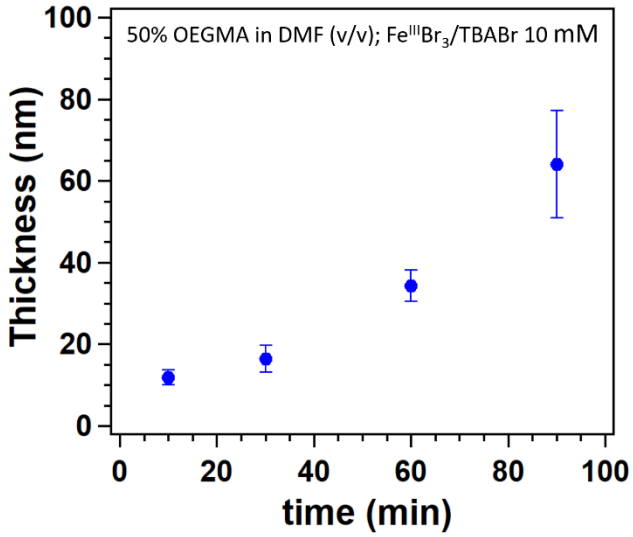


**Figure A.2.** SI-$Zn^0$-ATRP of OEGMA using Fe-based catalyst. $Fe^{III}Br_3$/tetrabutylammonium bromide (TBABr) is readily reduced to $Fe^{II}Br_2$/TBABr activators by the $Zn^0$ surface, triggering the growth of more than 30 nm-thick POEGMA brushes in just 60 min of reaction.

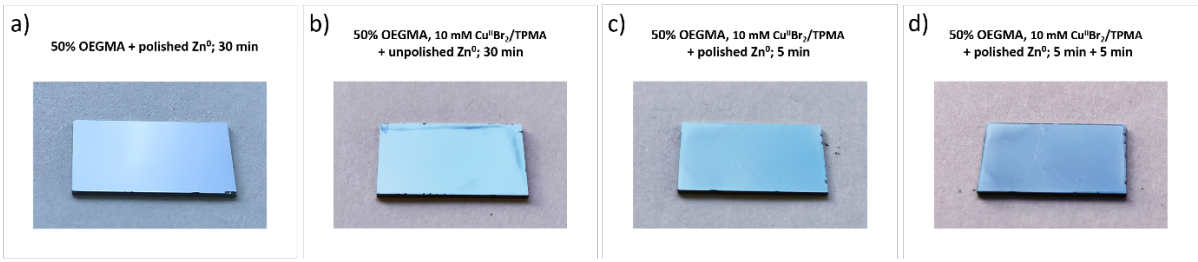


**Figure A.3.** (a) When SI-$Zn^0$-ATRP was performed in the absence of $Cu^{II}Br_2$ and ligand, by sandwiching a 50% OEGMA in DMF (v/v) between an initiator-bearing substrate (reported in the picture) and a polished $Zn^0$ plate, no appreciable growth of brushes was recorded, with the dry thickness of polymer layer < 5 nm. (b) When SI-$Zn^0$-ATRP was carried out using 50% OEGMA in DMF (v/v) and 10 mM $Cu^{II}Br_2$/TPMA but without polishing the $Zn^0$ plate a relevant brush growth was not recorded, with average polymer thickness < 5 nm, and just few areas presenting very inhomogeneous growth. (c,d) Re-initiation efficiency was demonstrated by first growing a 18 ± 2 nm-thick POEGMA brush (c), using 50% OEGMA in DMF + 10 mM $Cu^{II}Br_2$/TPMA and carrying out the polymerization for 5 min. Later on, the same substrate was subjected to a freshly prepared reaction solution (50% OEGMA in DMF + 10 mM $Cu^{II}Br_2$/TPMA) while carrying out polymerization for further 5 min (d). The final POEGMA brush-thickness resulted 35 ± 3 nm, reaching nearly twice the value recorded for the first "brush block".

# Chapter 8

## APPENDIX B

**Supplementary Information for "Fabrication of Three-Dimensional Polymer Brush Gradients Within Elastomeric Supports by $Cu^0$-mediated Surface-Initiated ATRP"**

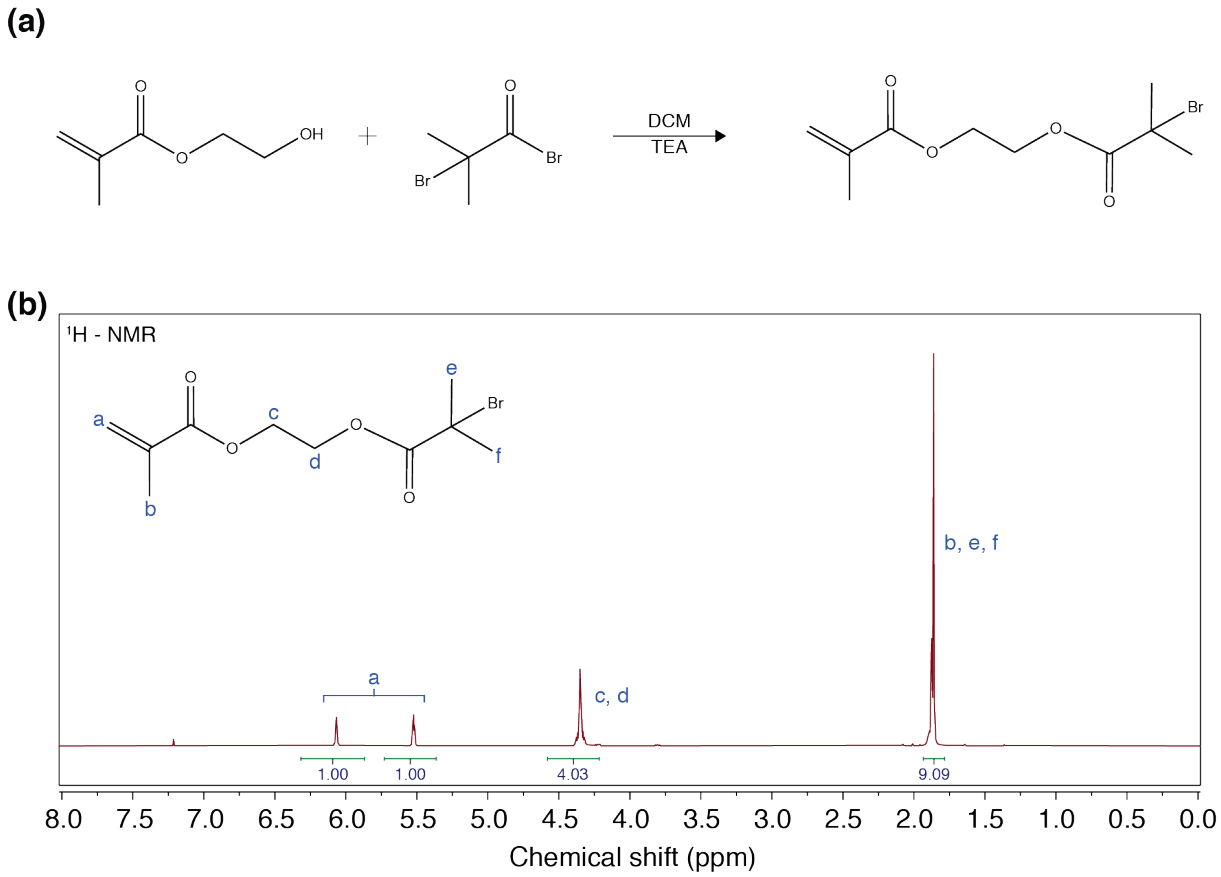


**Figure B.1.** Synthesis (a) and ¹H-NMR spectrum (b) of ATRP inimer 2-(2-bromoisobutyryloxy) ethyl methacrylate (BIEM).

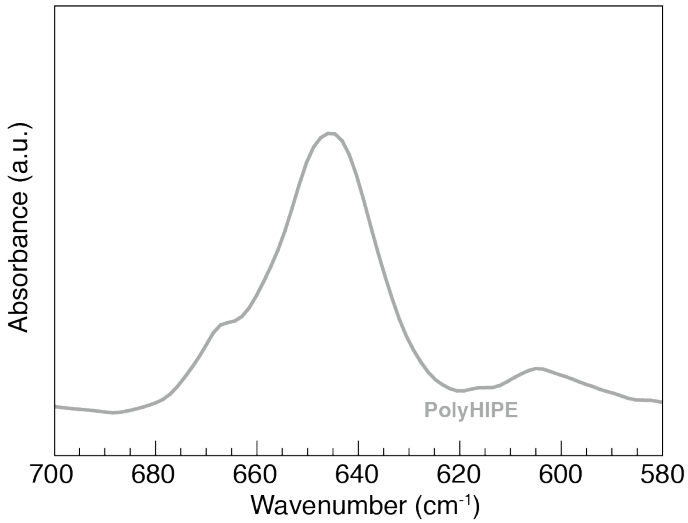


**Figure B.2.** (a) ATR-IR spectrum of PolyHIPE, band at 645 $cm^{-1}$ corresponding to C-Br stretching.

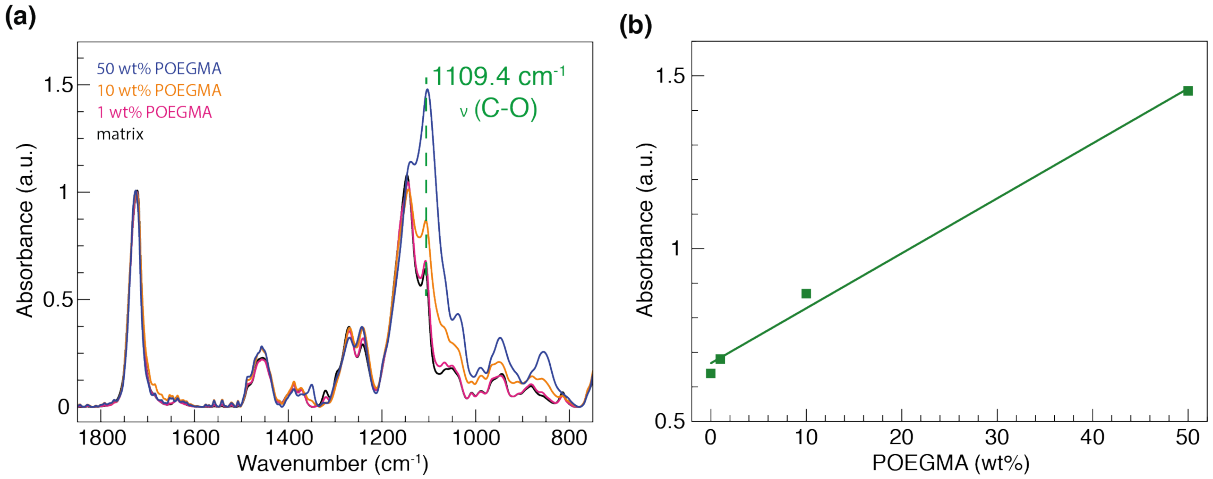


**Figure B.3.** (a) ATR-IR spectra of polyHIPE, and polyHIPE containing 1, 10 and 50 wt% of POEGMA. (b) Calibration curve built from the normalized absorbance values of the band at 1109.4 $cm^{-1}$ as a function of wt% of POEGMA.

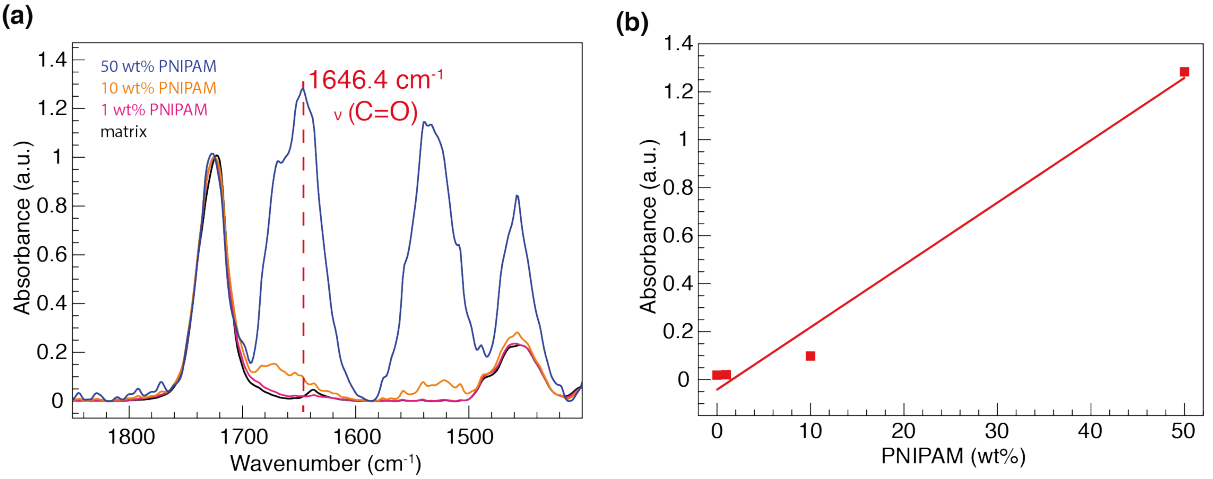


**Figure B.4.** (a) ATR-IR spectra of polyHIPE, and polyHIPE mixed with 1, 10 and 50 wt% of PNIPAM. (b) Calibration curve built from the normalized absorbance values of the band at 1646.4 $cm^{-1}$ as a function of wt% of PNIPAM.

# Chapter 9

## APPENDIX C

**Supplementary Information for "Fabrication of 2D-$MoS_2$-reinforced composites with interfacial loop-chain entanglements through selective vulcanization of interfaces"**

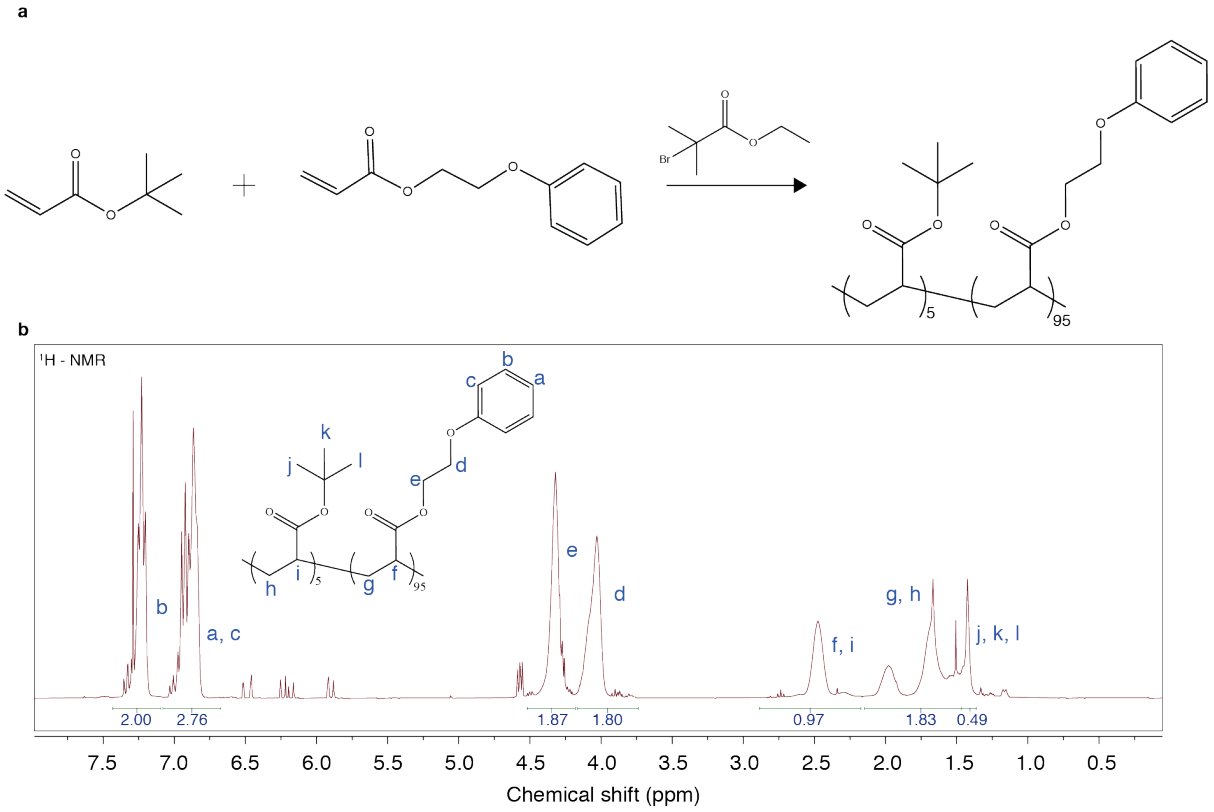


**Figure C.1.** Loop-forming polymer fabrication. Synthesis (a) and $^{1}$H-NMR spectrum (b) of poly(2-Phenoxyethyl acrylate-co-tert-butyl acrylate).

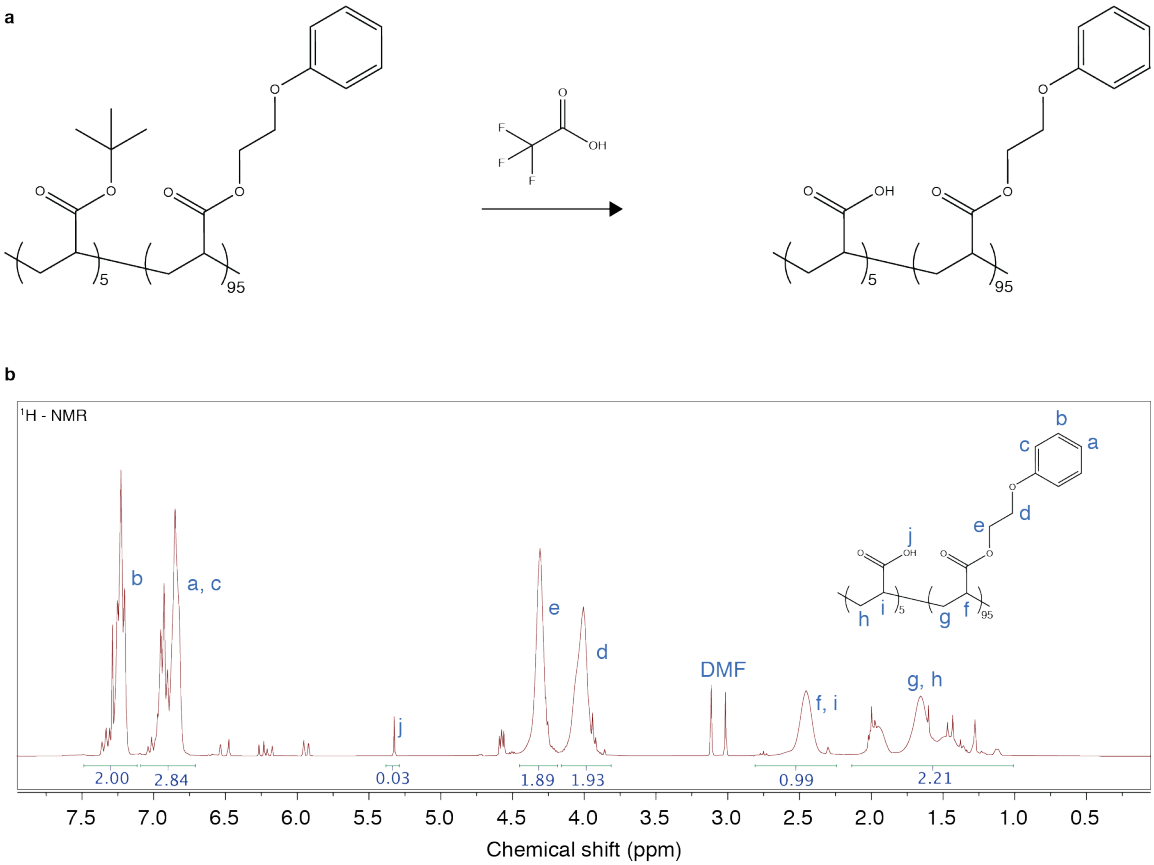


**Figure C.2.** 1st step of loop-forming polymer modification. (a) Deprotection of tert-butyl groups with TFA; (b) ¹H-NMR spectrum of poly(2-Phenoxyethyl acrylate-co-acrylic acid).

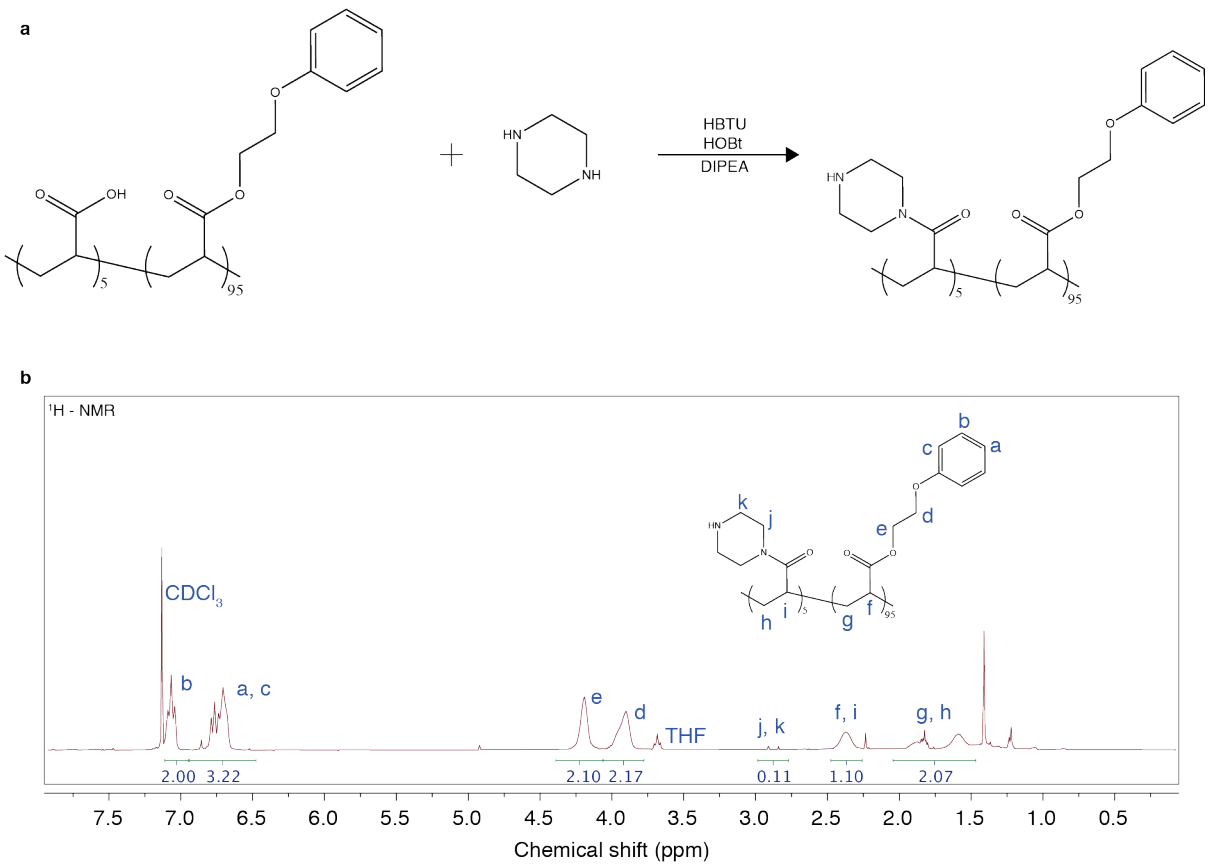


**Figure C.3.** 2nd step of loop-forming polymer modification. (a) Coupling reaction between carboxylic acid groups and piperazine; (b) $^{1}$H-NMR spectrum of poly(2-Phenoxyethyl acrylate-co-1-(piperazin-1-yl)prop-2-en-1-one).

a

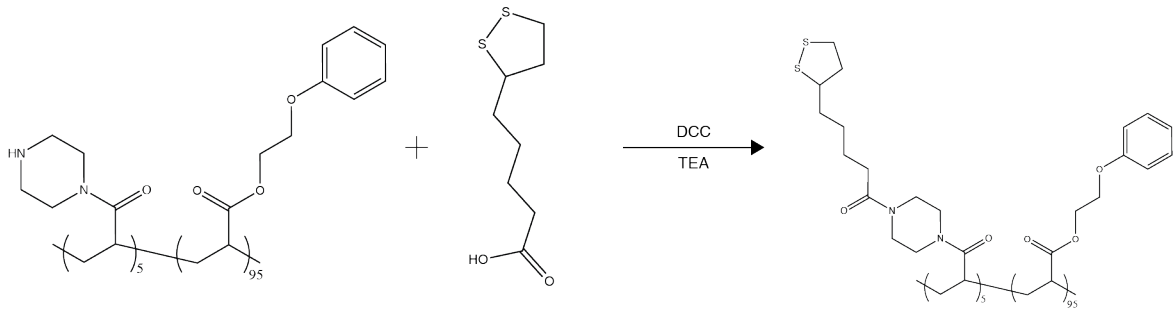


b

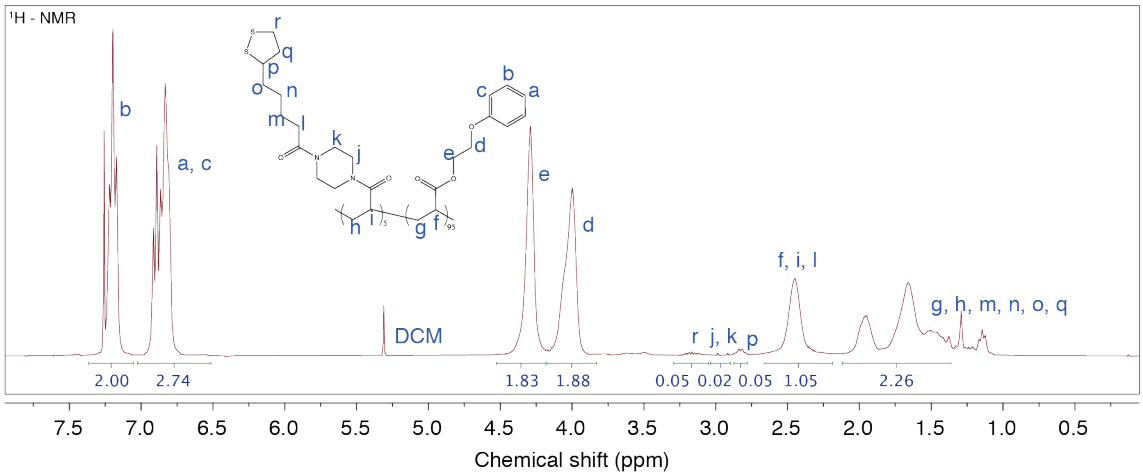


**Figure C.4.** 3rd step of loop-forming polymer modification. (a) Coupling reaction between amine groups and lipoic acid; (b) $^{1}$H-NMR spectrum of poly(2-Phenoxyethyl acrylate-co-1-(4-acryloylpiperazin-1-yl)-5-(1,2-dithiolan-3-yl)pentan-1-one).

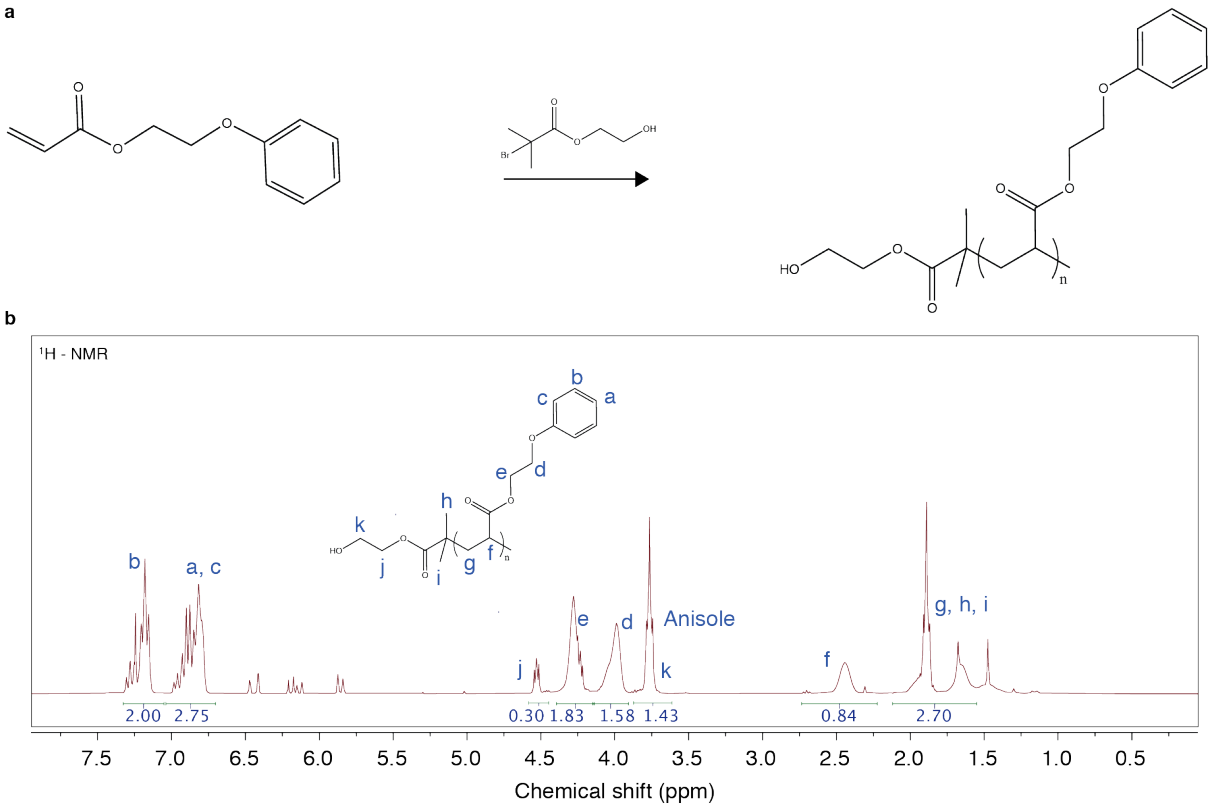


**Figure C.5.** Linear brushes polymer fabrication. Synthesis (a) and $^{1}$H-NMR spectrum (b) of poly(2-Phenoxyethyl acrylate).

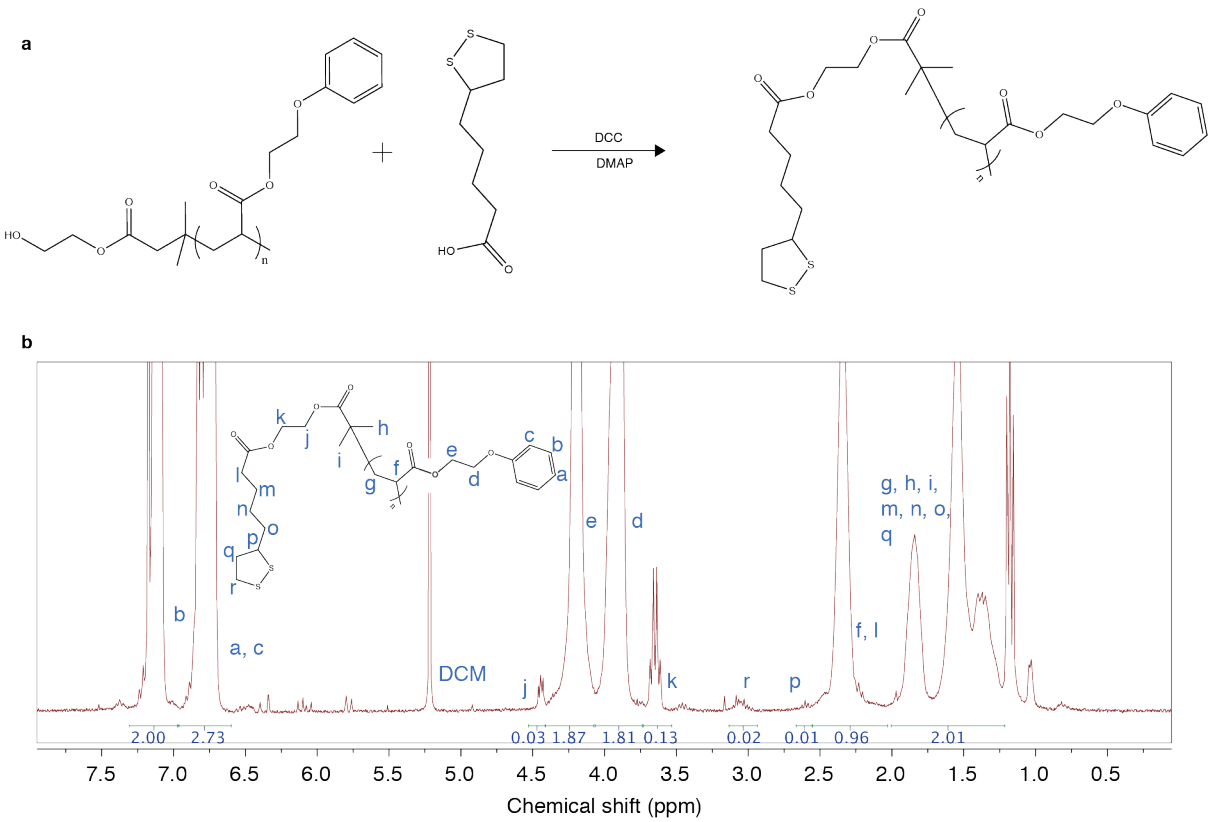


**Figure C.6.** Linear brushes polymer modification. (a) Coupling reaction between hydroxy groups and lipoic acid; (b) $^{1}$H-NMR spectrum of disulfide-poly(2-Phenoxyethyl acrylate).

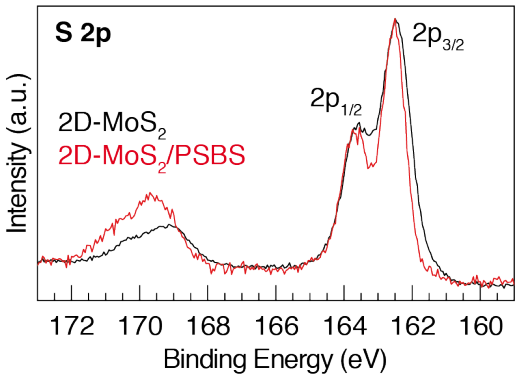


**Figure C.7.** High resolution XPS sulfur spectra of 2D-$MoS_2$ (black curve) and 2D-$MoS_2$-PSBS interfacial vulcanized composite after thermal treatment at 150 °C for 3 hours (red curve).

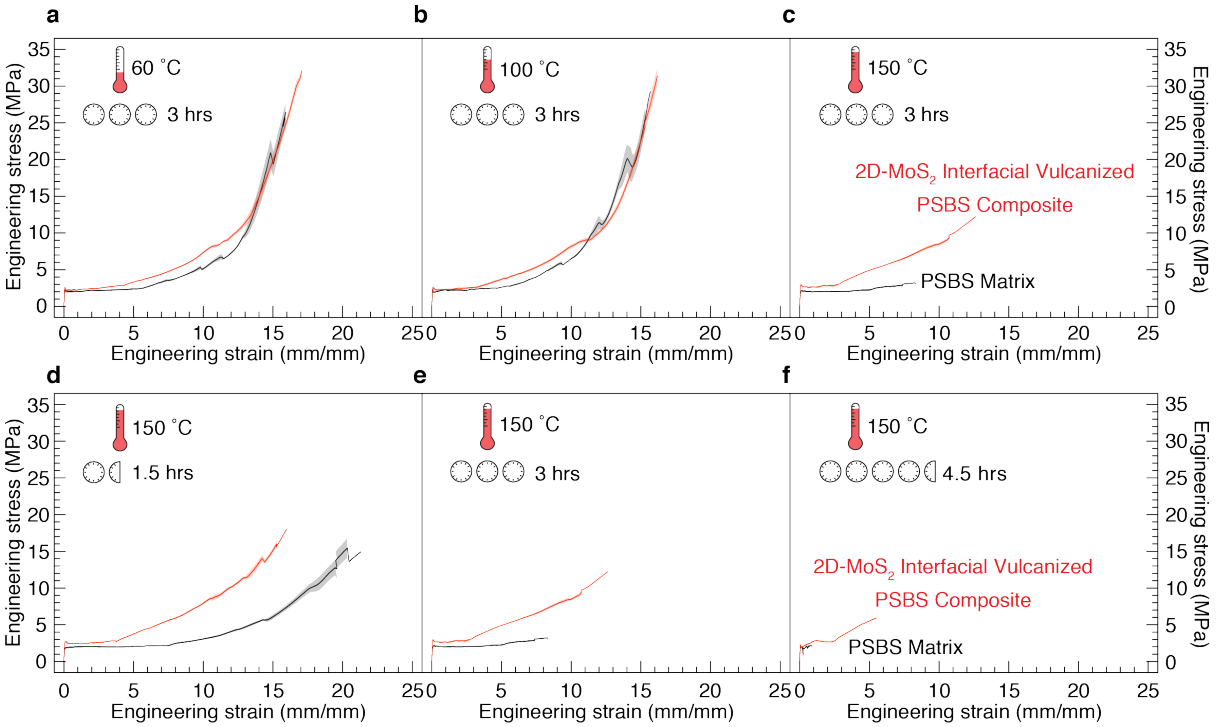


**Figure C.8.** Engineering stress versus engineering strain curves of quasi-static tensile tests of 2D-$MoS_2$-reinforced-PSBS composite after thermal treatment at (a) 60 °C; (b) 100 °C; and (c) 150 °C for 3 hours; and 150 °C for (d) 1.5; (e) 3 (f) 4.5 hours.

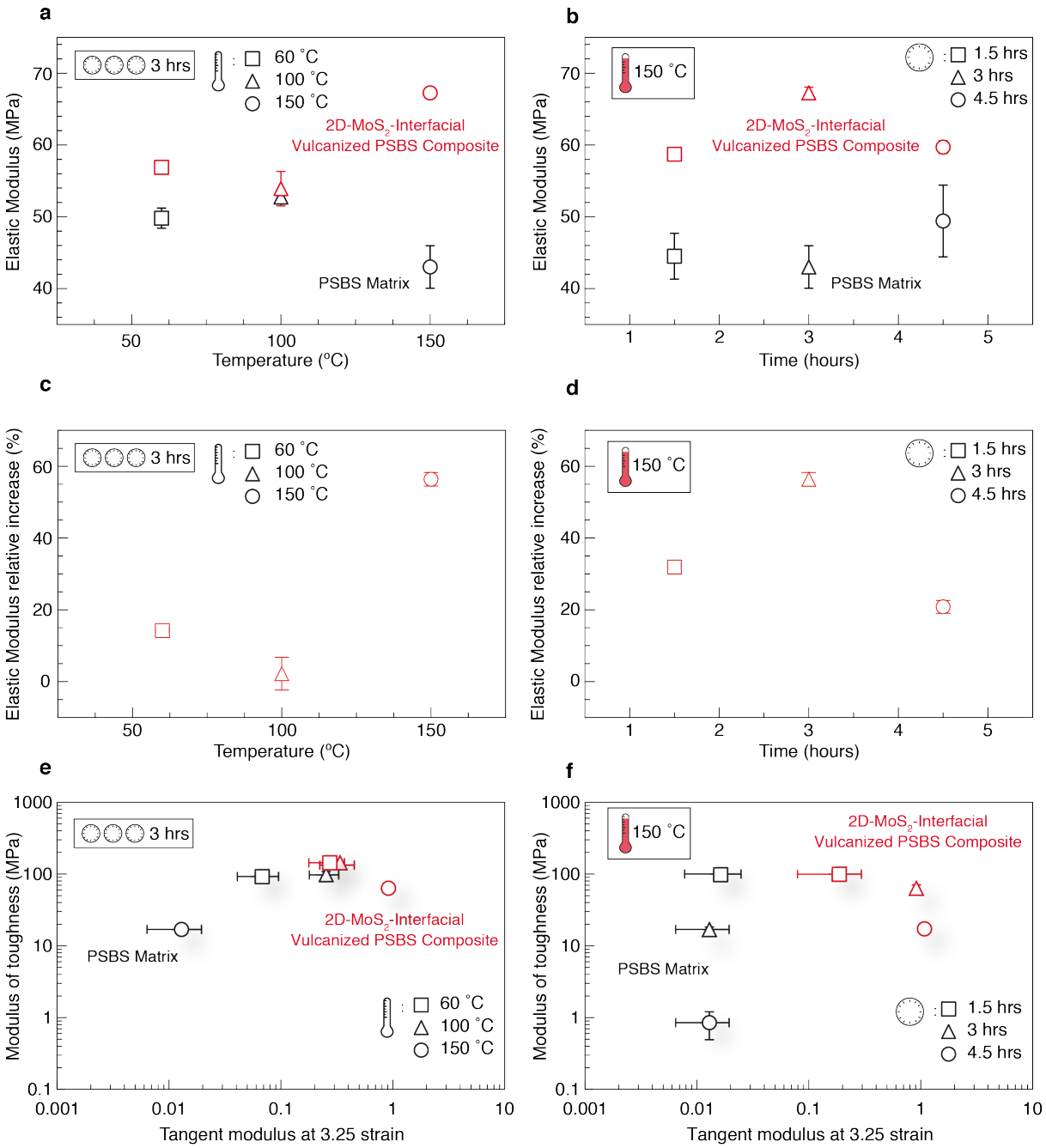


**Figure C.9.** Elastic modulus as a function of (a) temperature and (b) time of the thermal treatment; elastic modulus relative increase as a function of (c) temperature and (d) time of the thermal treatment; Ashby-like plot of Modulus of toughness versus tangent modulus at 3.25 strain as a function of (e) temperature and (f) time of the thermal treatment.

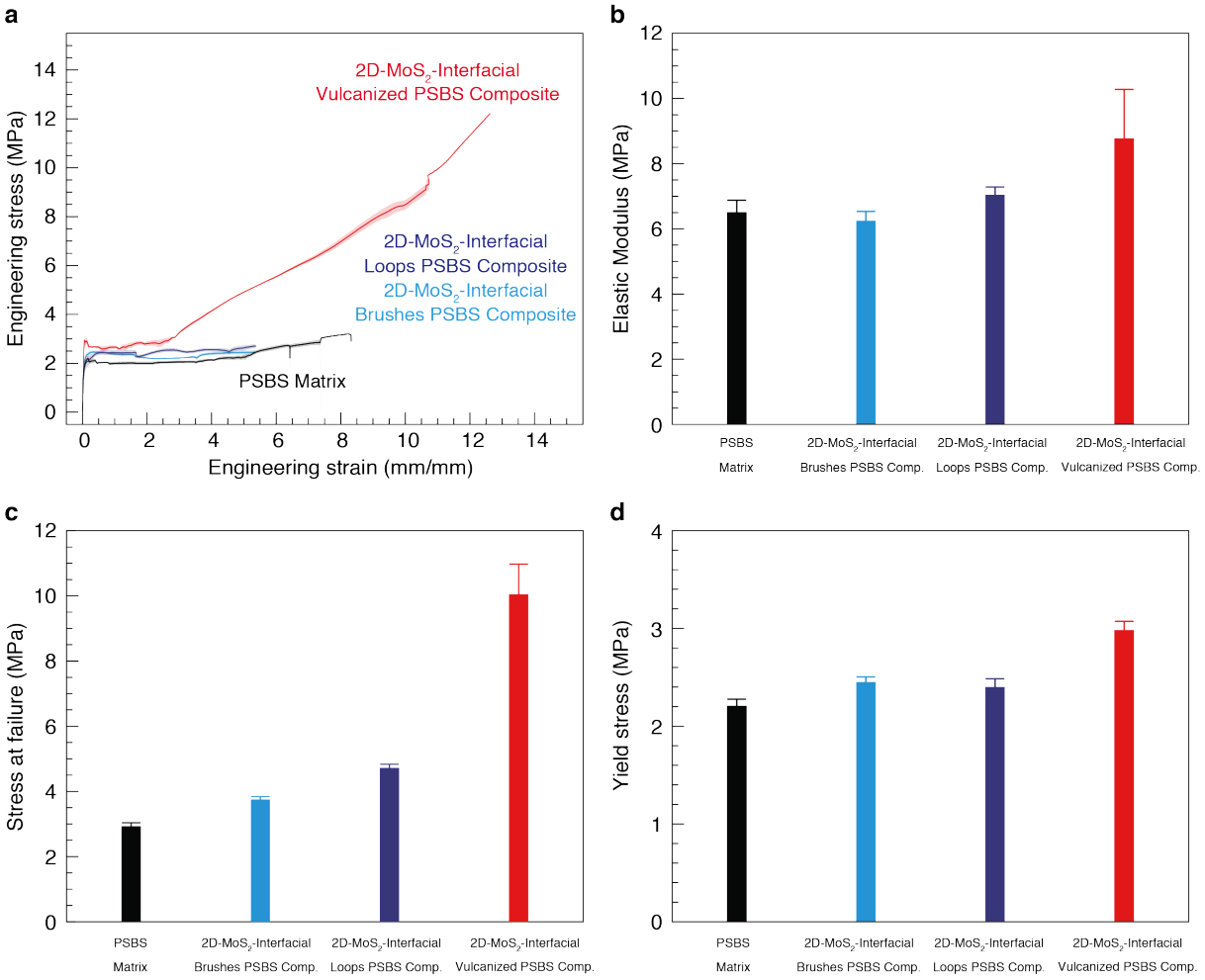


**Figure C.10.** (a) Engineering stress versus engineering strain curves of quasi-static tensile tests of PSBS matrix (black), 2D-$MoS_2$-interfacial brushes PSBS composite (light blue), 2D-$MoS_2$-interfacial loops PSBScomposite (purple) and 2D-$MoS_2$-interfacial vulcanized PSBS composite (red); (b) Elastic modulus; (c) Stress at failure; (d) Yield stress of the composites tested after thermal treatment ate 150 °C for 3 hours.